

**I. Episodic Volcanism of Tidally Heated Satellites with
Application to Io II. Thermal State of an Ice Shell
on Europa III. Polar Wander of a Synchronously
Rotating Satellite with Application to Europa**

Thesis by

Gregory W. Ojakangas

In partial fulfillment of the requirements
for the Degree of
Doctor of Philosophy

California Institute of Technology
Pasadena, California

1988

(submitted September 18, 1987)

©1988

Gregory W. Ojakangas

All Rights Reserved

To my wife, Tracie Lynn,
and to my parents,
in love and gratitude.

Acknowledgements

My first thanks go to God, in whom I believe and trust, for creating me, and allowing me the privilege of contemplating (in a small way) the dynamics of the Jupiter system — a part of His creation which is of unparalleled and astounding beauty. Three unique and beautiful moons, each the size of a planet, whose orbits are synchronized like clockwork, is a reality that will never grow dull for me. I feel like a very small child to whom was given a marvelous rattle to play with — a cleverly crafted thing of gyroscopes and wheels within wheels, a work which could only have been crafted by the greatest Artist of all.

I am deeply grateful to my thesis advisor and friend, Dave Stevenson, for his clever ideas, great support, encouragement, and virtually infinite patience with me during my years at Caltech. It is an understatement to say that none of this work would have been possible without his inspiration. His ideas seeded this work and often revived it when it appeared to be “dead, Jim.” I will always admire the remarkable breadth of his knowledge of science as well as his endless creativity, but what I will carry closest to my heart is the warmth and genuineness of his friendship.

I also wish to express my thanks to my academic advisor, Dr. Andrew Ingersoll, for his guidance and encouragement over the years. However, I will always resent the fact that he can run faster than me, despite the difference in our ages. I would also like to thank Dr. Duane Muhleman for his encouragement and belief in me, Dr. Yuk Yung for his support and good sense of humor, and Dr. Bruce Murray. Special thanks must also go to Dr. Peter Goldreich, for very valuable direction and insight into the problems I’ve attempted to tackle. I am also grateful to Dr. Robert Sharp for several stimulating field trips, especially for that wonderful trip to the flows of living lava, Project Pahoehoe 1987! Many thanks also to Dr. Eugene

Shoemaker and his charming wife Carolyn, for their kind instruction and especially for the opportunity to participate in the search for new asteroids, which allowed me the tremendous pleasure of discovering a minor planet and naming it after my wife!

I must express deep thanks to all of my fellow students with whom I shared the minor eternity of grad school. Thanks to Randolph Livingstone Kirk (alias RLK-divided-by-two-pi) who managed to repeatedly attain my complete attenuation. Always remember: there are only three (spatial) dimensions, so have as much fun as you can in them! Don Rudy, I can only hope that someday I will once again assume the glorious title of “Greg Of Down The Hall” for you. John Louie, you will always occupy the same fond region of my memories as does the frittata omelette. Don’t ever come out of retirement! To Ken Herkenhoff (sheesh, Musky!) I have one departing syllable: ‘sack?!’ Jim Friedson, I will always remember you as a central figure in the legacy of the “tough office.” Arie Grossman (alias Grossbeak), may you always command your life with the same grace with which I’ve seen you hurl your body out of an airplane. I am grateful to you for all your help in producing the first version of this thesis while I blew town! Carol Polansky, I’ll never forget how your cat “trashed the house.” Thanks to all of the rest of you, and to those of you who may still (as this is written) be occupying states in “the minor eternity”, may you all “tunnel” out eventually!

I cannot express enough thanks to Donna Lathrop, for beautifully and skillfully typing this entire behemoth, complete with hundreds of cryptic equations! I don’t know what I would have done without her. I am also grateful to Kay Campbell and Lorna Griffith for their friendship and help in maintaining contact with administrative realities.

Finally, I am deeply grateful to my wonderful wife Tracie Lynn and to my wonderful parents, for continually supporting me and tolerating my neurosis during the sometimes-painful birth of this work.

Great Jupiter, ominous hydrogen lord,
no casual sun-nearing bodies have missed him,
his ponderous presence cannot be ignored,
the “man-about-town” of the whole solar system.

When comets, in pilgrimage, close on our star,
he cruelly and coldly determines their fates,
he hurls them hopelessly, helplessly far,
but keeps, close by, four lovely mates.

Among these four favorites (all of them know),
bright Io is the liveliest,
the “life of the party”, she’s stealing the show —
if she were to vanish, she sure would be missed!

A lovely girl in graceful dance,
she waxes eloquent to see —
to Jupiter, with great romance,
we hear her singing, “13 D!”

She shakes her head as if to fight,
but knows that she is firmly caught —
he spins her ’round, he holds her tight,
it makes her nervous, flushed and hot.

Europa, petite and elegant,
spins farther off, plays hard to get,
she causes Io to resent
her apparent calmness, lack of sweat.

She plays it cool, as if to say,
“Later on I may join in ...
I may decide I want to play ...
especially if my crust is thin.”

Europa inquired of Jupiter,
“Might there be room for another guest?
This poor girl is lonely, just look ’it her —
we’re always lining up abreast.”

Jupiter answered with great show of sport,
“Come dance with us, don’t be so shy!
at ten-to-the-ten years, life is too short,
we must all dance before we die.”

But Ganymede’s a quiet one,
she bears the scars of reckless youth —
she’s sowed her oats, she’s had her fun —
she’s wiser than her years, forsooth.

She wasn't sure she'd take the chance,
but after many million years,
she joined at last the resonance,
the music of the spheres.

Yet dances she a quiet way —
no slowly drifting polar caps,
no brilliant plumes of sulfur spray,
conjunction clings to neither apse.

Callisto is a placid hulk,
with pimples, sad, complacent face
like wholesale ice, once bought in bulk —
then left, forgotten, beached in space.

And has she no chance to join in the fun?
Is there reason for anger? Cause to feel slighted?
she may be the saddest sphere under the sun,
and the reason is simple: she wasn't invited!

She's looking peaked, feeling sick,
it seems that she could use a rest,
her wits are slow, her crust is thick —
her eyeball sports a palimpsest.
we've all had bags under our eyes,
but never of such tremendous size!
we'll leave her be — we'll let her sleep —
at 120 K, she'll keep!

Thesis Abstract

Two examples of planetary bodies that may have coupled thermal and dynamical evolutions are investigated. The work is presented in three individual papers.

The first example is that of a tidally heated satellite in an orbital resonance, for which the tidal dissipation rate is a strongly increasing function of the internal temperature. For such a satellite, a feedback mechanism exists between the orbital and thermal energies, which may lead to periodic variations in tidal heating within the satellite and its orbital eccentricity. A simple model of this mechanism is presented in the first paper and is applied specifically to Io.

The second example is that of an ice shell on Europa, which is decoupled from the silicate core by a layer of liquid water. In the second paper, the spatially varying thickness that such a shell would have in thermal equilibrium with tidal dissipation within it, surface solar insolation and heat flow from the core is calculated for reasonable rheological laws for ice. The contribution of these variations in ice thickness to Europa's inertia tensor is estimated, and the implications for nonsynchronous rotation of Europa are discussed. In the third paper, a detailed dynamical model is developed, which demonstrates that such a shell may exhibit large-scale polar wander as it approaches thermal equilibrium, because of the destabilizing effect of the variations in ice thickness on the inertia tensor of the shell.

The abstracts of the three papers are reproduced below.

Episodic Volcanism of Tidally Heated Satellites with Application to Io

A simple model of the coupled thermal and orbital evolution of a tidally heated satellite in an orbital resonance is presented and applied specifically to Io.

The model quantitatively demonstrates how a feedback mechanism between the orbital and thermal energy of such a satellite can lead to periodic variations in surface heatflow and orbital eccentricity. The convective heatflow and (k/Q) of the satellite are parameterized as local power laws of the temperature, where Q is the quality factor and k is the second-degree tidal potential Love number. The time evolution of the model is determined by two nonlinear equations: an equation governing the orbital eccentricity, and a simple heat-balance equation determining the temperature. A linear stability analysis reveals that the time-independent solution is unstable if $n > m + p$, where n and m are the exponents in the power laws for (k/Q) and convective heatflow, respectively, and p is the ratio of the convective cooling time scale to the time scale for equilibration of the eccentricity. Numerical integration of the nonlinear equations reveals behavior in qualitative agreement with this relation. Laboratory data on near-solidus peridotites suggest $20 \lesssim n \lesssim 30$, and parameterized convection schemes suggest $m \sim 10$. Since p is of order unity, it follows that tidally heated satellites are probably in the unstable regime if they are operating near the solidus. It is thus probable that Io has no thermal steady state. The model is made more realistic by (1) arresting the reduction of (k/Q) at low temperature, and (2) arresting the growth of temperature at the mantle solidus and allowing volcanism to remove the excess heat. When the second modification is included, the unstable regime becomes periodic. In addition, a global k substantially larger than the elastic value is possible for a mostly solid Io because the body may begin to behave viscously when the tidal period is longer than, or comparable to, the Maxwell time. This requires a solid-state viscosity of $\lesssim 4 \times 10^{15}$ Pa s, which may be achievable with a small amount of partial melt. The model can easily be adjusted to pass through Io's current observed heatflow ($1\text{--}2 \text{ W m}^{-2}$) and eccentricity (~ 0.004)

for reasonable choices of parameters $(Q/k)_{\min} \sim 100$, $(Q/k)_{\max} \sim \text{few} \times 10^3$, solidus viscosity $\sim 10^{15}\text{--}10^{17}$ Pa s, and Q_J within the required dynamical bounds. The periods of high heatflow and acceptable eccentricity typically have duration of $\sim 20\text{--}20$ myr, separated in time by $\sim 80\text{--}100$ myr. Spatial heterogeneities in Io's thermal structure are likely to make the behavior more complicated. The model predicts that Io's mean motion may be currently increasing, a possibility suggested by recent estimates of \dot{n}_1 from eclipse data. Since Europa's eccentricity mimics that of Io, the model also implies that the tidal stresses in Europa's ice shell may have recently been large enough to produce the observed fracturing. The episodic heating mechanism may be responsible for the resurfacing of Enceladus $< 10^9$ years ago.

Thermal State of an Ice Shell on Europa

We consider a model of Europa consisting of an ice shell that is decoupled from a silicate core by a layer of liquid water. The thickness of the shell is calculated as a function of colatitude and longitude, assuming that a state of conductive equilibrium exists with the incident annual average solar insolation, tidal dissipation within the shell, and heat flow from the core. Ice thickness profiles are calculated for each of two plausible rheological behaviors for ice: the Maxwell rheology and the generalized flow law rheology. In both cases the strong temperature-dependence of the dissipation rate is explicitly included as well as the temperature-dependence of the thermal conductivity of ice. Because of the strong temperature dependence of the dissipation rate, nearly all of the tidal dissipation is concentrated in the lowermost few kilometers of the shell. Even though the effective Q of the greater part of the shell is $\gg 100$ in our models, average shell thicknesses do not exceed 25 km. Thus, if the total thickness of H_2O which mantles Europa is $\gtrsim 25$ km, none

of the models admit the possibility of a completely frozen H₂O layer. The total dissipation rates in our models are comparable to those of a constant Q model with $Q \sim 10$. The thickness profiles are relatively insensitive to heat flow from the core. The second degree spherical harmonic components of the ice thickness are given and the resulting contributions to the quantities $\frac{B-A}{C}$ and $\frac{B-C}{A}$ of Europa are estimated. Although the contribution to $\frac{B-A}{C}$ is perhaps larger than the permanent value needed to prevent nonsynchronous rotation, its dependence on the shell's orientation relative to synchronicity suggests that very slow nonsynchronous rotation will persist, with reorientation of the shell relative to the satellite-planet direction occurring on a timescale \gtrsim the thermal diffusion timescale for the shell ($\sim 10^7$ yr). The existence of a significant "fossil" bulge on the shell due to long-term elastic behavior of its outer, coldest regions would eliminate nonsynchronous rotation. Since the contribution to $(\frac{B-C}{A})$ of the thickness variations in most of our models is > 0 , Europa may experience polar wander as thermal equilibrium is approached, if the above is the most important permanent contribution to $(\frac{B-C}{A})$. The magnitudes of the principal moment differences are insensitive to the details of the parameterization of the tidal dissipation.

Polar Wander of a Synchronously Rotating

Satellite with Application to Europa

An ice shell on Europa that is decoupled from the silicate core by a layer of liquid water has a thermal-equilibrium thickness profile that varies with position over its surface, because of spatial variations in the surface temperature and tidal dissipation within the ice (see previous paper). The second spherical harmonic degree components of these thickness variations and of any fossil rotational and tidal bulges present on the shell contribute to the inertia tensor of the body. The problem

is that of a planetary elastic lithosphere that is topographically loaded from below. Following the development of Willemann and Turcotte (1981) we develop equations describing the variations in the inertia tensor of a body, which are caused by the addition of second harmonic degree topography to the base of the crust. Applied to the case of an ice shell on Europa, it is found for many choices of parameters that a state of thermal equilibrium for the shell will involve an orientation of Europa's principal axes of inertia (when the hydrostatic bulges are relaxed), which is unusual for a synchronously rotating satellite. Specifically, the intermediate and maximum principal moments are reversed. To reach the preferred orientation for synchronous satellites, a thermal equilibrium ice shell must execute a net reorientation of ninety degrees about the satellite-planet direction. We present a simple model of a rigid, synchronously rotating satellite in a circular orbit for which the difference between the intermediate and maximum principal moments is linear in time, passing through zero when $t = 0$. The model demonstrates that the expected reorientation is indeed dynamically favored.

We then consider a more realistic model, including the effects of various torques which act to couple the motions of the core, shell, and liquid water layer, as well as the effect of viscous dissipation which arises in the shell due to the predicted polar wander. It is found that the Poincaré torque, gravitational coupling, and the torque due to viscous shear in the liquid water layer are unable to induce significant motion of the core during polar wander of the shell. However, the Poincaré torque exerted on the liquid water layer by the shell is believed to cause the liquid water layer to reorient in coincidence with the shell. The model suggests that viscous friction in the shell eliminates the possibility that polar wander will occur unless preexisting fractures (e.g., due to tidal stresses (Crawford and Stevenson, 1988))

extend from the surface to a depth where the ice behaves viscously on the polar wander time scale. If the temperature T_f at the base of the fractured region is as high as $\sim 140\text{--}145$ K, the model indicates that polar wander occurs on a time scale of $10^6\text{--}10^5$ y (shorter as T_f increases) after the sign of the difference between the maximum and intermediate principal moments reverses. In the absence of dissipation, polar wander would occur in $\sim \text{few} \times 10^3$ y. Polar wander must occur on a time scale significantly shorter than $\sim 10^7$ y, or the thickness profile of the ice will be in continuous equilibrium with its thermal environment regardless of its orientation, and the mechanism driving the polar wander will be virtually eliminated. It is likely that events of large scale polar wander occur episodically, separated in time by periods on the order of the time scale for thermal diffusion through the shell ($\sim 10^7$ y), although a state of slow, continuous drifting of the pole is also possible. The time scale of viscous flow of topography at the base of the ice is also near 10^7 y. If dissipation in the shell due to polar wander is a few orders of magnitude smaller than our simple model suggests, polar wander as described here is a much more effective means for fracturing the ice than is tidal flexing, and it may contribute to producing the observed global fracture systems in Europa's ice.

Table of Contents

Acknowledgements	iv
Thesis Abstract	ix
List of Figures	xvii
List of Tables	xix
I Episodic Volcanism of Tidally Heated Satellites with Application to Io	1
1. Introduction	2
2. The Mechanism, Equations, and Nondimensionalization	6
3. A Linear Stability Analysis	9
4. Finite Amplitude Models	10
5. Discussion	12
References	18
Update	20
Additional References	22
II Thermal State of an Ice Shell on Europa	23
1. Introduction	27
2. Thickness of an Ice Shell in Conductive Equilibrium	30
3. The Maxwell Rheology	34
4. The Generalized Flow Law Rheology	40
5. Discussion	42
6. Conclusions	54
Appendix A: Surface Temperature of Europa	56
Appendix B: Tidal Strains in a Thin Shell	60
References	67

III Polar Wander of a Synchronously Rotating Satellite with Application to Europa	71
1. A Review of Polar Wander	75
2. Introduction	78
3. The Iceberg Effect	79
3.1 Development with Finite Rigidity	83
4. An Ice Shell on Europa: A Case of Loading from Below	88
5. Polar Wander of a Rigid Synchronously Rotating Body	99
6. A More Realistic Model for Europa	112
6.1 Dissipation in the Shell during Polar Wander	113
6.2 Polar Wander of the Shell	121
6.3 Discussion	135
7. Conclusions	142
Appendix A: The Coupling Torques	145
A.1 Shell-Ocean Coupling	145
A.2 Core-Shell Coupling	152
Appendix B: Viscous Relaxation at the Ice-Ocean Interface .	161
References	165

List of Figures

Paper I

Figure 1	7
Figure 2	7
Figure 3	10
Figure 4	10
Figure 5	11
Figure 6	11
Figure 7	12
Figure 8	13
Figure 9	13
Figure 10	14
Figure 11	14

Paper II

Figure 1	37
Figure 2	38
Figure 3	39
Figure 4	43
Figure 5	44

Paper III

Figure 1	81
Figure 2	82
Figure 3	84
Figure 4	101
Figure 5	102

Figure 6 107

Figure 7 109

Figure 8 131

Figure 9 133

List of Tables

Paper I

Table I	9
---------------	---

Paper II

Table I	45
---------------	----

PAPER I

Episodic Volcanism of Tidally Heated
Satellites with Application to Io

Episodic Volcanism of Tidally Heated Satellites with Application to Io¹

G. W. OJAKANGAS AND D. J. STEVENSON

*Division of Geological and Planetary Sciences, California Institute of Technology,
Pasadena, California 91125*

Received June 17, 1985; revised February 7, 1986

A simple model of the coupled thermal and orbital evolution of a tidally heated satellite in an orbital resonance is presented and applied specifically to Io. The model quantitatively demonstrates how a feedback mechanism between the orbital and thermal energy of such a satellite can lead to periodic variations in surface heatflow and orbital eccentricity. The convective heatflow and (k/Q) of the satellite are parameterized as local power laws of the temperature, where Q is the quality factor and k is the second-degree tidal potential Love number. The time evolution of the model is determined by two nonlinear equations: an equation governing the orbital eccentricity, and a simple heat-balance equation determining the temperature. A linear stability analysis reveals that the time-independent solution is unstable if $n > m + p$, where n and m are the exponents in the power laws for (k/Q) and convective heatflow, respectively, and p is the ratio of the convective cooling time scale to the time scale for equilibration of the eccentricity. Numerical integration of the nonlinear equations reveals behavior in qualitative agreement with this relation. Laboratory data on near-solidus peridotites suggest $20 \leq n \leq 30$ and parameterized convection schemes suggest $m \sim 10$. Since p is of order unity, it follows that tidally heated satellites are probably in the unstable regime if they are operating near the solidus. It is thus probable that Io has no thermal steady state. The model is made more realistic by (1) arresting the reduction of (k/Q) at low temperature, and (2) arresting the growth of temperature at the mantle solidus and allowing volcanism to remove the excess heat. When the second modification is included, the unstable regime becomes periodic. In addition, a global k substantially larger than the elastic value is possible for a mostly solid Io because the body may begin to behave viscously when the tidal period is longer than or comparable to the Maxwell time. This requires a solid-state viscosity of $\leq 4 \times 10^{15}$ Pa sec, which may be achievable with a small amount of partial melt. The model can easily be adjusted to pass through Io's current observed heatflow ($1-2 \text{ W m}^{-2}$) and eccentricity (~ 0.004) for reasonable choices of parameters $(Q/k)_{\min} \sim 100$, $(Q/k)_{\max} \sim \text{few} \times 10^3$, solidus viscosity $\sim 10^{15}-10^{17}$ Pa sec, and Q , within the required dynamical bounds. The periods of high heatflow and acceptable eccentricity typically have durations of $\sim 20-30$ myr, separated in time by $\sim 80-100$ myr. Spatial heterogeneities in Io's thermal structure are likely to make the behavior more complicated. The model predicts that Io's mean motion may be currently increasing, a possibility suggested by recent estimates of \dot{n}_1 from eclipse data. Since Europa's eccentricity mimics that of Io, the model also implies that the tidal stresses in Europa's ice shell may have recently been large enough to produce the observed fracturing. The episodic heating mechanism may be responsible for the resurfacing of Enceladus $< 10^9$ years ago. © 1986 Academic Press, Inc.

1. INTRODUCTION

Peale and Cassen (1978) derived analytical expressions for tidal heat production as a function of position in incompressible bodies of uniform and nonuniform rigidities. Peale *et al.* (1979) applied the same

modeling to Io and successfully predicted that tidal heating should be of great importance in that object's history because of its substantial forced orbital eccentricity and large tides. Although modifications have been suggested (cf. Schubert *et al.*, 1981), their model has become the basis for subsequent work toward understanding Io's thermal history.

The phenomenal production of heat

¹ Contribution Number 4212 of the Division of Geological and Planetary Sciences, California Institute of Technology, Pasadena, Calif. 91125.

within Io is intimately coupled to, and maintained by, a commensurability in the orbits of Io, Europa, and Ganymede known as the Laplace resonance, which holds the mean motions of the three satellites near the ratio of 4:2:1 (cf. Greenberg, 1982).

The Laplace resonance and Io's dissipation are mutually maintained by a combination of three effects:

(1) The tidal bulge raised by Io on Jupiter leads the planet-satellite line by a slight angle ($\sim 1/Q_J$, where Q_J is Jupiter's quality factor) due to dissipation within the planet. This causes a net torque on Io which pumps energy and angular momentum into its orbit, propels it outward from Jupiter, and reduces its mean motion, n_1 .

(2) The near equality of n_1 and $2n_2$ causes the conjunctions of Io with Europa (and similarly with Europa and Ganymede) to occur repeatedly near the same points in their orbits causing their mutual gravitational impulses at conjunction to add constructively. This maintains eccentricity in their orbits, which would otherwise tend toward circularity (because of tidal dissipation discussed below). The nearer each adjacent pair of satellites is to a 2/1 ratio of mean motions, the larger the forced eccentricities become, e.g., for Io,

$$e_1 = \frac{M_2 \alpha |C_1| n_1}{M_1 \nu_{11}} \quad (1)$$

$$\nu_{11} = n_1 - 2n_2 + \dot{\omega}_{1s}$$

where M_2 , J_J , α , $\dot{\omega}_{1s}$, and C_1 are considered to be constants, e_1 is Io's forced eccentricity, and n_1 and n_2 are Io's and Europa's mean motions, respectively (Greenberg, 1982). (All parameters are defined in the appendix.)

(3) These maintained eccentricities cause the tidal stresses within each satellite to vary periodically, as the magnitude of the tidal bulge varies with the distance to Jupiter and the sub-Jupiter point on each (synchronously rotating) satellite librates over its surface. The anelastic response to these

time-varying stresses causes tidal dissipation within each satellite at a rate

$$\dot{E}_T = \frac{21}{2} \frac{GM_J^2 R_i^5 n_i}{a_i^6} \left(\frac{k_i e_i^2}{Q_i} \right) = \frac{7}{3} \frac{GM_J M_i}{a_i} c_i D_i e_i^2 \quad (2)$$

(Peale *et al.*, 1982), where

$$c_i = \frac{9}{2} \left(\frac{R_J}{a_i} \right)^5 \left(\frac{M_i}{M_J} \right) n_i \left(\frac{k_J}{Q_J} \right) \quad (3)$$

$$D_i = \left(\frac{R_i}{R_J} \right)^5 \left(\frac{M_J}{M_i} \right)^2 \left(\frac{Q_J}{k_J} \right) \left(\frac{k_i}{Q_i} \right) \quad (4)$$

and the subscript "i" refers to the *i*th satellite (cf. Greenberg, 1982). This dissipation occurs instantaneously at constant orbital angular momentum and in the absence of other effects causes n_i to increase and e_i to decrease (Kaula, 1964). The balance between the above effects for Io is described by (e.g., Eq. (54), Greenberg, 1982)

$$\dot{\nu}_{11} = -0.32 c_1 n_1 (1 - 13D_1 e_1^2). \quad (5)$$

$\dot{\nu}_{11}$ can be related to \dot{e}_1 through differentiation of Eq. (1), yielding

$$\dot{e}_1 = \left[\frac{0.32 M_J c_1}{M_2 \alpha |C_1|} \right] e_1^2 (1 - 13D_1 e_1^2). \quad (6)$$

This equation is valid as long as $\dot{\nu}_{11} \ll \nu_{11}^2$. Note from equation (6) that Io's forced eccentricity is in a stable equilibrium when its square is $1/13D_1$.

Estimates of the heatflow from Io's surface from Voyager data and Earth-based IR measurements of its brightness temperature give surface-averaged values on the order of 1 to 2 W m⁻² (Matson *et al.*, 1980; Sinton, 1981; Pearl and Sinton, 1982), and although revised estimates are slightly downward revisions, they are still ~ 1 W m⁻² and possibly greater (Johnson *et al.*, 1984). Moreover, Io's measured IR brightness is almost entirely dominated by radiation from anomalously hot regions of its surface (hot spots) even though the background conductive heatflow, amounting to only a few degrees of elevation of surface temper-

EPISODIC TIDAL HEATING OF IO

343

ature, probably transports a comparable amount of heat to Io's surface. The true surface heatflow could exceed 2 W m^{-2} . If Io is in thermal equilibrium so that the observed heatflow is equal to the instantaneous rate of tidal dissipation, it follows from Eq. (2) that for heatflows between 1 and 2 W m^{-2} , (k_1/Q_1) lies between ~ 0.007 and ~ 0.014 . If Io is treated as an elastic body with a rigidity similar to the outer layers of the Earth's Moon ($\mu \sim 6.5 \times 10^{10} \text{ Pa}$), the second-degree potential Love number, k , for Io is ~ 0.027 , implying that $Q_1 \sim 1$, which is below the generally accepted range for Q in solid silicate bodies by about two orders of magnitude (Knopoff, 1964; Pollack, 1977; Mavko, 1980). Peale *et al.* (1982) were marginally able to explain a thermal equilibrium (k_1/Q_1) of ~ 0.01 (heatflow = 1.6 W m^{-2}) by invoking a model of Io's interior involving a thin solid outer shell decoupled from a solid interior by a liquid or partially molten zone. The shell is capable of much greater distortion under the tidal potential than a completely solid body, allowing dissipation in the thin shell to be greater than the total dissipation in a completely solid body of equal outer radius by a factor of ~ 10 . A shell as thin as their model requires ($\sim 40 \text{ km}$) is probably unable to support the observed mountainous topography on Io (O'Reilly and Davies, 1981). A rigidity contrast between the shell and the low rigidity layer of a factor of ≥ 100 is needed in order to decouple the shell from the solid interior. Although a contrast as large as this is possible, the analogous ratio for the Earth's crust versus asthenosphere is only ~ 1.1 (Schubert *et al.*, 1981). Furthermore, the observed highly localized surface heatflow (Johnson *et al.*, 1984) implies efficient transport and convergence of heat from large dissipating volumes. Dissipation confined to a shell leads to rather uniform conductive transport to the surface, and hence is difficult to reconcile with localization of heat output.

Ross and Schubert (1985) find Io's observed heatflow consistent with viscous

dissipation in a largely molten interior (crystals in magma) which is forced to circulate by the thin, rigid, flexing shell of the Peale *et al.* model. Their model is also capable of producing more than the observed heatflow. However, it is not clear whether the satellite could reach such a high-temperature state as their model requires, since a large degree of melting is implied, and melt migration can be a very rapid and efficient transporter of heat once low degrees of partial melt are reached (Turcotte, 1982; McKenzie, 1984; Scott and Stevenson, 1985).

Although dissipation localized in a thin, rigid shell or in a largely fluid interior are conceivable, they are perhaps not needed to explain the observed heatflow. In near-solidus silicate rocks, Q minimizes at $\sim 1-10$ (Murase and McBirney, 1973; Sacks and Murase, 1983). The assumption that a substantial fraction of Io's volume is near solidus is supported by the observed extensive volcanism. With an elastic value of k for Io of ~ 0.027 , k/Q can probably be as large as ~ 0.01 without an enhanced response due to a molten layer. If μ is as small as $2 \times 10^{10} \text{ Pa}$ (a value appropriate to the deep lunar interior), the elastic $k = 0.088$ for Io and k/Q is proportionately larger.

If Io behaves as a Maxwell viscoelastic body, the dissipation rate can be substantially larger than the elastic value, if the body is tidally forced at a frequency that is less than or comparable to the reciprocal of its Maxwell time,

$$\frac{1}{\tau_M} = \frac{\mu}{\eta}$$

(η = dynamic viscosity, μ = rigidity).

The Maxwell time is the characteristic time scale that separates predominantly creep response from predominantly elastic response in the stress-strain behavior of viscoelastic bodies (cf. Eirich, 1956). For a simple Maxwell body, the equivalent of k/Q is the imaginary part of the complex Love number:

$$\text{Im}(k) = \frac{1.5 \bar{\mu} \omega \tau_M}{1 + \omega^2 \tau_M^2 (1 + \bar{\mu})^2} \quad (7)$$

$$\bar{\mu} = \frac{19\mu}{2\rho g R}, \quad \omega = \text{forcing frequency}$$

(cf. Lambeck and Nakiboglu, 1983). Using the values of ρ , g , and R for Io and $\mu = 6.5 \times 10^{10}$ Pa, Eq. (7) gives $\text{Im}(k) \sim 0.01$ for $\omega \sim 2.5/\tau_M$. This corresponds to a viscosity $\eta \sim 4 \times 10^{15}$ Pa sec for $\omega \sim 4 \times 10^{-5}$ sec $^{-1}$, the frequency of Io's orbit. The actual range of viscosity in solid silicate rocks at high temperatures is currently uncertain. Typical Earth-mantle rheological laws suggest solidus viscosities of $\geq 10^{17}$ Pa sec (Turcotte and Schubert, 1982), because of the presence of a low melting point component (basalt). It is possible, however, that Io has differentiated and melting in the mantle may not be achieved until a higher temperature corresponding to a viscosity $\sim 10^{15}$ Pa sec. Partial melting can reduce the viscosity still further, perhaps by a large factor (Shaw, 1969), although more recent experiments suggest less dramatic effects (Cooper and Kohlstedt, 1984). Thus dissipation rates in a mostly solid Io may be enhanced further.

Equation (7) does not include the effects of spherical geometry and is thus an additional source of uncertainty of (k/Q) . The application to Io of a complete viscoelastic model, including spherical geometry, would be useful.

In the model proposed in this paper, the dissipation rate given by Eq. (2) will be used, and it will be assumed that (k/Q) can be as large as ~ 0.01 in a mostly solid Io.

If the Laplace resonance is in a steady state and the orbital eccentricities of Io, Europa, and Ganymede are not changing, the dissipation rate in Io is a direct measure of Jupiter's anelasticity. This can be verified by substitution of the equilibrium value $1/\sqrt{13D_1}$ of e_1 from Eq. (6) into Eq. (2) for Io's tidal dissipation. The dissipation in equilibrium is seen to be

$$\dot{E}_1)_{\text{equil}} = \frac{7}{39} \frac{GM_J M_I}{a_1} c_1 \quad (8)$$

which is $\propto 1/Q_J$, and independent of the dissipative properties of Io. Heat flows of 1 to 2 W m $^{-2}$ imply $2 \times 10^4 \leq Q_J \leq 4 \times 10^4$ (for $k_J = 0.5$). Q_J values less than $\sim 2.5 \times 10^4$ require a tidal torque from Jupiter which, acting over the age of the Solar System, would have propelled the satellites farther out from the planet than their current positions. Alternatively stated, $Q_J < 2.5 \times 10^4$ implies such rapid orbital evolution that, integrating backward in time, Io would have been at the surface of Jupiter less than 4.6×10^9 years ago (Schubert *et al.*, 1986; for earlier work see Yoder and Peale, 1981; Goldreich and Soter, 1966).

Although current observational estimates of Io's heatflow are not inconsistent with these dynamical bounds, a simple steady-state scenario cannot be inferred with confidence for the following reasons:

(1) The total heatflow cannot be measured in the IR and may well exceed 2 W m $^{-2}$. In fact, in the models proposed here, conductive flux usually exceeds volcanic flux.

(2) Reasonable estimates of Q_J from theoretical mechanisms give $Q_J \geq 10^5$. If this range reflects reality, Io's current heatflow must be in excess of its time-averaged value.

(3) The dissipation rate in solid bodies is a very strong temperature-dependent quantity. As will be explained later, the result may be that Io does not possess a thermal steady state.

Greenberg (1982) has suggested that the three resonating satellites may have formed deeper in the Laplace resonance, and that we are observing the system as it decays through the present state toward lower eccentricities and heatflows. Thus, the equilibrium heatflow from Io would be lower than the current value, allowing a larger Q_J . However, in addition to debate concerning the stability of the Laplace resonance for large eccentricities (greater than $\sim 3 \times$ the current value), Yoder and Peale (1981) argue that whether or not the resonance is primordial, relaxation from deeper resonance still implies that the current configu-

ration is near equilibrium. Thus the upper limit on Q_1 cannot be relaxed.

Another possibility is that Q_1 was larger in the past and has decreased relatively recently toward the value indicated by the steady-state assumption. The only suggested mechanisms capable of producing Q_1 as small as steady state requires ($\leq 4 \times 10^4$), imply large variations in this parameter through geologic time (Stevenson, 1983). If Q_1 was indeed higher in the past, the Laplace resonance could be geologically recent as well, as Yoder (1979) has suggested.

A third plausible solution to the problem involves the possibility of instabilities or periodic variations in Io's heatflow and orbital eccentricity over geologic time. The existence of feedback mechanisms potentially capable of producing cyclic behavior in the coupled thermal and orbital evolution of the satellites in the Laplace resonance has already been suggested (cf. Greenberg, 1982). The possibility that Io has no thermal steady state was demonstrated in Schubert *et al.* (1981). This paper describes an attempt to model such behavior quantitatively, and to explore its consequences for Q_1 , and the thermal and orbital history of Io.

In Section 2, we describe qualitatively the mechanism which can cause instabilities in the heat production and eccentricity of Io, and how it arises from an inverse temperature dependence of the quantity (Q_1/k_1) . We present a simple heat-balance equation for Io's internal temperature with Eq. (6) for the eccentricity evolution. (Q/k) and the convective heat loss for Io are parameterized as local power laws of the temperature, and experimental as well as theoretical motivation for this approach is given. The resulting two coupled nonlinear equations in temperature and eccentricity are then nondimensionalized in terms of convenient units. In Section 3, the equations are linearized about their steady state, and a stability analysis is performed. It is found that instability is inevitable for a strong enough inverse temperature dependence of (Q_1/k_1) , and that Io is in the unsta-

ble regime for choices of parameters consistent with theory and experiment. In Section 4, the model is modified to allow for (1) efficient removal of heat by volcanism once the solidus temperature is reached, and (2) more realistic behavior of (Q/k) at temperatures well below the solidus. Some examples of numerically integrated solutions of the model for various parameter choices are given. It is found that the model can easily be adjusted to reproduce Io's current orbital eccentricity and heatflow for reasonable choices of parameters. Finally, in Section 5, we discuss the consequences of the model for the history of the Laplace resonance and Io's heatflow through geologic time, as well as implications for the acceleration of n_1 and tidal stresses on Europa. The disadvantages and limitations of the analysis are also discussed.

2. THE MECHANISM, EQUATIONS, AND NONDIMENSIONALIZATION

Consider a satellite in which (Q/k) has a very strong inverse dependence on temperature. We start with a cold satellite (the internal temperature is well below the solidus) and an eccentricity which is less than the equilibrium value, $1/\sqrt{13D_1}$, which is relatively large because $1/\sqrt{13D_1} \propto (Q_1/k_1)^{1/2}$ [see Eq. (4)]. Tidal dissipation increases as $e^2/(Q/k)$ [Eq. (2)], and it may exceed the rate of heat loss, causing the internal temperature of Io to grow. Thus heat loss from the surface increases, and the satellite may become volcanically active. However, the increased temperature causes (Q/k) to decrease, and so also the equilibrium value of the eccentricity, $1/\sqrt{13D_1}$. If it decreases fast enough, $1/\sqrt{13D_1}$ falls below e , so that the eccentricity and tidal dissipation begin to decrease. When tidal dissipation becomes less than the rate of heat loss, the satellite cools off and returns to the cold, low-eccentricity state. The process can then repeat itself. This process is shown schematically in Fig. 1.

In order to support the above mechanism quantitatively, we will consider the evolu-

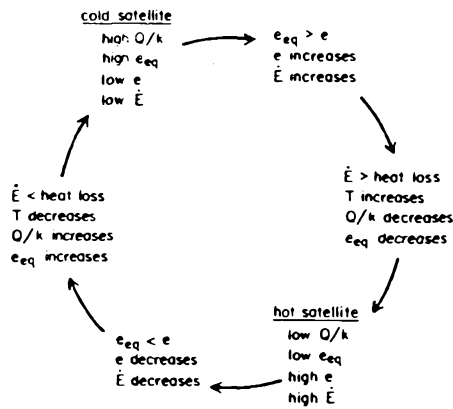


FIG. 1. Schematic diagram of the mechanism which can cause episodic tidal heating.

tion of Eq. (6), coupled with the following equation for the thermal state:

$$MC_p \frac{dT}{dt} = \frac{21}{2} \frac{GM_j^2 R^3 n_1}{a^6} \left(\frac{k(T)c^2}{Q(T)} \right) - 4\pi R^2 \rho C_p K \frac{T}{d} \left[\frac{g\alpha_T T d^3}{\nu(T) K R \alpha_c} \right]^{1/3} \quad (9)$$

(convective heat loss)

(see the Appendix for symbol definitions. All satellite parameters from here on refer to Io unless otherwise indicated, so we have dropped the subscripts.)

Equation (9) is a simple parameterization of the heat balance of a convecting satellite, where the adiabatic interior is approximated as isothermal at temperature T , and tidal dissipation in the (completely solid) body is occurring at the rate given by Peale *et al.* (1982), our Eq. (2). Although the heating rate is a function of position in the satellite, we assume that convection keeps the interior well mixed, so that the body can be characterized by a single temperature. Adiabatic temperature profiles in small convecting planets are nearly isothermal (Schubert *et al.*, 1979). The second term on the r.h.s. of (9) represents heat loss from the satellite due to Rayleigh–Benard convection (Schubert *et al.*, 1979), where we

have for simplicity assumed $T \sim \Delta T$, the temperature drop driving the convection. This parameterization is highly idealized; an accurate parametrization of convection is not important in the context of the model. The convective heat loss in a more complete model would “turn off” more rapidly at low temperatures. Note also that Q , k , and ν are written as functions of temperature.

Dissipative mechanisms are typically activated processes with relaxation times (τ) obeying the relation $\tau \propto \exp(E/RT)$, where E is an activation energy, R is the gas constant, and T is the absolute temperature. Typical activation energies for dissipative mechanisms in rocks are on the order of few $\times 10^5$ J mole $^{-1}$ (Turcotte and Schubert, 1982; Anderson, 1967). Since Q for a given mechanism is a function of $\omega\tau$, where ω is the forcing frequency, Q should be a very strong function of temperature.

Laboratory data indicate that Q in near-solidus silicates is indeed a very strong function of temperature. Figure 2 shows a semi-log plot of Q versus temperature data for near-solidus peridotites in the frequency range of ~ 100 kHz (taken from Sacks and Murase, 1983). The superimposed dashed lines show the relations $d \ln Q / d \ln T \approx -30$ and $d \ln Q / d \ln T \approx -20$. Of course, it is not correct to assume that this Q is applicable to the tidal problem because the frequency is very different. However, the probable existence of the same or a similar attenuation mechanism at tidal frequencies,

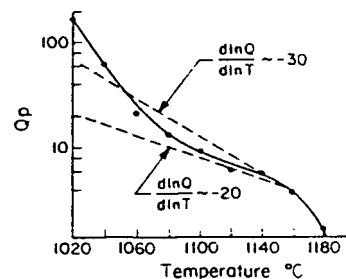


FIG. 2. Q vs temperature for peridotite near the solidus (Sacks and Murase, 1983).

EPISODIC TIDAL HEATING OF IO

347

the activated nature of dissipative mechanisms, and the known weak frequency dependence of Q lead us to expect that the tidal Q is also very temperature sensitive near the solidus.

Additional support for a strong inverse dependence of Q on temperature comes from the fact that for a Maxwell body, $\text{Im}(k)$ [see Eq. (7)] has the form

$$\text{Im}(k) \propto (\omega\tau_M)^{-1} = \frac{\mu}{\omega\rho\nu(T)} \quad (10)$$

when $\omega\tau_M \gg 1/(1 + \bar{\mu}) \sim 0.02$.

Typical rheological laws for the viscosity of steady-state creep in silicates give $-20 > d \ln \nu/d \ln T > -30$ (cf. Murase and McBirney, 1973; Turcotte and Schubert, 1982). It has already been argued that Io may be tidally forced at a period close to its Maxwell time. We assume that viscoelastic friction, where the relevant viscosity is that of steady-state creep, is the dominant source of dissipation in a near-solidus Io.

We have chosen to parameterize the strong inverse temperature dependence of (Q/k) near the solidus by a local power law:

$$\frac{Q}{k}(T) = C_Q T^{-n} \quad (11)$$

and similarly, for the kinematic viscosity,

$$\nu(T) = C_\nu T^{-L} \quad (12)$$

Using (11) and (12), (9) can be written

$$\frac{T_0}{\tau_{\text{th}}} \frac{dT_N}{dt_N} = \left[\left(\frac{63}{8\pi} \right) \left(\frac{GM_J^2 R^5 n_1}{\rho C_p a^6 C_Q} \right) T_0^n e_0^2 \right] T_N e_N^2 - \left[\frac{3}{R} \left(\frac{g\alpha_T K^2}{Ra_c} \right) T_0^{(4+L)/3} \right] T_N^{(4+L)/3} \quad (13)$$

where $T_N \equiv T/T_0$, $t_N \equiv t/\tau_{\text{th}}$, $e_N \equiv e/e_0$, and T_0 , e_0 , τ_{th} are, respectively, the characteristic temperature, eccentricity, and convective cooling time scale for the system. Equation (6) can be treated similarly using (4), (11), and the above nondimensional parameters, yielding

$$\frac{e_0}{\tau_{\text{th}}} \frac{de_N}{dt_N} = \left[\frac{0.32 M_J c_1 e_0^2}{M_2 \alpha |C_1|} \right] e_N^2 \left[1 - \left\{ \left(\frac{13 M_J^2 R^5}{M^2 C_Q R^5} \right) \left(\frac{Q_J}{k_J} \right) T_0^n e_0^2 \right\} T_N^n e_N^2 \right]. \quad (14)$$

We define T_0 and e_0 as the values of T and e in the steady-state solution to (13) and (14). By setting the r.h.s. of (13) and (14) to zero when $T_N = e_N = 1$, we find

$$T_0 = \left[\frac{7}{26} \left(\frac{k_J}{Q_J} \right) \frac{GM_J R^5 n_1}{C_p a^6} \left(\frac{c_\nu Ra_c}{g\alpha_T K^2} \right)^{1/3} \right]^{1/m} \quad (15)$$

$$e_0 = \left[\frac{M^2 C_Q R_J^5}{13 M_J^2 R^5} \left(\frac{k_J}{Q_J} \right) \right]^{1/2} T_0^{-n/2} \quad (16)$$

where $m \equiv (L + 4)/3$ represents the strength of the temperature dependence of the convective heat loss.

We further define the convective cooling time scale τ_{th} as the heat content of the satellite at $T = T_0$ divided by the rate of convective heat loss at that temperature, i.e.,

$$\tau_{\text{th}} \equiv \frac{M_1 C_p T_0}{4\pi R^2 \rho C_p K T_0 \left(\frac{g\alpha_T T_0}{\nu(T_0) K Ra_c} \right)^{1/3}} = \frac{R}{3} \left(\frac{C_\nu Ra_c}{g\alpha_T K^2} \right)^{1/3} T_0^{1-m}, \quad (17)$$

and we identify the leading coefficient on the r.h.s. of (14) as $(e_0/2\tau_e)$, where τ_e is the characteristic time scale for equilibration of the eccentricity near equilibrium. Thus,

$$\frac{de}{dt} = -\left(\frac{e - e_0}{\tau_e} \right) \quad \text{for } e - e_0 \ll e_0$$

and

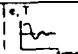

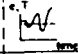

$$\tau_e = \frac{M_2 \alpha |C_1|}{2 M_J (0.32) c_1 e_0}. \quad (18)$$

Inserting (15)–(18) into (13) and (14), we finally obtain

$$\frac{dT_N}{dt_N} = T_N^n e_N^2 - T_N^m \quad (19)$$

$$\frac{de_N}{dt_N} = \left(\frac{p}{2} \right) e_N^2 [1 - T_N^n e_N^2] \quad (20)$$

TABLE I
BEHAVIOR OF THE SOLUTIONS TO EQUATIONS (21)
AND (22)

$\frac{1}{\tau_*}$	$4\omega_0^2 - \frac{1}{\tau_*^2}$	Behavior	
$\frac{1}{\tau_*} > 0$	$4\omega_0^2 - \frac{1}{\tau_*^2} > 0$	STABLE: Oscillatory decay to steady state	
$\frac{1}{\tau_*} < 0$	$4\omega_0^2 - \frac{1}{\tau_*^2} > 0$	UNSTABLE: Oscillatory growth of solutions	
$\frac{1}{\tau_*} < 0$	$4\omega_0^2 - \frac{1}{\tau_*^2} < 0$	UNSTABLE: Pure growth of solutions	

where $p \equiv \tau_{th}/\tau_c$, the ratio of the two time scales. In the following sections, we will use (19) and (20) to explore the coupled thermal and orbital evolution of our model as it applies to Io.

3. A LINEAR STABILITY ANALYSIS

The solutions of the coupled Eqs. (19) and (20) completely describe the thermal and orbital history of the model Io. Unfortunately, their nonlinearity renders analytical solutions impossible. We can, however, determine their stability by considering the behavior of small oscillations about the steady state $e_N = T_N = 1$. Let

$$\begin{aligned} T_N &= 1 + \varepsilon_T e^{i\omega t} \\ e_N &= 1 + \varepsilon_e e^{i\omega t} \end{aligned} \quad (21)$$

where ε_T and ε_e can be complex valued and $|\varepsilon_T|, |\varepsilon_e| \ll 1$. To first order in ε_T and ε_e , (19) and (20) become

$$\begin{aligned} i\omega\varepsilon_T &= (n - m)\varepsilon_T + 2\varepsilon_e \\ i\omega\varepsilon_e &= -\frac{p}{2}(n\varepsilon_T + 2\varepsilon_e). \end{aligned} \quad (22)$$

When Eqs. (22) are combined, eliminating ε_T and ε_e , the quadratic

$$\omega^2 - \frac{i\omega}{\tau_*} - \omega_0^2 = 0 \quad (23)$$

$$\frac{1}{\tau_*} = (m + p - n)$$

$$\omega_0^2 = pm$$

is obtained. The nondimensional ω represents a characteristic frequency of oscillation of T and e , which in dimensional units is

$$\frac{\omega_0}{\tau_{th}} = \sqrt{\frac{m}{\tau_{th}\tau_c}} \text{ sec}^{-1}. \quad (24)$$

Thus, the time scale for small oscillations goes as the geometric mean of τ_{th} and τ_c . The solution of (23) is

$$\omega = \frac{1}{2} \left[\frac{i}{\tau_*} \pm \sqrt{4\omega_0^2 - 1/\tau_*^2} \right]. \quad (25)$$

Inserting expression (25) for ω back into Eqs. (21), we find the behaviors shown in Table I.

Stability of the linearized solutions depends on the sign of $1/\tau_*$. If $n > m + p$, the solution diverges; and if $n < m + p$, the solution is stable. This behavior is intuitively reasonable: If the convective heat loss is a stronger function of temperature than the tidal heat production, then the satellite is able to relieve itself of the increased heat production at increased temperatures, thus avoiding a "thermal runaway." The presence of p in $1/\tau_*$ can be interpreted as a stabilizing "thermal inertia"; it represents the fact that it is harder to produce a thermal runaway in a body that takes a longer time to heat.

The sign of the quantity $4\omega_0^2 - 1/\tau_*^2$ determines whether the system oscillates during the growth or decay dictated by $1/\tau_*$. The boundary $4\omega_0^2 - 1/\tau_*^2 = 0$ is the conic section

$$m^2 + n^2 + p^2 - 2mp - 2mn - 2np = 0 \quad (26)$$

which is a cone in (m, n, p) space whose axis is the line $m = n = p$. The time scale ratio p is a weak function of m and n in the region of our interest, and is generally of order unity. Both τ_{th} and $\tau_c \sim 10^7$ years. Figure 3

EPISODIC TIDAL HEATING OF IO

349

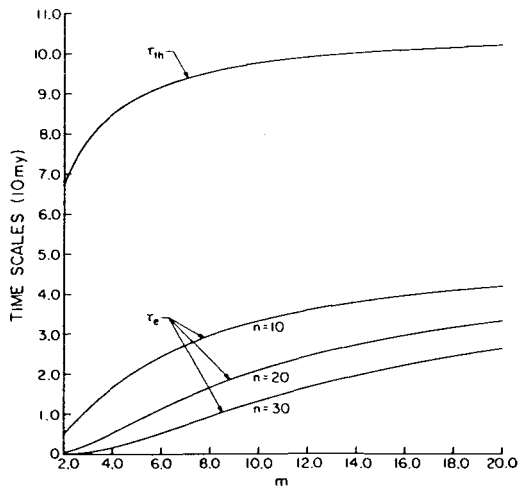


FIG. 3. τ_{th} and τ_c from Eqs. (17) and (18). τ_{th} depends only on the convective parameterization and is independent of n . The behavior of τ_c , a function of both m and n , is depicted by level curves for different values of n . $\nu_{TM} = 10^{12} \text{ m}^2 \text{ sec}^{-1}$, $(Q/k)_{min} = 100$, $Q_1 = 10^5$.

shows τ_{th} and τ_c for a wide range of m and n .

Figure 4 shows schematically the behavior of the linearized solutions in the (m, n) plane, for $p = 1$. The shaded region represents $20 < -d \ln \nu / d \ln T = L < 30$ (which is roughly equivalent to $8 < m < 12$), and $20 < [-d \ln(Q/k)] / d \ln T = n < 30$. This is the region that we expect applies to Io from the experimental and theoretical grounds discussed in Section 2. It is well within the unstable regime. In reality, of course, temperatures and eccentricities cannot diverge. In the next section, we present numerical integrations of modified versions of Eqs. (19) and (20), which prevent divergence of the temperature and eccentricity and make our model more plausible on theoretical grounds.

4. FINITE AMPLITUDE MODELS

We have performed extensive numerical integrations of Eqs. (19) and (20), and we have found good qualitative agreement between their solutions and the predictions of the linearized analysis given in Section 3. However, the diverging growth of the unstable solutions is clearly unrealistic. The

strong increase of k/Q with temperature cannot persist for temperature well in excess of the solidus. Motivated by the expectation that melt migration is very rapid, we propose that when the satellite's internal temperature reaches the solidus, its growth is arrested by the efficient removal of heat by volcanism. We have consequently altered our algorithm for the integration of (19) and (20) so that when $T = T_m$, where T_m is the solidus temperature, $dT/dt = 0$, and the heatflow at the surface (convective plus volcanic heat loss) is equal to the tidal heat production from Eq. (2), i.e., we insert a volcanic heat loss term equal to the difference between tidal heating and convective loss on the r.h.s. of Eq. (9). This is, of course, at best an approximation to Io's behavior; i.e., at best, $dT/dt \approx 0$ once the solidus is reached. This modification is equivalent to asserting that the magma is buoyant, so that essentially all of the melt that is produced is able to reach the surface and the satellite never becomes appreciably molten. The rate-limiting step is probably melt-percolation but this can be rapid (few cm/year) even at low degrees of partial melting (Turcotte, 1982; McKenzie, 1984; Scott and Stevenson, 1985). When this mechanism is incorporated into the model, the unstable regime ($1/\tau_* < 0$) becomes periodic. Note that the behavior of (Q/k) given by Eq. (11)

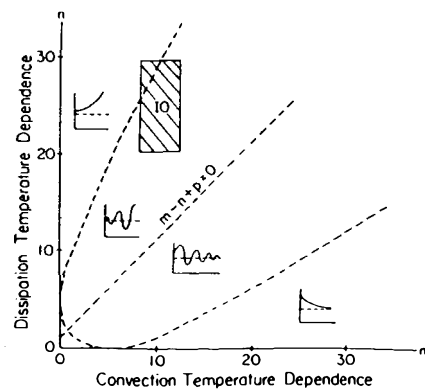


FIG. 4. Behavior of the linearized solutions to Eqs. (19) and (20) in the (m, n) plane.

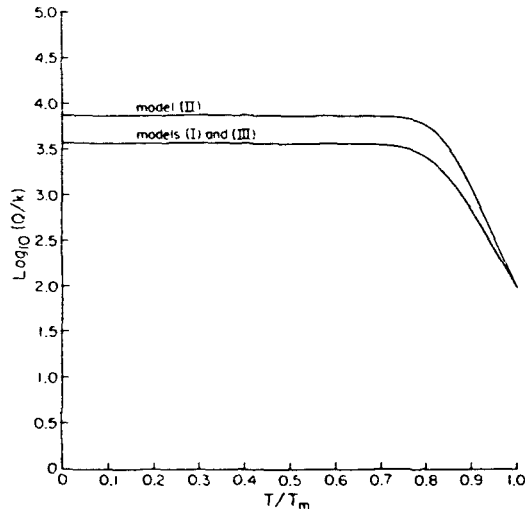


FIG. 5. $Q/k \equiv f(T)$ for models I-III.

could not persist at temperatures well above the solidus because dissipation in a purely viscous medium ($\mu = 0$) is proportional to the viscosity and thus decreases with temperature.

A modification in the functional form of (Q/k) is necessary in order to bring the model into closer accord with theory and experiment. Although (Q/k) is a strong function of temperature near the solidus, it must saturate well below the solidus at a finite and nearly constant value, since k must approach the elastic value of ~ 0.027 , and Q must approach the accepted low-temperature, high-frequency range of a few $\times 10^2$ (see the Introduction for references). We have chosen the functional form

$$f(T) = \frac{Q}{k}(T) = \left[\left(\frac{Q}{k} \right)_0^{-1} + A \left(\frac{T}{T_m} \right)^n \right]^{-1} \quad (27)$$

where $(Q/k)_0$ is the low-temperature value, and

$$A = \left(\frac{Q}{k} \right)_{\min}^{-1} - \left(\frac{Q}{k} \right)_0^{-1} \quad (28)$$

allows a variable minimum value $(Q/k)_{\min}$ of (Q/k) , which we assume to occur at the solidus temperature, T_m . The "solidus temper-

ature" of our model can be slightly above the true solidus, i.e., perhaps a few percent partial melt. Figure 5 shows $f(T)$ for some of the specific models presented below. Although this functional form is a gross simplification of the experimental behavior, it exhibits the proper behavior at low and high temperatures.

With the revised form for (Q/k) given by Eq. (27), Eqs. (19) and (20) become

$$\frac{dT_N}{dt_N} = \left[\frac{f(T_0)}{f(T)} \right] e_N^2 - T_N^m \quad (29)$$

$$\frac{de_N}{dt_N} = \left(\frac{p}{2} \right) e_N^2 \left[1 - \frac{f(T_0)}{f(T)} e_N^2 \right]. \quad (30)$$

Equations (15) and (17) for T_0 and τ_{th} are unchanged, but Eq. (16) becomes

$$e_0 = \left[\frac{M^2}{13M_j^2} \left(\frac{k_j}{Q_j} \right) \left(\frac{R_j}{R} \right)^5 f(T_0) \right]^{1/2} \quad (31)$$

and Eq. (18) for τ_e remains the same but e_0 now is given by (31). Figure 6 shows the new τ_{th} and τ_e for the range of m and n of interest.

Extensive testing of our model indicates that its solutions are independent of the initial values of T and e . In Fig. 7, the results of a typical unstable case for two choices of

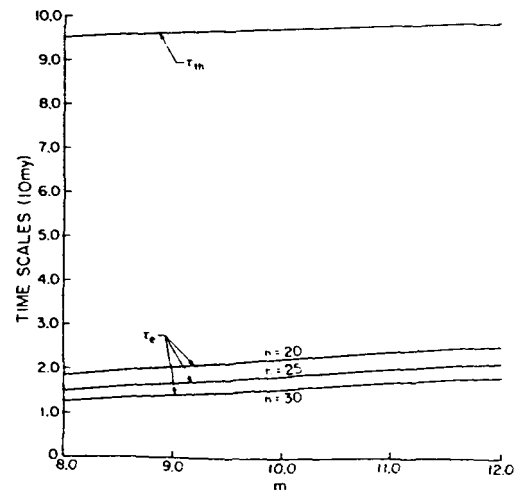


FIG. 6. τ_{th} and τ_e for the modified model with $\nu_{TM} = 10^{12} \text{ m}^2 \text{ sec}^{-1}$, $(Q/k)_0 = 10^4$, $(Q/k)_{\min} = 100$, $Q_j = 10^5$.

EPISODIC TIDAL HEATING OF IO

351

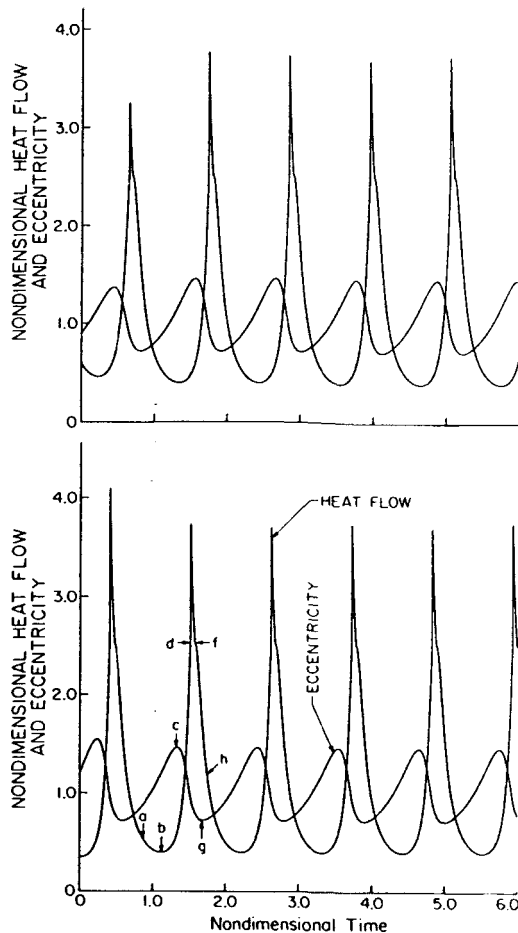


FIG. 7. Generic unstable case $(m,n) = (10,15)$ for two different combinations of initial temperature and eccentricity. The solutions are identical after decay of transients. Symbols are discussed in text.

initial conditions are shown. After the decay of transients, their behaviors are identical. Figure 8 shows the stable case $(m,n) = (10,11)$. More than 50 numerical integrations were performed representing numerous choices of the relevant parameters in the model. All unstable cases have post-transient behavior similar to the model in Fig. 7; e.g., the eccentricity maxima and minima always occur (respectively) before the maxima and minima in heatflow; initial peaks in heatflow are always sharp. These are, in fact, essential features of the episodic heating mechanism (see the Discus-

sion). Finally, Figs. 9a, 10a, and 11a demonstrate three examples in which reasonable choices of parameters relevant to Io produce curves which pass roughly through Io's current state of $e \sim 0.004$ and heatflow $\sim 1.0\text{--}2.0 \text{ W m}^{-2}$. The models predict that Io is volcanically active for periods of $\sim 10\text{--}30$ myr, separated by quiescent periods of ~ 60 to 200 myr. The values of all parameters used are listed in the appendix. For all three cases, Q_1 is $\geq 10^5$, above the limit from theoretical and orbital evolution considerations.

5. DISCUSSION

Consider the model shown in Fig. 7 as an example of the cycle shown in Fig. 1. At point (a) the convective heat loss is greater than \dot{E} and the satellite is cooling off. The eccentricity is increasing toward the equilibrium value, which is also increasing because of the decreasing temperature [see Eq. (4)]. \dot{E} is increasing as $e^2/(Q/k)$ [Eq. (2)], and becomes greater than the convective heat loss at point (b) causing the temperature to increase and Q/k to decrease. This causes the equilibrium eccentricity to decrease, and at point (c) it falls below the eccentricity. A thermal runaway is in progress and energy is drawn out of the orbit, decreasing the eccentricity. The satellite reaches the solidus at point (d) and remains at that temperature while volcanism and convection remove heat at a total rate equal to \dot{E} . \dot{E} drops below the convective heat loss (due to decreasing eccentricity) at point (f), and the temperature again begins to decrease. The resulting Q/k again causes the equilibrium eccentricity to increase, surpassing the eccentricity at point (g). When interpreting the plots, bear in mind that the heatflow mimics the internal temperature of the satellite, except between points (d) and (f) where the temperature is constant and the heatflow equals \dot{E} .

Note the discontinuity in slope at point (f). Inflections such as these are present on the decreasing sides of all of the heatflow plots presented. They occur at the points

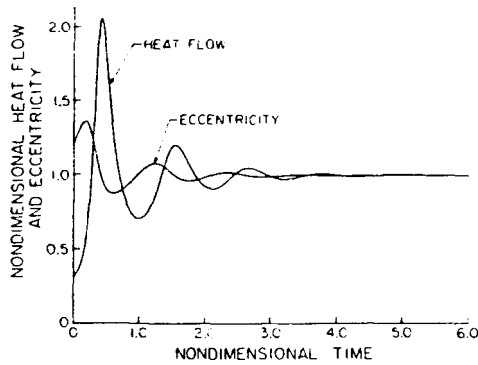


FIG. 8. Generic stable case $(m,n) = (10,11)$.

where the temperature begins to drop below the solidus. The value of heatflow at which this occurs is the convective loss throughout the period when $T = T_m$, and the volcanic component is simply the excess above this level during that period.

The values chosen for most of the parameters employed in the model are listed in the appendix. A range of values for $(Q/k)_0$, $(Q/k)_{\min}$, Q_j , and the kinematic viscosity at the solidus, ν_{TM} , were considered since these parameters are more poorly constrained. Values of $(Q/k)_0 \sim \text{few} \times 10^2/0.027$ and $(Q/k)_{\min} \sim (1-10)/0.027$ were chosen, with various values of $Q_j \geq 10^5$, consistent with known theoretical mechanisms as well as orbital evolution constraints. The solidus kinematic viscosity, ν_{TM} (i.e., the kinematic viscosity at a few percent partial melt), was assumed to lie in the range $10^{11}-10^{14} \text{ m}^2 \text{ sec}^{-1}$. These values are the best estimates given earlier in this paper.

The model can easily be adjusted to pass through the current orbital and thermal state of Io (heatflow $\sim 1-2 \text{ W m}^{-2}$ and $e \sim 0.004$) for parameter values in the above range. The value of $(Q/k)_{\min}$ is chosen that produces the required heatflow at the solidus when $e \sim 0.004$, using Eq. (2). During the periods of high heatflow the eccentricity typically drops from $\sim 1.1e_0$ to $\sim 0.6e_0$. By choosing a range for e_0 [Eq. (31)] such that $(0.6-1.1)e_0 \sim 0.004$, the model will pass through the required state during the peri-

ods of high heatflow. e_0 is in the required range for a wide region of the parameter space spanned by the above values of $(Q/k)_0$, $(Q/k)_{\min}$, Q_j , and ν_{TM} , with $8 \leq m \leq 12$ and $20 \leq n \leq 30$. Figures 9a, 10a, and 11a show three examples.

Nevertheless there are combinations that do not produce adequate models. For $\nu_{TM} \leq 10^{11} \text{ m}^2 \text{ sec}^{-1}$ and/or $Q_j \geq 10^6$ the characteristic temperature T_0 becomes low enough that the temperature dependence of Q/k at T_0 is too weak to allow unstable solutions in the desired range of m and n . For $\nu_{TM} \geq 10^{14} \text{ m}^2 \text{ sec}^{-1}$ the characteristic eccentricity, e_0 ,

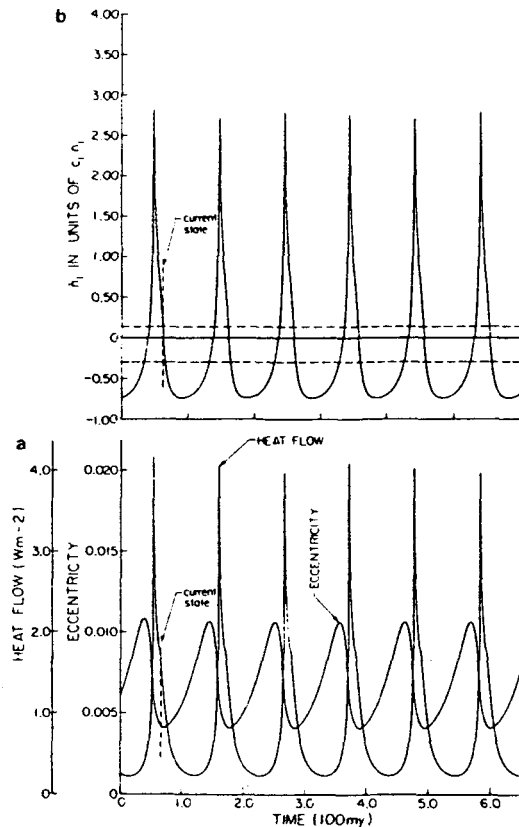


FIG. 9. Model I: $(m,n) = (10,20)$, $(Q/k)_0 = 100/0.027$, $(Q/k)_{\min} = 3/0.027$, $Q_j = 10^5$, $\nu_{TM} = 10^{12} \text{ m}^2 \text{ sec}^{-1}$. The model passes through Io's current state at the point shown. The value of n_1 is also shown, in units of $c_1 n_1 = 2.55 \times 10^{-22} \text{ sec}^{-2}$. Horizontal dashed lines show bounds on n_1 from eclipse data (Goldstein, 1975). Very recent observational estimates are considerably larger (see text).

EPISODIC TIDAL HEATING OF IO

353

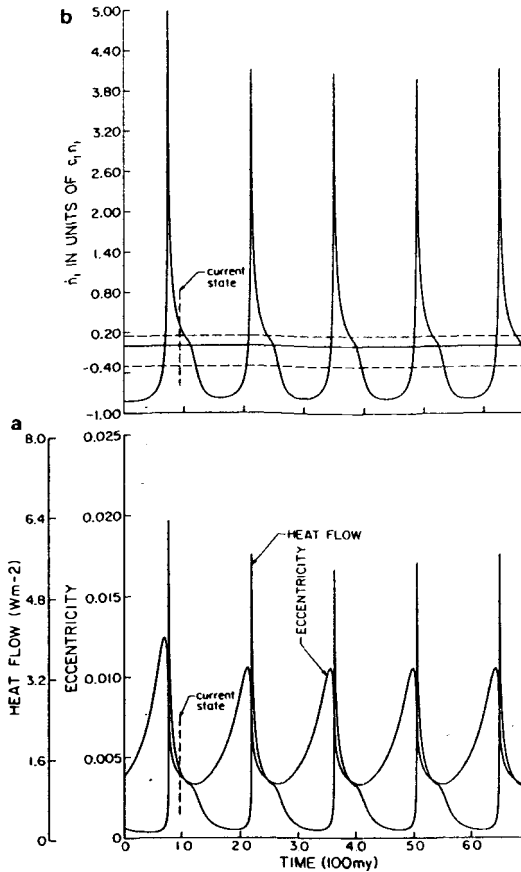


FIG. 10. Model II: $(m,n) = (12,25)$, $(Q/k)_0 = 200/0.027$, $(Q/k)_{\min} = 3/0.027$, $Q_J = 10^5$, $\nu_{TM} = 5 \times 10^{12} \text{ m}^2 \text{ sec}^{-1}$. Io's current state is shown. \dot{h}_1 is also shown as in Fig. 9. $c_1\eta_1 = 2.55 \times 10^{-22} \text{ sec}^{-2}$.

is too small to allow the model to pass through $e \sim 0.004$ during the periods of high heatflow, unless $Q_J \geq 10^6$. The reason is that higher viscosities require a higher characteristic temperature, T_0 , in order to relieve by convection the heat supplied by Jupiter (unless that supply is simultaneously reduced by increasing Q_J), and the resulting lower $(Q/k)(T_0)$ requires a lower e_0 in steady state. For $\nu_{TM} \approx 10^{13} \text{ m}^2 \text{ sec}^{-1}$, e_0 is too large for $m \leq 9$ and/or $n \geq 27$.

The model is most easily adjusted to pass through the current state during roughly the part of the cycle between the points marked (d) and (h) in Fig. 7, when the heatflow is decreasing and the eccentricity is either de-

creasing or is just beyond its minimum, since this region allows the largest acceptable range of e_0 . Models I and II are two such examples (see Figs. 9a and 10a). The parameters chosen are given in the captions. Note that $Q_J = 10^5$ in both cases. Periods of high heatflow ($\geq 1 \text{ W m}^{-2}$) for models I and II have durations of ~ 20 myr separated by quiescent periods of ~ 80 myr, and ~ 35 myr, separated by ~ 95 myr, respectively. Decreasing Q_J allows more energy into the system, increasing the periods of high heatflow. If the value of Q_J used in model II is reduced from 10^5 to 8×10^4 (still within the dynamical bounds), the periods of high heatflow increase from ~ 27 to

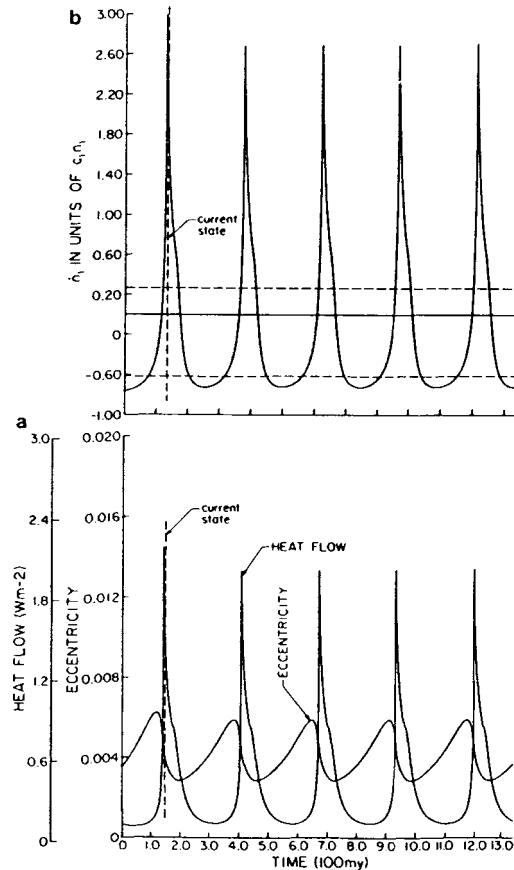


FIG. 11. Model III: $(m,n) = (12,20)$, $(Q/k)_0 = 100/0.027$, $(Q/k)_{\min} = 3/0.027$, $Q_J = 2 \times 10^5$, $\nu_{TM} = 10^{13} \text{ m}^2 \text{ sec}^{-1}$. Io's current state is shown. \dot{h}_1 is also shown. $c_1\eta_1 = 1.275 \times 10^{-22} \text{ sec}^{-2}$.

~38% of the total cycle. Increasing Q_1 to 10^6 is undesirable because it similarly reduces the high heatflow periods to $\leq 10\%$ of the total cycle. Model III (Fig. 11a) is an example which passes through the current state near its peak heatflow. $Q_1 = 2 \times 10^5$. In this case the heatflow is $\geq 1 \text{ W m}^{-2}$ for periods of ~30 myr separated by colder periods of ~200 myr duration.

Typically, $e \approx e_0$ when the heatflow is near its peak in the models. Hence, the magnitude of the peak heatflow can be crudely estimated by inserting $e = e_0$ and $(Q/k) = (Q/k)_{\text{min}}$ into Eq. (2) for \dot{E} . This yields a peak of $\sim 0.7(Q/k)T_0/(Q/k)T_m \text{ W m}^{-2}$. The peak eccentricity is limited by the equilibrium value, $1/\sqrt{13D_1}$ when $Q/k = (Q/k)_0$ [see Eq. (4)]. Note that the eccentricity for all models shown never exceeds the limit for stability of the resonance given by Yoder and Peale (Yoder and Peale, 1981).

An interesting prediction of the model is that Io's mean motion, n_1 , may currently be increasing rather than decreasing, as is usually assumed. Although n_1 must be on the average decreasing at the rate $\dot{n}_1 = -0.23c_1n_1$ (Yoder and Peale, 1981), Yoder's equation (65) implies that if Io's eccentricity exceeds ~1.36 times the equilibrium value, n_1 increases. For our purposes this equation can be written

$$\dot{n}_1 = -0.87c_1n_1(1 - 9.56D_1e_1^2). \quad (32)$$

The evolution of \dot{n}_1 from Eq. (32) is shown for models I–III in Figs. 9b, 10b, and 11b. The horizontal dashed lines show previous upper and lower bounds on \dot{n}_1 from estimates based on ~300 years of eclipse timings (Goldstein, 1975). Very recent reanalysis of the data (Goldstein and Jacobs, 1985) favors a large positive value for \dot{n}_1 of $\sim 7 \times 10^{-22} \text{ sec}^{-2}$. For model I, \dot{n}_1 is within Goldstein's (1975) bounds when the system passes through Io's current state. Model II exceeds the upper bound by a small amount during the relevant period, and model III exceeds the upper bound by a wide margin. Although models I–III predict a currently positive value for \dot{n}_1 ($\sim \text{few} \times 10^{-22}$ to

$\sim \text{few} \times 10^{-22} \text{ sec}^{-2}$), negative values are not disallowed. Note that the peak values of \dot{n}_1 for all three models are comparable to or greater than the large recent estimate ($\sim 7 \times 10^{-22} \text{ sec}^{-2}$) given by Goldstein and Jacobs. Cases could easily be found which pass through Io's current eccentricity and measured heatflow while \dot{n}_1 is as large as (or larger than) this most recent value, although such large values could admittedly only persist for a small fraction of the total period. Refined analysis of eclipse data may test our model.

The model of the coupled orbital and thermal evolution of Io presented in this paper is successful in that it allows orbital eccentricities of ~0.004 and heatflows of 1–2 W m^{-2} for part of the time, consistent with current observations. Although the details of the model are speculative, the essential elements that lead to episodic heatflow are well founded (most importantly, a strong inverse temperature dependence of the dissipation). The fact that models containing these characteristics can be easily chosen to pass through the current thermal and orbital state of Io for a range of acceptable parameter values is strong support for the plausibility of episodic heating of the satellite.

Nevertheless, the model has disadvantages. It requires that Io is currently in a state that only persists for 10 to 30% of the time. It also assumes homogeneity of the interior, while in fact large heterogeneities are probable, not only radially (dissipation may occur predominantly in an asthenospheric layer), but laterally as well. Nevertheless, the thermal runaway mechanism described in our model can operate equally well over a limited lateral length scale. If a local thermal instability is initiated within a single "convection cell," the likely result would be local volcanism since convection drives vertical heat transport more effectively than horizontal heat transport. If only part of the satellite participates in the heating the effective Love number, k , is less liable to significantly exceed the elastic

EPISODIC TIDAL HEATING OF IO

355

value due to the rigidity of the cold regions acting as a rigid "frame." The possible presence of a number of distinct coupled regions capable of local thermal runaways would certainly result in a more complicated evolution for Io.

Although the tidal Q of Io is expected to be a strong inverse function of temperature from both theory and experiment, existing viscoelastic theory is largely phenomenological (detailed microscopic descriptions do not yet exist), and data for Q at tidal frequencies is lacking.

Another consequence of the episodic model is that Europa's tidal stresses would have been greater in the past, since the cyclical tidal stress varies as the eccentricity, and the eccentricity of Europa (and Ganymede) mimics variations in Io's eccentricity (Yoder and Peale, 1981). Current cyclical tidal stresses on Europa are <10 bar. The tensile strength of ice is ~ 10 – 20 bar somewhat below its melting point. The consequences of the episodic model for Europa's history deserve study.

Tidal heating is probably also responsible for the resurfacing of Saturn's moon Enceladus $\sim 10^8$ to 10^9 years ago (Smith *et al.*, 1982), because Enceladus is in a 2:1 orbital resonance with Dione, similar to the 2:1 resonance of Io with Europa. However, Squyres *et al.* (1983) estimate that tidal heating must exceed $\sim 2.5 \times 10^{10}$ W to initiate melting, and that the current heating rate probably cannot exceed $\sim 6 \times 10^7$ W. If the satellite has a substantial NH_3 – H_2O component, the tidal heating required to initiate melting is a few times smaller than the Squyres estimate (Stevenson, 1982). Yoder (1981) has suggested that the tidal

heating of Enceladus may be episodic due to the inverse dependence of Q on tidal stress, and that dissipation rates large enough to cause melting are possible if energy is built up in Enceladus' orbit over $\sim 10^8$ years and then deposited due to a reduction in Q during periods of $\lesssim 10^6$ -years duration. The model presented in this paper can produce a similar phenomenon due to the temperature dependence of Q . Assuming that a heating rate of $\sim 10^{10}$ W is required to initiate a thermal runaway, the required eccentricity is $\sim \text{few} \times 0.01$ and can be attained every $\sim 10^8$ years if $Q(\text{low } T) \geq \text{few} \times 10^2$, $Q(T_m) \sim 1$ – 10 , and $Q_{\text{Saturn}} \sim \text{few} \times 10^4$. A longer eccentricity-building time and higher low-temperature Q are required if Q_{Saturn} is larger. The recent resurfacing of the satellite can be explained since all that is required is that a "spike" in heatflow has occurred at some time $< 10^9$ years ago. However, Enceladus is probably the source of the material in Saturn's E ring, which must be resupplied on a time scale of 10^2 to 10^4 years (Cheng *et al.*, 1982). It should be emphasized that although the episodic model can produce high heatflows for limited periods of time, the average dissipation rate is unchanged; the energy available from the orbital evolution of Enceladus must be supplied in "bursts" amounting to $\lesssim 1\%$ of the total time. The recent replenishment of material in the E ring, probably by volcanic activity (Herkenhoff and Stevenson, 1984, and in preparation) argues for large lateral heterogeneities of tidal heating, but a quantitative demonstration of the sufficiency of tidal heating is lacking.

APPENDIX: LIST OF SYMBOLS

a_i Semimajor axis of i th satellite
 A equation (30)
 c_i $\frac{9}{2} \left(\frac{R_j}{a_i} \right)^5 \left(\frac{M_i}{M_j} \right) n_i \left(\frac{k_j}{Q_j} \right)$

$a_1 = 4.22 \times 10^8 \text{ m}$

C_p	Specific heat	$800 \text{ J kg}^{-1} \text{ }^\circ\text{K}^{-1}$
C_Q	$\left(\frac{Q}{k}\right)_{\min} T_m^n$	
C	$\nu(T_m)T_m^L$	$\nu_{TM} (1400)^L \text{ m}^2 \text{ }^\circ\text{K}^L \text{ sec}^{-1}$
C_1	A function of α	-1.18
d	Depth of convecting layer, assumed $\sim R$	
D_i	Equation (4)	
e_{eq}	Equilibrium forced eccentricity of Io, $(13D)^{-1/2}$	
e_i	Forced eccentricity of i th satellite	
e_N	Rescaled forced eccentricity e/e_0	
e_0	Forced eccentricity of time-independent solution	
E_T	Tidal dissipation rate, W	
$f(T)$	Equation (29)	
g	Surface gravity of Io	1.8 m sec^{-2}
G	Gravitational constant	$6.67 \times 10^{-11} \text{ NM}^2 \text{ kg}^{-2}$
k_i	Second-degree tidal potential Love number of i th satellite	
k_J	Second-degree tidal potential Love number of Jupiter	0.5
L	$-d \ln \nu / d \ln T$	
m	Power law exponent for convective heatflow	$(4 + L)/3$
M_i	Mass of i th satellite	$M_1 = 8.9 \times 10^{22} \text{ kg},$ $M_2 = 4.9 \times 10^{22} \text{ kg}$
M_J	Mass of Jupiter	$1.9 \times 10^{27} \text{ kg}$
n_i	Mean motion of i th satellite	$n_1 = 4.1 \times 10^{-5} \text{ sec}^{-1},$ $n_2 = 2.0 \times 10^{-5} \text{ sec}^{-1}$
\bar{n}_1	Average acceleration of Io's mean motion	
n	Power law exponent for tidal dissipation	
P	Ratio of time scales τ_{th}/τ_c	
Q_i	Quality factor of i th satellite	
Q_J	Quality factor of Jupiter	
$(Q/k)_0$	Low-temperature value of (Q/k)	
$(Q/k)_{\min}$	Minimum value of (Q/k) , assumed to occur at solidus	
R_i	Radius of i th satellite	$R_1 = 1.82 \times 10^6 \text{ m}$
R_J	Radius of Jupiter	$7.2 \times 10^7 \text{ m}$
Ra_c	Critical Rayleigh number	800
t	Time	
t_N	Nondimensional time t/τ_{th}	
T	Temperature of adiabatic interior	
T_m	Temperature of mantle solidus	1400°K
T_N	Nondimensional temperature T/T_0	
T_0	Temperature of time-independent solution	
α	Semimajor axis ratio. a_i/a_{i+1}	0.63
α_T	Thermal expansion coefficient	$3 \times 10^{-5} \text{ }^\circ\text{K}^{-1}$
ϵ_e, ϵ_T	Defined in Eq. (23)	
η	Dynamic viscosity	
K	Thermal diffusivity	$10^{-6} \text{ m}^2 \text{ sec}^{-1}$
λ_i	Mean longitude of i th satellite	

EPISODIC TIDAL HEATING OF IO

357

μ	Rigidity	6.5×10^{10} Pa
$\bar{\mu}$	$19\mu/2\rho gR$	54
ν	Kinematic viscosity	
ν_{TM}	Kinematic viscosity at solidus (~few percent partial melt)	
ν_{11}	$n_1 - 2n_2 + \dot{\omega}_{1s}$	
ρ	Density of Io	3.5×10^3 kg m ⁻³
τ_e	Time scale for equilibration of e , Eq. (20)	
τ_M	Maxwell time η/μ	
τ_{th}	Convective cooling time scale	
τ_*	$1/(m + p - n)$	
ϕ	$\lambda_1 - 3\lambda_2 + 2\lambda_3$	
ω	Forcing frequency	
ω_0	$(pm)^{1/2}$	
$\dot{\omega}_{1s}$	Secular rate of change of Io's argument of pericenter	

ACKNOWLEDGMENTS

This work is supported by NASA Grant NAGW-185 of the Planetary Geophysics program. The second author acknowledges useful conversations with C. F. Yoder early in the development of this work. We also acknowledge helpful reviews and comments from M. Ross and G. Schubert.

REFERENCES

- ANDERSON, D. L. (1967). The anelasticity of the mantle. *Geophys. J.R. Astron. Soc.* **14**, 135–164.
- CHENG, A. F., L. J. LANZEROTTI, AND V. PIRONELLO (1982). Charged particle sputtering of the ice surfaces in Saturn's magnetosphere. *J. Geophys. Res.* **87**, 4567–4570.
- COOPER, R. F., AND D. L. KOHLSTEDT (1984). Solution-precipitation enhanced diffusional creep of partially molten olivine-basalt aggregates during hot pressing. *Tectonophysics* **107**, 207–233.
- ETRICH, F.R. (1956). *Rheology: Theory and Applications*, Vol. 1. Academic Press, New York.
- FINNERTY, A. A., G. A. RANSFORD, D. C. PIERI, AND K. D. COLLERSON (1980). Is Europa's surface cracking due to thermal evolution? *Nature* **289**, 24–27.
- GOLDREICH, P., AND S. SOTER (1966). Q in the Solar System. *Icarus* **5**, 375–389.
- GOLDSTEIN, S. J., JR. (1975). On the secular change in the period of Io, 1668–1926. *Astron. J.* **80**, 532–539.
- GOLDSTEIN, S. J., JR., AND K. C. JACOBS (1985). The contraction of Io's orbit. *Bull. Amer. Astron. Soc.* **17**, 873.
- GREENBERG, R. (1982). Orbital evolution of the Galilean satellites. In *Satellites of Jupiter* (D. Morrison, Ed.), pp. 65–92. Univ. of Arizona Press, Tucson.
- HERKENHOFF, K. E., AND D. J. STEVENSON (1984). Formation of Saturn's E-ring by evaporation of liquid from the surface of Enceladus. *Lunar Planet. Sci. XV*, 361–362.
- JOHNSON, T. V., D. MORRISON, D. L. MATSON, G. J. VEEDER, R. H. BROWN, AND R. M. NELSON (1984). Io volcanic hotspots: Stability and longitudinal distribution. *Science* **226**, 134–137.
- KAULA, W. M. (1964). Tidal dissipation by solid friction and the resulting orbital evolution. *Rev. Geophys.* **2**, 661–685.
- KNOPOFF, L. (1964). *Q. Rev. Geophys.* **2**, 625–660.
- LAMBECK, K., AND S. M. NAKIBOGLU (1983). Long-period Love numbers and their frequency dependence due to dispersion effects. *Geophys. Res. Lett.* **10**, 857–860.
- MATSON, D. K., G. A. RANSFORD, AND T. V. JOHNSON (1980). Heat flow from Io. *Lunar Planet. Sci. XI*, 686–687.
- MAVKO, G. M. (1980). Velocity and attenuation in partially molten rocks. *J. Geophys. Res.* **85**, 5173–5189.
- MCKENZIE, D. P. (1984). The generation and compaction of partial melts. *J. Petrology* **25**, 713–765.
- MURASE, T., AND A. R. MCBIRNEY (1973). Properties of some common igneous rocks and their melts at high temperatures. *Geol. Soc. Amer. Bull.* **84**, 3563–3592.
- O'REILLY, T. C., AND G. F. DAVIES (1981). Magma heat transport on Io: A mechanism allowing a thick lithosphere. *Geophys. Res. Lett.* **8**, 313–316.
- OXBURGH, E. R., AND D. L. TURCOTTE (1978). Mechanisms of continental drift. *Rep. Progr. Phys.* **41**, 1249–1312.
- PEALE, S. J., AND P. CASSEN (1978). Contribution of tidal dissipation to lunar thermal history. *Icarus* **36**, 245–269.
- PEALE, S. J., P. CASSEN, AND R. T. REYNOLDS (1979). Melting of Io by tidal dissipation. *Science* **203**, 892–894.
- PEALE, S. J., P. CASSEN, AND R. T. REYNOLDS (1982). Structure and thermal evolution of the Galilean sat-

- ellites. In *Satellites of Jupiter* (D. Morrison, Ed.), pp. 93-128. Univ. of Arizona Press, Tucson.
- PEARL, J. C., AND W. M. SINTON (1982). Hot spots of Io. In *Satellites of Jupiter* (D. Morrison, Ed.), pp. 720-755. Univ. of Arizona Press, Tucson.
- POLLACK, J. B. (1977). Phobos and Deimos. In *Planetary Satellites* (J. A. Burns, Ed.), pp. 319-345. Univ. of Arizona Press, Tucson.
- ROSS, M., AND G. SCHUBERT (1985). Tidally forced viscous heating in a partially molten Io. *Icarus* **64**, 391-400.
- ROULT, G. (1975). Attenuation of seismic waves of very low frequency. *Phys. Earth Planet. Inter.* **10**, 159-166.
- SACKS, I. S., AND T. MURASE (1983). *The Anelasticity of Peridotite and Partial Melt in the Asthenosphere*. Dept. Terrestrial Mag. Ann. Rep. 1982-1983. Reprinted from *Carnegie Institution of Washington Year Book* **82**, pp. 509-512. Washington, D.C.
- SCHUBERT, G., P. CASSEN, AND R. E. YOUNG (1979). Subsolidus convective cooling histories of terrestrial planets. *Icarus* **38**, 192-211.
- SCHUBERT, G., T. SPOHN, AND R. T. REYNOLDS (1986). Thermal histories, compositions and internal structures of the moons in the Solar System. In *Natural Satellites* (D. Morrison and J. Burns, Eds.). Univ. of Arizona Press, Tucson, in press.
- SCHUBERT, G., D. J. STEVENSON, AND K. ELLSWORTH (1981). Internal structures of the Galilean satellites. *Icarus* **47**, 46-59.
- SCOTT, D., AND D. J. STEVENSON (1985). Magma Ascent by Porous Flow. *J. Geophys. Res.*, submitted.
- SHAW, H. R. (1969). Rheology of basalt in the melting range. *J. Petrol.* **10**, 510-535.
- SINTON, W. M. (1981). The thermal emission spectrum of Io and a determination of the heat flux from its hot spots. *J. Geophys. Res.* **86**, 3122-3128.
- SMITH, B. A., L. A. SODERBLOM, R. BATSON, P. BRIDGES, J. INGE, H. MASURSKY, E. M. SHOEMAKER, R. F. BEEBE, J. BOYCE, G. A. BRIGGS, A. BUNKER, S. A. COLLINS, C. J. HANSEN, T. V. JOHNSON, J. L. MITCHELL, R. J. TERRILE, A. F. COOK, J. CUZZI, J. B. POLLACK, G. E. DANIELSON, A. P. INGERSOLL, M. E. DAVIES, G. E. HUNT, D. MORRISON, T. OWEN, C. SAGAN, J. VEVERKA, R. G. STROM, AND V. E. SUOMI (1982). A new look at the Saturn system: The Voyager 2 images. *Science* **215**, 504-537.
- SOUYRES, S. W., R. T. REYNOLDS, AND P. M. CASSEN (1983). The evolution of Enceladus. *Icarus* **53**, 319-331.
- STEVENSON, D. J. (1982). Volcanism and igneous processes in small icy satellites. *Nature* **298**, 142-144.
- STEVENSON, D. J. (1983). Anomalous bulk viscosity of two-phase fluids and implications for planetary interiors. *J. Geophys. Res.* **88**, 2445-2455.
- TURCOTTE, D. L. (1982). Magma migration. *Annu. Rev. Earth Planet. Sci.* **10**, 397-408.
- TURCOTTE, D. L., AND G. SCHUBERT (1982). *Geodynamics*. Wiley, New York.
- YODER, C. F. (1979). How tidal heating in Io drives the Galilean orbital resonance locks. *Nature* **279**, 767-770.
- YODER, C. F. (1981). Tidal friction and Enceladus' anomalous surface. *EOS* **62**, 939.
- YODER, C. F., AND S. J. PEALE (1981). The tides of Io. *Icarus* **47**, 1-35.

Update

Since the publication of the preceding paper, additional relevant work has been published. New estimations of IR heatflux from Io are again near 2 Wm^{-2} (McEwen et al., 1985). Greenberg et al. (1986) demonstrated that the large positive value of \dot{n}_1 derived by Goldstein and Jacobs (1985, 1986) was consistent with the IR heat flux in the absence of any significant torque from the tidal bulge raised on Jupiter by Io (i.e., $\frac{1}{Q_J} \approx 0$), thus lending support to his suggestion (Greenberg, 1982) that the satellites may be evolving outward from a state of primordial deep resonance. In addition support of this conjecture, he also demonstrated that the resonance is, in fact, stable at values of ν_{11} much smaller than Yoder and Peale had claimed (Yoder and Peale, 1981), but that the stable states involve equilibrium values of ϕ different from 180° (Greenberg, 1987a).

However, Greenberg subsequently showed that Goldstein and Jacobs' estimate of \dot{n}_1 was flawed due to their use of an incorrect radius for Jupiter, aliasing, and clock-correction problems (Greenberg, 1987b). A more reliable estimate of \dot{n}_1 was made by Lieske (1987) using apparently more complete and accurate methods of data reduction, as well as a considerably larger data set. He found $\frac{\dot{n}_1}{n} = (-7.4 \pm 8.7) \times 10^{-12} \text{ yr}^{-1}$ (or $\dot{n}_1 = (-9.6 \pm 11.1) \times 10^{-24} \text{ s}^{-1}$). As Greenberg (1987b) demonstrates, this value, although negative, is an order of magnitude too small to give consistency with Yoder's (1981) equilibrium hypothesis ($\dot{\nu}_{11} = 0$). Using the measured IR flux to estimate the parameter D_1 together with the above estimate of \dot{n}_1 , gives $\dot{\nu}_{11} > 0$, which suggests that the system is currently evolving out of resonance (toward smaller eccentricities). For $Q_J = 10^5$, our model gives $\dot{\nu}_{11} \approx 2.4 \times 10^{-23} \text{ s}^{-1}$, for example. Thus it would appear that the system is currently dominated by dissipation in Io rather than by dissipation in Jupiter.

However, Lieske has also derived $\dot{\nu}_{11}$ directly, using his measurements of both \dot{n}_1 and \dot{n}_2 ($\frac{\dot{\nu}_{11}}{\dot{n}_1} < 0.5 \times 10^{-11} \text{ yr}^{-1}$ or $\dot{\nu}_{11} < 6 \times 10^{-24} \text{ s}^{-2}$). Greenberg (1987b) suggests that this inconsistency would be rectified if Io has been very near equilibrium ($\dot{\nu}_{11} \approx 0$) during the past ~ 300 years (the time span over which the eclipse data were taken) but that Io's thermal activity has increased by an order of magnitude within the last few decades, perhaps due to a temporary storage and release of pent-up heat.

These new results are easily accommodated by the episodic heating model for Io that is present here. Inspection of Figures 9a, 10a, and 11a reveal that the time rate of change of \dot{n}_1 is typically very large (and negative) in the region of the curves marked "current state." Slight adjustments of model parameters would therefore undoubtedly produce cases which approximately pass through Io's current heatflow and orbital eccentricity at a time when \dot{n}_1 is equal to Lieske's calculated value.

Additional References

- Goldstein, S.J. and Jacobs, K.C. (1986). The contraction of Io's orbit. *Astron. J.* **92**, 199–202.
- Greenberg, R. (1987a). Galilean satellites: Evolutionary paths in deep resonance. *Icarus* **70**, 334–347.
- Greenberg, R. (1987b). Time-varying orbits and tidal heating of the Galilean satellites. Paper presented at the *International Workshop on Time-Variable Phenomena in the Jovian Systems*, at Flagstaff, Arizona.
- Greenberg, R., Goldstein, S.J., and Jacobs, K.C. (1986). Orbital acceleration and the energy budget in the Galilean satellite system. *Nature* **323**, 789–791.
- Lieske, J.H. (1987). Galilean satellite evolution: Observational evidence for secular changes in mean motions. *Astron. Astrophys.* **176**, 146–158.
- McEwen, A.S., Matson, D.L., Johnson, T.V., and Soderblom, L.A. (1985). Volcanic hot spots on Io: Correlation with low-albedo calderas. *J. Geophys. Res.* **90**, 12345–12379.

PAPER II**Thermal State of an Ice Shell on Europa**

Thermal State of an Ice Shell on Europa

Gregory W. Ojakangas and David J. Stevenson

Division of Geological and Planetary Sciences

California Institute of Technology

Pasadena, California 91125

Submitted to: *Icarus*

May, 1988

Contribution number 4519 from the Division of Geological and Planetary Sciences,
California Institute of Technology, Pasadena, California 91125.

Abstract

We consider a model of Europa consisting of an ice shell that is decoupled from a silicate core by a layer of liquid water. The thickness of the shell is calculated as a function of colatitude and longitude, assuming that a state of conductive equilibrium exists with the incident annual average solar insolation, tidal dissipation within the shell, and heat flow from the core. Ice thickness profiles are calculated for each of two plausible rheological behaviors for ice: the Maxwell rheology and the generalized flow law rheology. In both cases the strong temperature-dependence of the dissipation rate is explicitly included as well as the temperature-dependence of the thermal conductivity of ice. Because of the strong temperature dependence of the dissipation rate, nearly all of the tidal dissipation is concentrated in the lowermost few kilometers of the shell. Even though the effective Q of the greater part of the shell is $\gg 100$ in our models, average shell thicknesses do not exceed 25 km. Thus, if the total thickness of H_2O which mantles Europa is ≥ 25 km, none of the models admit the possibility of a completely frozen H_2O layer. The total dissipation rates in our models are comparable to those of a constant Q model with $Q \sim 10$. The thickness profiles are relatively insensitive to heat flow from the core. The second degree spherical harmonic components of the ice thickness are given and the resulting contributions to the quantities $\frac{B-A}{C}$ and $\frac{B-C}{A}$ of Europa are estimated. Although the contribution to $\frac{B-A}{C}$ is perhaps larger than the permanent value needed to prevent nonsynchronous rotation, its dependence on the shell's orientation relative to synchronicity suggests that very slow nonsynchronous rotation will persist, with reorientation of the shell relative to the satellite-planet direction occurring on a timescale \geq the thermal diffusion timescale for the shell ($\sim 10^7$ yr). The existence of a significant "fossil" bulge on the shell due to long-term

elastic behavior of its outer, coldest regions would eliminate nonsynchronous rotation. Since the contribution to $(\frac{B-C}{A})$ of the thickness variations in most of our models is > 0 , Europa may experience polar wander as thermal equilibrium is approached, if the above is the most important permanent contribution to $(\frac{B-C}{A})$. The magnitudes of the principal moment differences are insensitive to the details of the parameterization of the tidal dissipation.

1. Introduction

The structure and composition of the outer regions of Europa's interior have been the subject of considerable debate (cf. Cassen et al., 1982). Water ice is known from spectroscopic studies to be present on its surface (cf. Pilcher et al., 1972), and the lack of substantial topographic relief or large impact craters supports the conjecture that the satellite is covered with a considerable mantle of water, concealing topography on the underlying silicates and capable of viscous relaxation on geologic timescales (Thomas and Schubert, 1987). Models of the formation of the Galilean satellites in orbit about a warm proto-Jupiter suggest that water should be increasingly abundant at increasing orbital radius (Consolmagno and Lewis, 1976), a prediction consistent with the observed densities of the satellites.

Cassen et al. (1982) pointed out that if Europa were differentiated, its mean density (3.03 g cm^{-3}) is consistent with a rocky core of Io's mean density (3.55 g cm^{-3}) overlain by ~ 120 km of water. Conversely, Europa may have retained its water in hydrated silicates, and its water layer may be only a few km thick. However, the paucity of impact craters as well as the abundance of crack-like lineaments on Europa's surface suggests that liquid water exists at depth, decoupling an outer shell of ice from the rocky core, allowing for much greater tidal response and stresses within the ice leading to fractures, and providing a source of liquid water to resurface the satellite.

A generally accepted value for the quality factor Q of solids at low frequencies and well below the melting point is ~ 100 (cf. Smith and Born, 1976). Previous attempts to evaluate the thickness of an ice shell in thermal equilibrium with tidal dissipation within it and heat flow from the core, have assumed a constant dissipation rate (i.e., constant Q) throughout the shell (cf. Squyres et al., 1983; Cassen et

al., 1982). Such models have predicted that a layer of liquid water would persist beneath the ice only if the effective Q of the ice is low ($\lesssim 70$) and a large tidal heat flow from the core is present, requiring a low quality factor for the core ($Q_{\text{core}} \lesssim 25$).

The criterion for a stable liquid layer was shown to be even more stringent by Ross and Schubert (1987), who found that the cyclic tidal strains in the shell are about a factor of two smaller than was previously believed, because the self-potential of the tidal bulge is dominated by low density ice, rather than rock as had been tacitly assumed. They found that a liquid layer is stable only when either or both Q_{core} and Q_{shell} are less than ~ 30 , even when they include an insulating regolith at the surface which enhances the near-surface temperature by 40 K.

Although data at tidal frequencies are sparse, there is much evidence from both theory and experiment that dissipation rates in solids are very strongly temperature-dependent, increasing dramatically as the melting point is approached. Q for silicates near the melting point drops to $\lesssim 10$ (Murase and McBirney, 1973). Data for near-solidus peridotites at high frequencies (Sacks and Murase, 1983) give $20 < \frac{-d \ln Q}{d \ln T} < 30$ near the melting point (Ojakangas and Stevenson, 1986). Q in polycrystalline ice at high frequencies (~ 300 – 500 Hz) is a complicated function of temperature (cf. Hobbs, 1974) due to the importance of a number of relaxation mechanisms. However, the contribution of any relaxation mechanism to the dissipation rate peaks when the forcing frequency is near the reciprocal of the relaxation time for the mechanism. The relaxation mechanisms that operate at high frequencies have relaxation times of $\sim 10^{-2}$ to 10^{-4} sec, far from the tidal frequency of $\sim 10^5$ sec. We can therefore expect them to be unimportant at the tidal frequency. The relevant relaxation time for a simple viscoelastic medium is the Maxwell time $\tau_M = \frac{\eta}{\mu}$, where η is the dynamic viscosity and μ is the rigidity. Since μ for poly-

crystalline ice is in the range of $1.1 \times 10^9 - 4 \times 10^{10}$ dynes cm^{-2} and $\eta \gtrsim 10^{14}$ Poise near the melting point (cf. Hobbs, 1974), τ_M is near the tidal forcing period (~ 3 days) for the ice near the base of the ice shell on Europa. It is therefore likely that at tidal frequencies the important relaxation mechanism that contributes to the effective Q is viscous creep. This differs from terrestrial planets where the tidal period is much less than the Maxwell time. As we shall see in Section 3, the dissipation rate (and hence the effective Q) in a Maxwell medium is very strongly dependent on temperature, because of the strong temperature-dependence of the viscosity η .

Shear stresses in a decoupled shell on Europa due to tidal forcing are on the order of a few bars. This is in a range in which laboratory experimentation indicates that ice behaves according to a Glen flow law (see Section 4). As is shown in Section 4, the dissipation rate (and hence the effective value of $\frac{1}{Q}$) for such a medium is also a very strongly increasing function of temperature. The probable low value of Q near the melting point of ice was assumed to be insignificant by Ross and Schubert (1987) on the basis that only a small fraction of the shell is at such temperatures. However, as we shall show, the relative importance of local dissipation rates on ice thickness is not equal at all depths, but is strongly weighted toward the base of the ice, where dissipation is probably dramatically greater than the average. We demonstrate here that approximating Q by a constant leads to overestimates of equilibrium shell thickness.

For shell thicknesses greater than 30 km, Squyres et al. (1983) contend that subsolidus convection will occur within the ice, and freezing of a liquid layer is inevitable. In the models presented here, nonuniform tidal heating with depth is explicitly included, and we find that average shell thicknesses of less than 30 km

are readily achieved when plausible forms for the dependence of dissipation on temperature are assumed. We thus claim that an insulating regolith and a large core heat flow, though they may be present, are not required for stability of a water ocean and decoupled shell on Europa.

In the following section, we develop a general equation for ice thickness as a function of surface temperature, local tidal strain rates, the variation of the dissipation rate with depth, and the temperature-dependence of the thermal conductivity of ice. Then in Sections 3 and 4 we calculate dissipation rates for two possible rheological laws for ice: that of a Maxwell body, and that of a medium which behaves according to a generalized Glen flow law. The resulting ice thickness profiles are given in each case. For ease of presentation, calculations of surface temperature and tidal strain rates in a thin shell overlying a hydrostatic ocean on a synchronously rotating satellite are confined to Appendices A and B, respectively.

Finally, we discuss the importance of the derived thickness profiles in the question of the existence of a decoupled shell, as well as nonsynchronous rotation and polar wander of Europa.

2. Thickness of an Ice Shell in Conductive Equilibrium

In a shell with a thickness of 25 km on Europa, vertical temperature gradients are at least 10^2 times larger than horizontal temperature gradients. Horizontal transport of heat may therefore be neglected, and the equilibrium temperature profile is everywhere determined, to a good approximation, by the solution of the one-dimensional time-independent thermal diffusion equation:

$$\frac{d}{dz} \left(k \frac{dT}{dz} \right) = -q \quad , \quad (2.1)$$

where z is depth below the surface, k is the thermal conductivity, and q is the volumetric dissipation rate,

The equilibrium thickness of an ice shell overlying a liquid water ocean on Europa is obtained by solving (2.1) with the appropriate conditions. The boundary conditions are that the temperature at the surface, $T(o)$, is equal to the local surface temperature T_s , as dictated by radiative equilibrium with the annual average solar insolation, the temperature at the base of the ice $T(b)$, is fixed at the melting temperature of Ice I, $T(b) = 273$ K, and that the heat flux, H , flowing from the interior is related to the basal temperature gradient by

$$H = k \left. \frac{dT}{dz} \right|_{z=b} \quad (2.2)$$

The thermal conductivity of polycrystalline ice is well approximated by the form:

$$k(T) = \frac{a_1}{T} + a_0 \quad (2.3)$$

$$a_1 \sim 4.88 \times 10^7 \frac{\text{erg}}{\text{cm s}}$$

$$a_0 \sim 4.68 \times 10^4 \frac{\text{erg}}{\text{cm K}^{-1} \text{s}}$$

(Hobbs, 1974), where T is the absolute temperature. At temperatures well below $\sim 10^3$ K, the constant a_0 may be neglected. Using this approximation, Equation (2.1) may be written

$$\frac{d^2 y}{dz^2} = \left(\frac{dy}{dz} \right) \frac{d}{dy} \left(\frac{dy}{dz} \right) = \frac{-q(T)}{a_1} \quad , \quad (2.4)$$

where

$$y \equiv \ln T \quad .$$

Integrating Equation (2.4) once with respect to y from the surface where $T = T_s$ to the base of the ice, where $T = T_M$, the equation

$$\left(\frac{dy}{dz}\right)_{T=T_s}^2 = \frac{2}{a_1} \int_{T=T_s}^{T=T_M} \frac{q(T) dT}{T} + \left(\frac{dy}{dz}\right)_{T=T_M}^2 \quad (2.5)$$

is obtained.

In the following two sections, we will give reasonable parameterizations of $q(T)$, which are consistent with theory and experiment. In all cases, $q(T)$ is a very strongly increasing function of temperature. Note in Equation (2.4) that the magnitude of $q(T)$ is proportional to the curvature of the profile $y(z)$. In the limit where $q(T)$ is a sufficiently strong function of temperature, it is evident that the curvature near the base of the ice is responsible for most of the temperature gradient throughout the ice, so that to a reasonable approximation,

$$\int_{T_s}^{T_M} \frac{q(T) dT}{T} \approx \int_0^{T_M} \frac{q(T) dT}{T}, \quad (2.6)$$

and the gradient of y is nearly constant through the majority of the shell. Thus,

$$\left(\frac{dy}{dz}\right)_{z=0} \approx \frac{y(T_M) - y(T_s)}{b} = \frac{\ln(T_M/T_s)}{b}. \quad (2.7)$$

Equations (2.2), (2.5), (2.6), and (2.7) then give

$$b \approx \frac{\ln(T_M/T_s)}{\left[\left(\frac{2}{a_1}\right) \int_0^{T_M} \frac{q(T) dT}{T} + \left(\frac{H}{a_1}\right)^2\right]^{1/2}}. \quad (2.8)$$

We shall use Equation (2.8) to estimate the thickness of an ice shell on Europa for various possible rheologies of ice.

It is easy to see that for a given temperature difference between the surface and the base of the shell, its thickness depends on the distribution of the dissipation

with depth. If the dissipation is homogeneously distributed, for example, the profile of $\ln T$ with depth is parabolic, reaching its maximum slope at the upper surface of the ice. If, by contrast, the same total dissipation is concentrated in a thin layer near the base of the shell, the same maximum slope is attained at the upper surface of the dissipative layer, and persists throughout the overlying ice. Thus the average slope is greater throughout the shell, and the required temperature difference across it is achieved with a smaller total thickness. This is analogous to the argument frequently made for a thicker lithosphere in continental regions than in oceanic regions on Earth, even for places where the surface heat flows are equal. The development leading to Equation (2.8) is exemplary of the case of heating from below rather than within because of the assumed temperature dependence of the dissipation.

In order to evaluate shell thickness profiles using equation (2.8), it is necessary to know the surface temperature, T_s , the integral of the dissipation given by Equation (2.6), and the heat flowing from the core at each latitude and longitude. In Appendix A, functions giving approximate values for the average solar insolation and the resulting surface temperature as a function of colatitude on Europa are derived. In Appendix B, the cyclical tidal strains experienced by a thin incompressible elastic shell overlying a fluid synchronously rotating satellite in an elliptical orbit are derived, following the development of Peale and Cassen (1978). As is discussed in Appendix B, when the thickness of such a shell is small, the strains become independent of the rheology of the shell material, so that the strains derived for an elastic shell may be applied to an arbitrary rheology. (This is intuitively reasonable since a very thin shell must assume the hydrostatic figure of the underlying fluid planet.) We will apply the results of Appendix B in calculating the dissipation

integral, Equation (2.6), for both of the rheologies discussed below.

The heat flux from the core may vary with latitude and longitude as well, thus affecting the thickness profile of the shell. However, the nature of such variations remains unsolved, and we will assume that any heat incident upon the shell from below is uniformly distributed. This problem is addressed further in the section labeled *Discussion*.

3. The Maxwell Rheology

The two simplest phenomenological models that attempt to describe the behavior of materials which possess the characteristics of both elastic and viscous media are the Kelvin–Voigt body and the Maxwell body (cf. Eirich, 1956). The Kelvin–Voigt and Maxwell bodies are visually represented by a spring and a dashpot arranged in parallel and in series, respectively. Of the two models, the Maxwell body more effectively reproduces the response of many real materials to imposed cyclic strains while the Kelvin–Voigt body usually does not. In particular, the Maxwell body behaves nearly elastically when it is forced on a time scale that is short compared to the Maxwell time (the strain is nearly in phase with the stress) while at long time scales it exhibits a creep–like, viscous response. Recent laboratory data and analyses of post glacial rebound data for the earth suggest that the effective viscosity for terrestrial crustal and mantle materials varies significantly with frequency (Sabadini et al., 1987). Consequently a more complex viscoelastic model, such the standard linear solid, is required to adequately describe the behavior of earth materials. However, corresponding data for ice are not available. In this section we calculate the dissipation integral, Equation (2.6), under the simplifying assumption that the ice shell of Europa behaves as a Maxwell medium. We then

give examples of ice thickness profiles for the model.

The constitutive relation for an incompressible Maxwell medium is

$$2\dot{\epsilon}_{ij} = \frac{\sigma_{ij}}{\eta} + \frac{\dot{\sigma}_{ij}}{\mu} \quad , \quad (3.1)$$

(cf. Eirich, 1956) where μ , η , σ_{ij} , and $\dot{\epsilon}_{ij}$ are the rigidity and the viscosity of the medium, and the stress and strain rate tensors, respectively.

It is easy to show, using Equation (3.1) that when the $\dot{\epsilon}_{ij}$ are sinusoidal functions of time, the average volumetric dissipation rate for a Maxwell medium is

$$q = \overline{\sigma_{ij}\dot{\epsilon}_{ij}} = \frac{2\mu\overline{\dot{\epsilon}_{ij}^2}}{\omega} \left[\frac{\omega\tau_M}{1 + (\omega\tau_M)^2} \right] \quad , \quad (3.2)$$

where ω is the frequency of the forcing and $\tau_M = \frac{\eta}{\mu}$ is the Maxwell time. We may equate ω with Europa's mean motion, n . The viscosity η of ice obeys an Arrhenius relation

$$\eta = \eta_o \exp \left[\ell \left(\frac{T_M}{T} - 1 \right) \right] \quad , \quad (3.3)$$

where T_M is the melting temperature, $\ell \approx 24$ and $\eta_o \approx 10^{14}$ Poise (cf. Turcotte and Schubert, 1982). For computational purposes, we use a local power law representation of Equation (3.3) for the viscosity η :

$$\eta = \eta_o \left(\frac{T}{T_M} \right)^{-\ell} \quad . \quad (3.4)$$

Equation (3.4) has the same value of the logarithmic derivative $\frac{d \ln \eta}{d \ln T} = -\ell$ as Equation (3.3), near the melting point. Using Equations (3.4) and (3.2), the dissipation integral, Equation (2.6), may be solved exactly, giving

$$\int_0^{T_M} q(T) \frac{dT}{T} = \frac{2\mu}{n\ell} \overline{\dot{\epsilon}_{ij}^2}(\phi, \lambda) \left[\frac{\pi}{2} - \tan^{-1}(n\tau_M)_{\text{min}} \right] \quad (3.5)$$

where $\overline{\dot{\epsilon}_{ij}^2}$ is a function of ϕ and λ , the colatitude and longitude of the shell (see Appendix B and Figure 1), and $(n\tau_M)_{\min}$ is the value of $n\tau_M$ at the base of the ice.

The shell thickness obtained by insertion of the results of Equation (3.5) into Equation (2.8) is a reasonable estimate of the actual ice thickness as long as the peak tidal dissipation occurs at a location which is at most only a small fraction of the distance between the base of the ice and the surface. This is probably true because the tidal frequency n ($n \simeq 2 \times 10^{-5} \text{ s}^{-1}$) is near $\frac{1}{\tau_M}$ for the reasonable values of $\eta_o \gtrsim 10^{14}$ Poise and $1.1 \times 10^9 \text{ dynes cm}^{-2} \leq \mu \leq 4 \times 10^{10} \text{ dynes cm}^{-2}$ (cf. Hobbs, 1974). In the specific cases presented here, we have chosen the nominal value of $n\tau_M = 1$ at the base of the ice.

Figures 2 and 3 show two thickness profiles that result from inserting Equation (3.5) into Equation (2.8) for the thickness of the ice, using values for the surface temperature and $\overline{\dot{\epsilon}_{ij}^2}$ as derived in the Appendices. In both cases, values for μ and ℓ of $4 \times 10^{10} \text{ dynes cm}^{-2}$ and 24 have been used. In calculating the profile shown in Figure 2, the heat flow from the core was taken to be zero, while in the profile of Figure 3, a uniform heat flow from the core of $\sim 10 \text{ ergs cm}^{-2} \text{ sec}^{-1}$ was used. $10 \text{ ergs cm}^{-2} \text{ sec}^{-1}$ is roughly the amount of tidal heat flux which would flow from the core if the Q of the core were ~ 25 . As stated above, both figures represent cases where $(n\tau_M)_{\min} = 1$. If $(n\tau_M)_{\min}$ differs from unity, the profile of Figure 2 (with zero heatflow from the core) is changed by a multiplicative factor of

$$\sim \left[\left(\frac{\mu}{4 \times 10^{10} \text{ dynes cm}^{-2}} \right) \left(2 - \frac{4}{\pi} \tan^{-1} (n\tau_M)_{\min} \right) \right]^{-1/2}$$

Thus, if the point where $n\tau_M = 1$ occurs above (but near) the base of the ice, the thicknesses in Figure 2 are overestimates, while if $n\tau_M$ does not reach a value as small as unity, the thicknesses are underestimates. Note that for $(n\tau_M)_{\min} = 1$

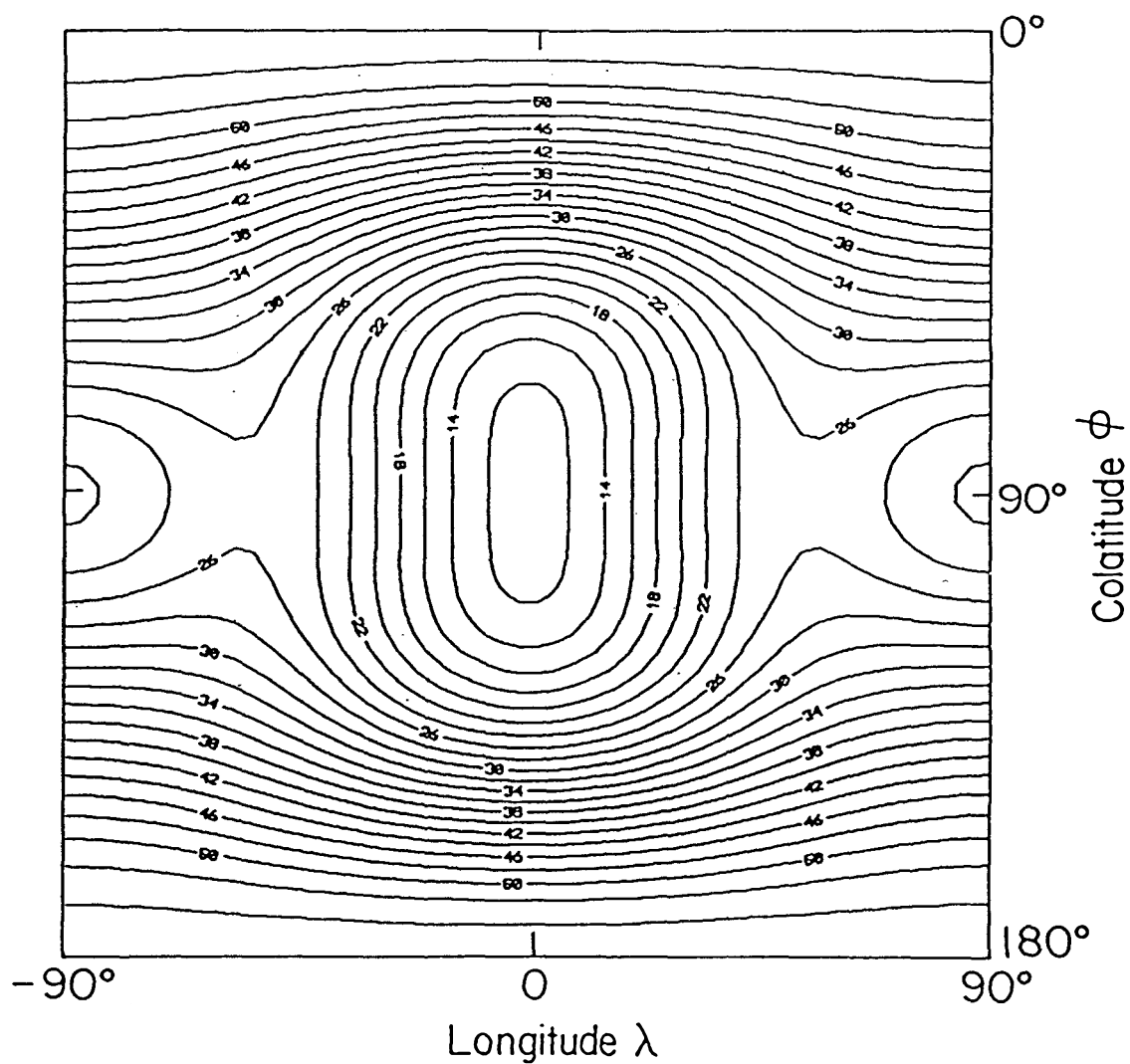


Figure 1. The quantity $\overline{\epsilon_{ij}^2}$, in units of $\frac{1}{2}(n\gamma eC_R)^2 \approx 1.2 \times 10^{-21} \text{sec}^{-2}$, as a function of Europa's colatitude ϕ and longitude λ .

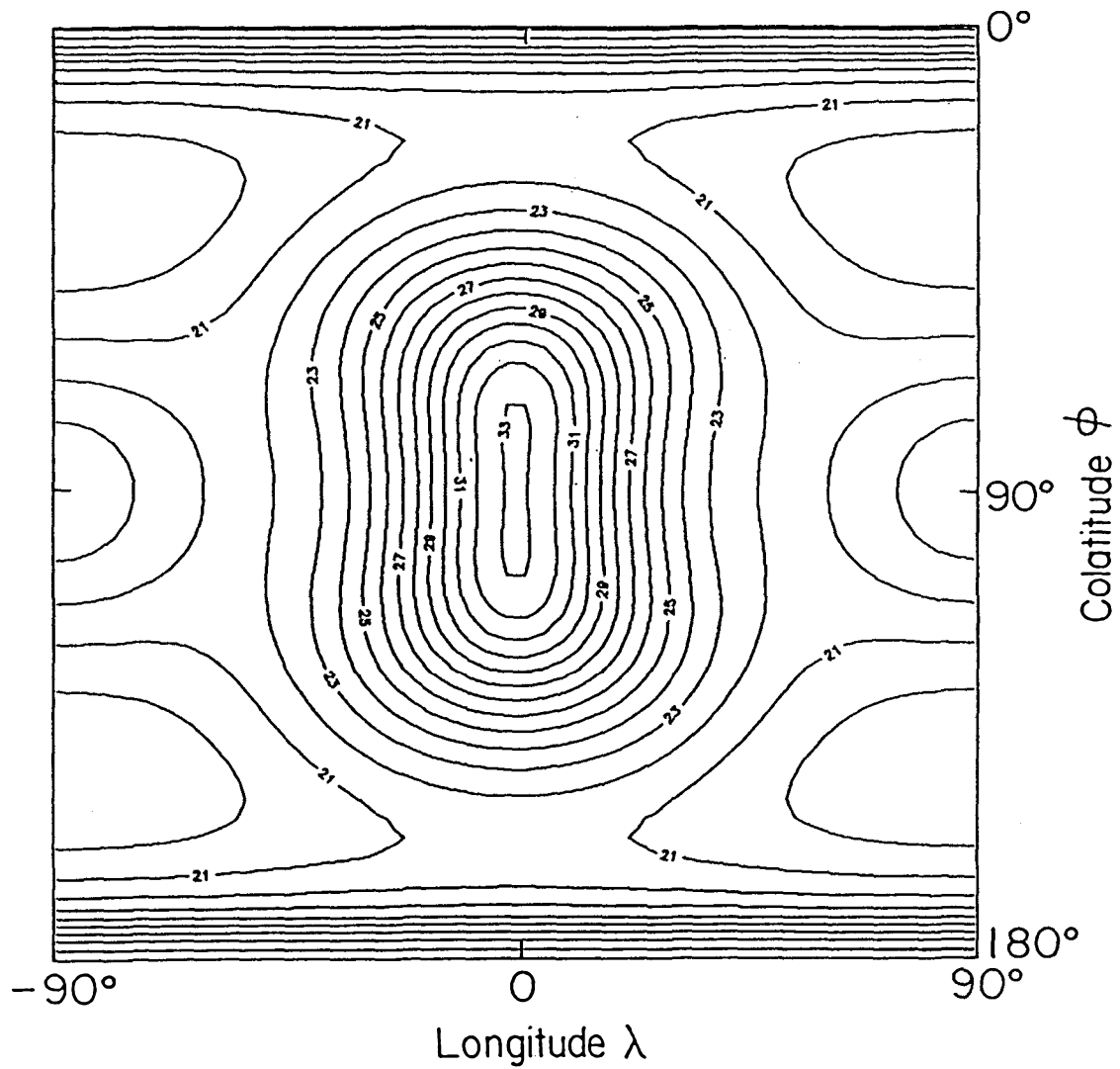


Figure 2. Equilibrium ice thickness for Maxwell rheology with no heat flow from the core. Units are kilometers. ϕ is colatitude and λ is longitude.

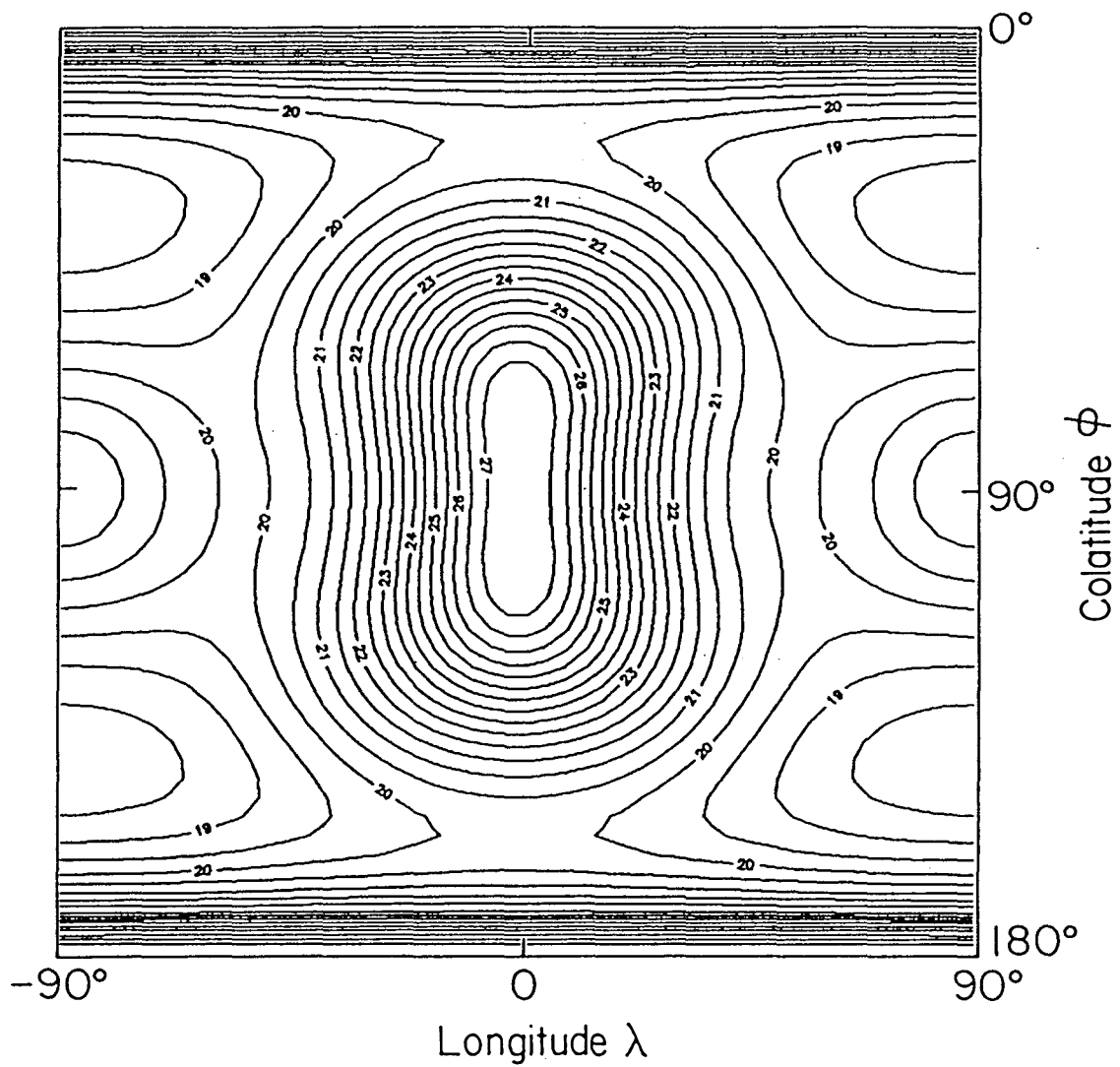


Figure 3. Equilibrium ice thickness for Maxwell rheology with heat flow from core of $\sim 10 \text{ ergs cm}^{-2} \text{ sec}^{-1}$. Units are kilometers. ϕ is colatitude and λ is longitude.

with $\mu = 4 \times 10^{10}$ dynes cm^{-2} it is implied that $\eta_o \simeq 2 \times 10^{15}$ Poise. If η_o is actually $\simeq 10^{14}$ Poise, the maximum dissipation rate occurs above the base of the ice, and Figure 2 is an overestimate of shell thickness by a factor of ~ 1.4 . If $\mu \simeq 4 \times 10^{10}$ dynes cm^{-2} , Figure 2 underestimates the ice thicknesses by a factor of $> \sqrt{2}$ only if $\eta_o \gtrsim 5 \times 10^{15}$ Poise. If the heatflow from the core is nonzero, as in Figure 3, the multiplicative correction factor if $(n\tau_M)_{\text{min}} \neq 1$ is similar to that given above, but is slightly closer to unity.

4. The Generalized Flow Law Rheology

Laboratory experimentation has shown that in the limit of pure creep and for a range of stresses between ~ 0.5 and several bars, the strain rates $\dot{\epsilon}_{ij}$ for ice are related to the stresses σ_{ij} by the relation

$$\dot{\epsilon}_{ij} = A \sigma_{ij}^{n_G} \quad , \quad (4.1)$$

where n_G is a constant, A varies with temperature according to an Arrhenius relation

$$A = A_o \exp \left[-n_A \left(\frac{T_M}{T} - 1 \right) \right] \quad , \quad (4.2)$$

and σ_{ij} are the elements of the stress tensor once the hydrostatic pressure is subtracted (i.e. σ_{ii} are the stress deviator components) (cf. Paterson, 1981). Equation (4.1) is commonly referred to as Glen's flow law.

The constant n_G has been found by different investigators to have values between 1.5 and 5.2 (Paterson, 1981). Above $\sim -10^\circ$ C the Arrhenius relation (4.2) is not strictly valid because several creep processes operate simultaneously, but Paterson (1981) suggests that it may still be used if an activation energy of ~ 139 kJ/mole is employed, which represents an average of the relevant activation energies and corresponds to a value for n_A of ~ 61 in our notation.

Nye (1957) proposed that Equation (4.1) may be generalized as the more tractable set of Equations

$$\dot{\epsilon}_{ij} = A \sigma_e^{n_G - 1} \sigma_{ij} \quad , \quad (4.3)$$

where

$$\sigma_e \equiv \left[\frac{1}{2} \sigma_{ij} \sigma_{ij} \right]^{1/2} \quad (4.4)$$

is called the *effective shear stress*. Using Equations (4.3) and (4.4) the volumetric dissipation rate can be shown to be

$$q = \overline{\sigma_{ij} \dot{\epsilon}_{ij}} = \frac{2}{A^{1/n_G}} \left[\frac{1}{2} \overline{\dot{\epsilon}_{ij}^2} \right]^{\frac{n_G + 1}{2n_G}} \quad . \quad (4.5)$$

It may easily be shown that for an incompressible material the product $\sigma_{ij} \dot{\epsilon}_{ij}$ is unaltered by replacing the σ_{ij} by the elements of the full stress tensor. We approximate the function A , (Equation (4.2)), by a local power law of temperature:

$$A = A_o \left(\frac{T}{T_M} \right)^{-n_A} \quad , \quad (4.6)$$

which has the same logarithmic derivative $\frac{d \ln A}{d \ln T}$ as Equation (4.2), near the melting point. Using Equation (4.6) in Equation (4.5), the dissipation integral given by Equation (2.6) may be evaluated, giving

$$\int_0^{T_M} \frac{q(T) dT}{T} = A_o^{-1/n_G} \left(\frac{n_G}{n_A} \right) 2 \left[\frac{1}{2} \overline{\dot{\epsilon}_{ij}^2} \right]^{\frac{n_G + 1}{2n_G}} \quad . \quad (4.7)$$

Note that the expression (4.7) does not reduce to Equation (3.5) when $n_G = 1$ because this development does not include the effects of elasticity. The nonlinearity of the generalized equation which is equivalent to Equation (3.1) makes such a computation difficult. However, the nonlinear generalization of the Maxwell time is not very different than the tidal period, so this deficiency is usually minor in this instance.

In Figures 4 and 5 thickness profiles are shown that were calculated using Equation (4.7) in Equation (2.8), for two choices of the parameters A_o and n_G . In both cases, n_A is taken to be 61 as discussed above. In Figure 4 the standard value of $n_G = 3$ was used, with a corresponding value for A_o of $5.1 \times 10^{-27} \text{ s}^{-1} (\text{dynes cm}^{-2})^{-3}$ taken from Table 3.2 of Paterson (1981). Figure 5 represents an extreme case where $n_G = 5.2$ and $A_o = 8.0 \times 10^{-41} \text{ s}^{-1} (\text{dynes cm}^{-2})^{-5.2}$. These values were taken from Table 3.1 of Paterson (1981). Because of the fractional power involved in the factor $[\frac{1}{2}\dot{\epsilon}_{ij}^2]^{\frac{n_G+1}{2n_G}}$, it has been averaged numerically over one orbital period at each latitude and longitude, using the expressions derived in Appendix B for the value of $\dot{\epsilon}_{ij}^2$ at each time.

5. Discussion

Various aspects of the thickness profiles given in this paper (Figures 2–5) are summarized in Table I. Profiles such as these have several implications for Europa's thermal and dynamical histories.

First, they indicate that the configuration consisting of an ice shell which is decoupled from a silicate core by a layer of liquid water is indeed a plausible one for Europa, if the total depth of the H_2O mantle exceeds ~ 30 km. This is true in spite of the fact that in our models, the effective Q throughout most of the shell is very large. The effective Q for the Maxwell model, for example, may be written

$$Q_{\text{Maxwell}} = \left[\frac{1 + (n\tau_M)^2}{2(n\tau_M)} \right] , \quad (5.1)$$

which, in the parameterization of Section (3) exceeds ~ 100 above the lowermost ~ 4 km of the shell (for both of the specific cases presented). It reaches a value of $\sim 10^{11}$ at the surface, for a mean surface temperature of ~ 80 K. The expression

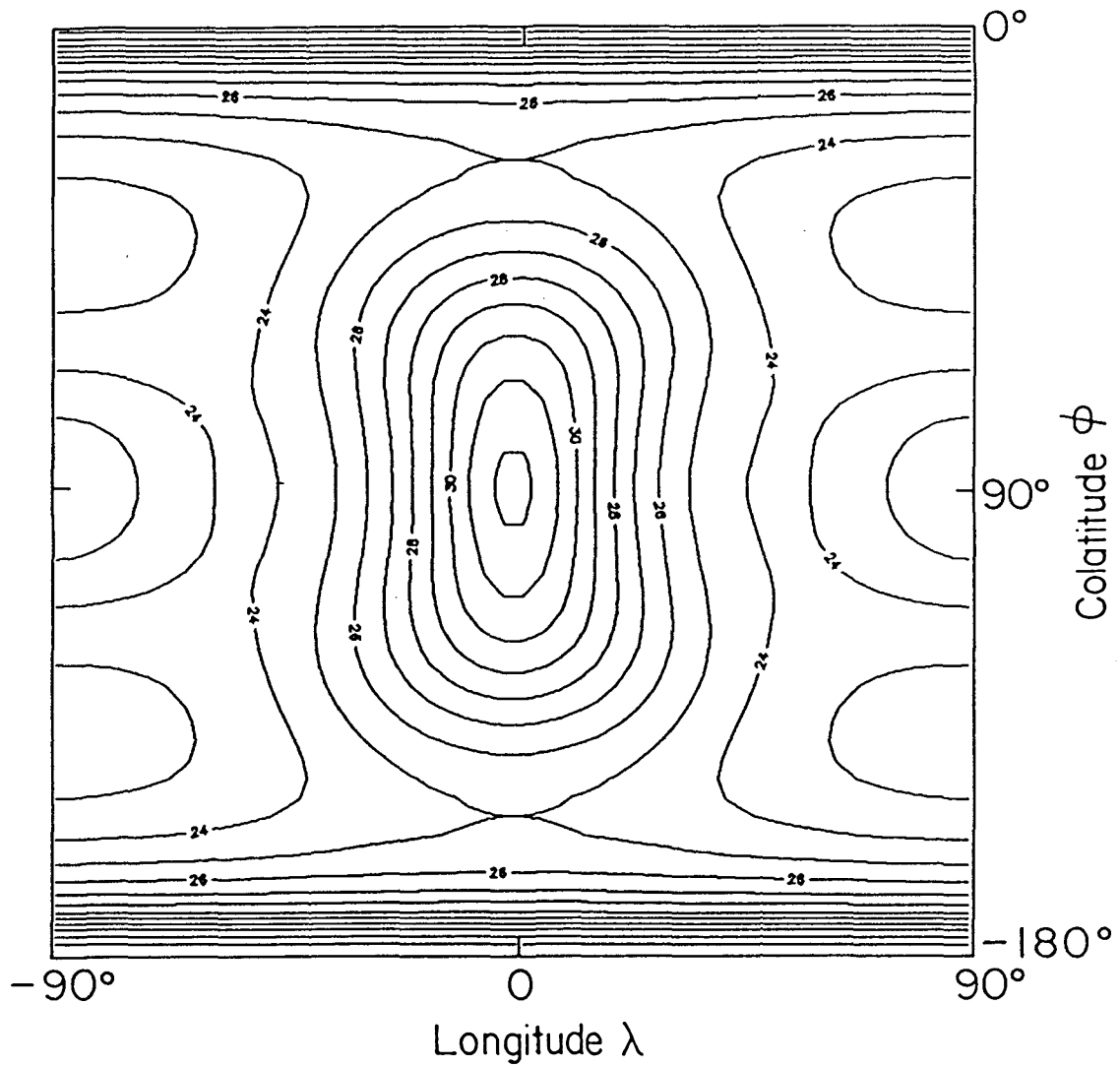


Figure 4. Equilibrium ice thickness for generalized flow law rheology, with $n_G = 3$ and $A_o = 5.1 \times 10^{-27} \text{ s}^{-1} (\text{dynes cm}^{-2})^{-3}$. Heat flow from core = 0. Units are kilometers.

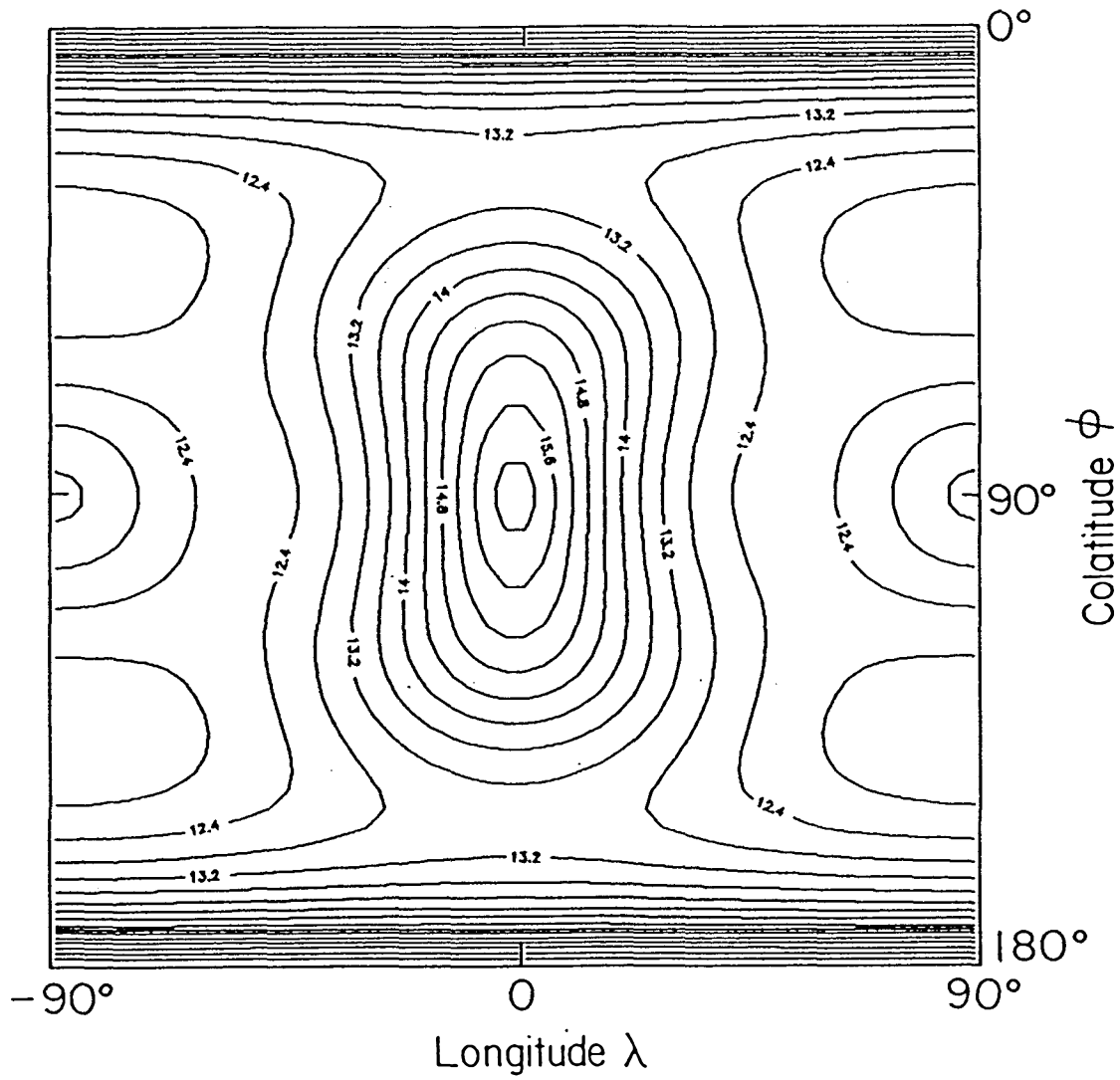


Figure 5. Equilibrium ice thickness for generalized flow law rheology with $n_c = 5.2$ and $A_c = 8.0 \times 10^{-41} \text{ s}^{-1} (\text{dynes cm}^{-2})^{-5.2}$. Heat flow from core = 0. Units are kilometers.

Table I

Properties of ice thickness profiles given in Figures

1-4. Other relevant parameters are given in text.

Figure	Type of Rheology	Parameters	Average Ice Thickness (km)	$4t_{22}$ (km)	$t_{20} + 2t_{22}$ (km)
2	Maxwell	$H_{\text{core}} = 0 \text{ erg cm}^{-2} \text{ s}^{-1}$	23	6.6	-0.1
3	Maxwell	$H_{\text{core}} = 10 \text{ erg cm}^{-2} \text{ s}^{-1}$	21	4.6	0.4
4	Generalized flow law	$H_{\text{core}} = 0 \text{ erg cm}^{-2} \text{ s}^{-1}$ $n_G = 3$ $n_A = 61$ $A_0 = 5.1 \times 10^{-27} \text{ s}^{-1} (\text{dynes cm}^{-2})^{-3}$	25	4.4	1.1
5	Generalized flow law	$H_{\text{core}} = 0 \text{ erg cm}^{-2} \text{ s}^{-1}$ $n_G = 5.2$ $n_A = 61$ $A_0 = 8.0 \times 10^{-41} \text{ s}^{-1} (\text{dynes cm}^{-2})^{-5.2}$	13	2.0	0.8

given by (5.1) has a minimum value of unity if $n_{TM} = 1$ at the base of the ice, as we have assumed.

The characteristic length scale over which the effective Maxwell Q grows by an order of magnitude is crudely $-b_o \ln(10) \frac{d \ln T}{d \ln Q} \sim 2 \frac{b_o}{\ell}$ or ~ 2 km for $b_o \sim 20$ km and $\ell = 24$, where b_o is the average shell thickness. The dissipation is therefore concentrated in the lowermost $\sim 2 \frac{b_o}{\ell}$ of the shell's thickness to within an order of magnitude. From this result, it follows that the total dissipation rate in the Maxwell

model is roughly equivalent to that of a constant Q model in which $Q \sim \frac{\ell}{2} \sim 10$.

The total dissipation rate in the shell is therefore ~ 10 times larger than the nominal constant Q model with $Q \sim 100$ and $b_o \sim 20$ km (cf. Cassen et al., 1982). The total tidal dissipation rate in the Maxwell model is roughly 2×10^{18} ergs $^{-1}$, implying an average tidal heat flux of ~ 7 erg cm $^{-2}$ sec $^{-1}$.

As is evident from Table I, a uniformly distributed heat flux from the core of ~ 10 erg cm $^{-2}$ sec $^{-1}$ reduces the average shell thickness by only ~ 2 km. The insensitivity of the ice thickness to the heatflow from the core which is implied by this result is not surprising. Heat flowing into the ice shell from the ocean requires a nonzero temperature gradient at the core/ocean interface, and such a temperature gradient reduces the thickness of the region of the warmest, most dissipative ice. Thus, heatflow from the core reduces the total tidal dissipation in the ice, and the net affect on shell thickness is reduced. A tidal heat flux of 10 erg cm $^{-2}$ sec $^{-1}$ would flow from the core if it has a constant Q of ~ 25 .

Because of the nonlinear nature of the generalized flow law, there is no simple expression for the effective Q for that rheology. However, note that the temperature dependence of the dissipation rate for the generalized flow law, with $n_A = 61$ and $n_G = 3$, is similar to that of the Maxwell rheology because $\frac{-d \ln q}{d \ln T} = \frac{n_A}{n_G} \approx 20 \approx \ell$ for that case. As in the Maxwell rheology, the total dissipation rates for the generalized flow law cases given here are on the order of a few $\times 10^{18}$ erg cm $^{-2}$ sec $^{-1}$.

Note the large maxima in the thickness profiles in Figures 2 through 5, at $\phi = \frac{\pi}{2}$ and $\lambda = 0, \pi$ (the sub- and anti-Jupiter points). These maxima are due to large minima in the average tidal strain rates at the same locations (Figure 1). Also note the presence of sharp maxima in the thickness profiles at the poles ($\phi = 0, \pi$). These are caused by acute minima in the surface temperature at the

poles as calculated from the expressions derived in Appendix A. The poles of Europa are particularly cold (~ 50 K) because of Europa's small inclination ($\sim 1^\circ$) with respect to Jupiter's equatorial plane, and Jupiter's small obliquity ($\sim 3^\circ$). The maxima in the ice thickness very near the poles persist in spite of a strong maximum in the tidal dissipation at the same locations.

The extrema in ice thickness discussed above may have important implications for Europa's rotational history because of their contributions to the inertia tensor of the satellite. Only components of the ice thickness variations of the second spherical harmonic degree affect the inertia tensor. It can easily be shown that the addition of such a thickness component t_{2m} to a perfectly isostatically compensated shell will affect the inertia tensor by a characteristic amount

$$\Delta I \sim (\rho_m - \rho_c) \frac{\rho_c}{\rho_m} a^4 \left(\frac{b}{a} \right) t_{2m} \quad , \quad (5.2)$$

where ρ_c , ρ_m , a , and b are the density of the ice and the underlying liquid water, the radius of the body, and the thickness of the shell, respectively.

Hence, the second degree components of the gravity field will be affected by a characteristic amount

$$C_{2m} \sim \frac{\Delta I}{I} \sim \frac{\rho_m - \rho_c}{\bar{\rho}} \frac{\rho_c}{\rho_m} \left(\frac{b}{a} \right) \left(\frac{t_{2m}}{a} \right) \quad , \quad (5.3)$$

where I is the characteristic magnitude of the moments of inertia of the body and $\bar{\rho}$ is its average density.

The principal moments of inertia of a body are related to the C_{2m} by

$$A \equiv I_{xx} = I' + Ma^2 \left(\frac{C_{20}}{3} - 2C_{22} \right) \quad (5.4)$$

$$B \equiv I_{yy} = I' + Ma^2 \left(\frac{C_{20}}{3} + 2C_{22} \right) \quad (5.5)$$

$$C \equiv I_{zz} = I' + Ma^2 \left(\frac{-2}{3} C_{20} \right) , \quad (5.6)$$

where I' is the average moment of inertia and M is the mass of the body (cf. Lambeck, 1980). We shall take the coordinate system in which (5.4)–(5.6) are defined to be the usual principal axis coordinate system of a synchronously rotating satellite (i.e., $A < B < C$).

Using (5.3) and (5.4)–(5.6) it may now be seen that the contributions of the t_{2m} to the quantities $\left(\frac{B-A}{C}\right)$ and $\left(\frac{B-C}{A}\right)$ go as

$$\Delta \left(\frac{B-A}{C} \right) \sim \left(\frac{\rho_m - \rho_c}{\bar{\rho}} \right) \left(\frac{\rho_c}{\rho_m} \right) \left(\frac{b}{a} \right) \left(\frac{4t_{22}}{a} \right) \quad (5.7)$$

$$\Delta \left(\frac{B-C}{A} \right) \sim \left(\frac{\rho_m - \rho_c}{\bar{\rho}} \right) \left(\frac{\rho_c}{\rho_m} \right) \left(\frac{b}{a} \right) \left(\frac{t_{20} + 2t_{22}}{a} \right) . \quad (5.8)$$

Using $b = 20$ km and other appropriate parameter values, (5.7) and (5.8) may be written

$$\Delta \left(\frac{B-A}{C} \right) \sim 10^{-7} \left(\frac{4t_{22}}{1 \text{ km}} \right) \quad (5.9)$$

$$\Delta \left(\frac{B-C}{A} \right) \sim 10^{-7} \left(\frac{t_{20} + 2t_{22}}{1 \text{ km}} \right) . \quad (5.10)$$

Actual values of $\Delta \left(\frac{B-A}{C}\right)$ and $\Delta \left(\frac{B-C}{A}\right)$ may be estimated by inserting values of t_{20} and t_{22} for our models (see Table I) into the above two equations. The values of both $\Delta \left(\frac{B-A}{C}\right)$ and $\Delta \left(\frac{B-C}{A}\right)$ are mostly due to the variation of tidal dissipation with latitude and longitude rather than the variation of surface temperature over the shell. (The surface temperature variation contributes nothing to t_{22} , and the fact that t_{20} is negative indicates that the maximum in tidal dissipation at high latitudes dominates over the minimum in surface temperature.)

Because the tidal torque only goes to zero for a synchronously rotating satellite when the orbital eccentricity is zero (Goldreich, 1966), planetary satellites will

in general rotate nonsynchronously unless they possess a small permanent component of $\left(\frac{B-A}{C}\right)$ which persists in a frame fixed in the body, regardless of its orientation. Greenberg and Weidenschilling (1984) have determined the magnitude of this permanent asymmetry which is required to induce synchronous rotation in several planetary satellites, for two models of tidal behavior: the MacDonald and Darwin tidal models. In the MacDonald model, the entire tidal bulge on the satellite is assumed to be offset by a constant angle $\sim \frac{1}{Q}$ from the instantaneous direction toward the planet. In the Darwin model, each Fourier component of the tide-raising potential raises its own bulge on the satellite, with its own specific phase lag. For synchronous rotation, each of the lowest order time-dependent terms in the potential have the frequency of the mean motion. Using a Q of ~ 10 for the MacDonald tidal bulge and for each component of the Darwin tidal bulge in synchronous rotation, Greenberg and Weidenschilling find that the magnitude of the permanent component of $\left(\frac{B-A}{C}\right)$ that is needed in order for Europa to rotate synchronously is $\sim 10^{-7}$ if the tides obey the Darwin model and $\sim 10^{-5}$ if they obey the MacDonald model.

As is clear from Table I and Equation (5.9), the contribution of a thermal equilibrium ice shell to the value of $\left(\frac{B-A}{C}\right)$ for Europa is between 10^{-6} and 10^{-7} for each of the models presented in this paper. These values are larger than the permanent component of $\left(\frac{B-A}{C}\right)$ which is required to prevent nonsynchronous rotation of Europa if the Darwin tidal model applies to that body. Furthermore, if the ice shell and a portion of the liquid ocean behave as a single entity which can reorient independently of the silicate core, as is suggested in the accompanying paper (Ojakangas and Stevenson, 1988), we may take the value of C in $\Delta\left(\frac{B-A}{C}\right)$ to be only due to the inertia of the shell and that portion of the ocean which reorients

with it. Then the relevant C is smaller than that of the entire satellite by at least a factor of ~ 10 for an H_2O mantle of ~ 100 km in thickness, and $\Delta \left(\frac{B-A}{C} \right)$ is proportionately larger. It is then possible that $\Delta \left(\frac{B-A}{C} \right)$ is as large as the permanent component of $\left(\frac{B-A}{C} \right)$ which is required to prevent nonsynchronous rotation if the MacDonald tidal model applies.

However, the contribution to $\left(\frac{B-A}{C} \right)$ due to variations in shell thickness given by Equation (5.7) is not truly permanent, but depends on the orientational history of the shell. This is because the tidal dissipation rate in the shell is a fixed function of latitude and longitude only in a coordinate system which is synchronously rotating, rather than one which is fixed in the body frame of the shell. As a relevant example, suppose that the ice shell were somehow "held" in synchronous rotation until it reached its equilibrium thickness at all geographic coordinates and was then "released," i.e. allowed to rotate naturally. Then, if $\Delta \left(\frac{B-A}{C} \right)$ as given by Equation (5.7) is large enough, the shell will reorient by an angle between zero and $\frac{\pi}{4}$ (with respect to the direction toward the planet) to an equilibrium state where the torque due to the gravitational influence of the planet acting on the asymmetry of the shell balances the tidal torque. In this orientation, however, the shell is no longer in thermal equilibrium with the tidal dissipation within it, and the shell thickness will begin to adjust toward its new equilibrium profile. As this occurs, both the magnitude and direction of the principal axes of the shell will evolve, the torques will no longer balance in that orientation, and the shell will begin to rotate nonsynchronously once again. Thus, even though a thermal equilibrium ice shell may possess a $\Delta \left(\frac{B-A}{C} \right)$ which is larger than the critical permanent asymmetry needed to prevent nonsynchronous rotation, thermal equilibrium involving synchronous rotation seems impossible for Europa's shell. Instead a state of dy-

dynamic equilibrium involving slightly nonsynchronous rotation is probable. In such a state, the shell is continually striving to achieve thermal equilibrium, but is continuously drifting relative to the synchronously rotating frame. This drift can only occur on a time scale comparable to, or longer than, the time scale for thermal diffusion through the shell's characteristic thickness. Thus for a shell thickness of ~ 20 km, a complete rotation relative to the satellite-planet direction must take place in $\sim 10^7$ years or more. However, it must be noted that if the shell were ever rotating with a much shorter period relative to synchronicity, it is unlikely that the state described above could ever be achieved. For example, if the shell at some time possessed no significant permanent component of $\left(\frac{B-A}{C}\right)$, its preferred rotation period relative to synchronicity is ~ 10 years if the MacDonald model is correct (see Equation (1) of Greenberg and Weidenschilling (1984)). At such a rotation rate, the longitudinal variations in tidal dissipation within the shell average to zero (in the frame of the shell). Consequently no significant contribution to $\left(\frac{B-A}{C}\right)$ can evolve, and the ~ 10 year period of nonsynchronous rotation will persist. Thus, a state of very nearly synchronous rotation must have existed at some time in the past if the state described above, of nonsynchronous rotation on the thermal diffusion time scale, is currently occupied by Europa's shell. This would be true if the Laplace resonance, and hence the forced eccentricity of Europa were not primordial (assuming free eccentricity is quickly damped). Then Europa's shell would have formed in synchronous rotation. This would also be true if a significant portion of the outermost, coldest ice behaves as a continuous elastic shell on a time scale of $\gtrsim 10^7$ years. Then a portion of its hydrostatic rotational and tidal bulges will persist in the frame of the shell upon reorientation. This "fossil" bulge, described in the following paper (Ojakangas and Stevenson, 1988), may itself be large enough

to prevent nonsynchronous rotation.

Another consequence of ice thickness variations on Europa's rotational history is possible due to the fact that the preferred dynamic equilibrium for synchronously rotating satellites is one in which $B < C$ (cf. Danby, 1962). Therefore, if $\Delta \left(\frac{B-C}{A} \right) > 0$ and it is the most important permanent component of the total $\left(\frac{B-C}{A} \right)$, it is possible that an ice shell in thermal equilibrium is incompatible with a state of dynamic equilibrium for Europa: the implication is that Europa may exhibit polar wander as thermal equilibrium is approached. $\Delta \left(\frac{B-C}{A} \right)$ is indeed greater than zero for three of the models presented here, as is evident from the tabulated values of $(t_{20} + 2t_{22})$ in Table I. However, note that the validity of these values (and hence the possibility of polar wander) requires that Europa's shell has never been rotating nonsynchronously on a time scale short compared to the thermal diffusion time ($\sim 10^7$ y), for then the longitudinal thickness variations described by t_{22} would not exist (see previous paragraph). The question of polar wander of Europa's shell is addressed in detail in the following paper (Ojakangas and Stevenson, 1988).

Because the ice possesses rigidity, the effect of the second degree ice thickness variations on the inertia tensor may be reduced due to elastic support of the topography at the base of the ice (see the following paper (Ojakangas and Stevenson, 1988)). However, for reasonable ice rigidities of $\mu \lesssim 4 \times 10^{10}$ dynes cm^{-2} , it is shown in the following paper that the effect of elasticity on the contributions of t_{20} and t_{22} to the inertia tensor is unimportant in this problem.

Despite the fact that an ice shell with horizontal thickness variations will be very nearly isostatically compensated, viscous flow of the topography will occur because of the horizontal pressure variations within the ice. This flow will act to

eliminate the thickness variations described in this paper. However, it is shown in the following paper that such flow would require $\sim 10^7$ years to eliminate the topography in the absence of all other effects. Since the topography grows on a similar time scale (the diffusion time through the shell) the flow can reduce but not eliminate the topography calculated here.

The question of the manner in which heat flowing from the silicate core of Europa is distributed with latitude and longitude at the lower surface of the ice is a difficult one which remains unanswered. Vertical heat transport below the level where $T \sim 277$ K is probably accomplished by a turbulent (mixing length theory) convection. This will eliminate any horizontal temperature gradients. Above the level where $T \sim 277$ K, upward transport of heat cannot occur by standard convection because the thermal expansivity of water is negative (warm parcels sink). We therefore expect conduction to operate, consequently requiring a much larger temperature gradient. In the case shown in Figure 3 we assumed that a heat flow from the core $10 \text{ erg cm}^{-2} \text{ sec}^{-1}$ was distributed uniformly with latitude and longitude. In the other cases given, the heat flow from the core was taken to be zero. The insensitivity of ice thickness to heatflow from the core described previously suggests that spatial variations in core heatflow need not eliminate the ice thickness components calculated in this paper. For example, if we assume that the core heatflow is channeled preferentially into the ice that protrudes deepest into the ocean, the ice thickness in those places will be reduced, but the topographic variations calculated in this paper will not be eliminated, even if the total heat produced in the core exceeds that in the shell.

6. Conclusions

We have calculated thermal equilibrium thicknesses of a thin decoupled ice shell on Europa for both the Maxwell rheology and the generalized flow law rheology, as functions of colatitude and longitude on the satellite. The models include explicitly the strong variation of the dissipation rate with temperature, as well as the temperature dependence of the thermal conductivity of ice.

In both models most of the dissipation is concentrated in the lowermost few kilometers of the shell. The effective Q of the majority of the shell in our models is very large ($\gg 100$), yet the shell thickness is nowhere more than 30 km in each case presented. Thus, our models predict that a decoupled ice shell on Europa is stable as long as the total thickness of the H_2O mantle is $\gtrsim 30$ km. The presence of an insulating regolith, though possible, is not needed to promote stability. A uniform core heatflow of $10 \text{ erg cm}^{-2} \text{ sec}^{-1}$, corresponding to the tidal dissipation rate with a constant Q for the core of ~ 25 , causes a reduction in the average shell thickness of only ~ 2 km. Because of spatial variations in tidal dissipation within the ice and the annual average solar insolation incident upon it, the equilibrium ice thickness varies markedly with position over the shell. We have calculated the second spherical harmonic degree components of the ice thickness profiles presented here and have estimated their contributions to Europa's principal moment differences. Even though these differences may be larger than the permanent values required to prohibit nonsynchronous rotation (as estimated by Greenberg and Weidenschilling (1984)), they are not able to prohibit nonsynchronous rotation because of their dependence on the orientation of the shell in a synchronously rotating frame. Instead, a state of continuous thermal disequilibrium and nonsynchronous rotation is probable, with a rotation period relative to synchronicity of $\gtrsim 10^7$ years. Such

a state will only be occupied if the shell rotated nearly synchronously at the time of its formation. If the shell rotated much more rapidly at any time, such rapid rotation would persist, and the thickness variations calculated in this paper would be nullified. Synchronous rotation may be ensured by the presence of a "fossil" bulge on the shell, due to elastic behavior of the near-surface, cold ice.

Since the contribution of the ice thickness variations to the quantity $B - C$ is typically greater than zero, a state of thermal equilibrium for Europa's shell may correspond to a state of dynamic disequilibrium, if the above is the most important permanent component of the mass distribution. Thus, Europa's shell may exhibit polar wander as thermal equilibrium is approached. This is analyzed in the following paper (Ojakangas and Stevenson, 1988).

Appendix A: Surface Temperature of Europa

In order to calculate the surface temperature as a function of colatitude ϕ on Europa, we first calculate the average solar insolation as a function of ϕ . The problem is nontrivial because the body possesses a finite obliquity, $i \approx 3$ degrees.

We choose a Cartesian coordinate system in which a point on Europa's surface has a unit direction vector

$$\hat{x} = (\sin \phi \cos nt, \sin \phi \sin nt, \cos \phi) \quad , \quad (\text{A.1})$$

where n is Europa's mean motion (equal to its rotational frequency). This is simply a non-rotating coordinate system whose z -axis is coincident with Europa's axis of rotation.

In this coordinate system, the unit vector directed toward the sun is

$$\hat{s} = (\cos i \cos \Omega t, \sin \Omega t, \sin i \cos \Omega t) \quad , \quad (\text{A.2})$$

where Ω is the mean motion of Jupiter in its orbit about the sun. Europa's equinoxes occur when $\Omega t = \frac{\pi}{2}, \frac{3\pi}{2}$, and $\Omega t = 0, \pi$ corresponds to its northern and southern solstices, respectively.

The quantity $\hat{x} \cdot \hat{s}$ is the cosine of the solar zenith angle. Therefore, a point on the surface of Europa that is described by \hat{x} will receive an incident solar flux F of

$$\begin{aligned} F &= \pi F_{\odot} (\hat{x} \cdot \hat{s}) \quad : \quad \hat{x} \cdot \hat{s} > 0 \\ F &= 0 \quad : \quad \hat{x} \cdot \hat{s} < 0 \quad , \end{aligned} \quad (\text{A.3})$$

where πF_{\odot} is the solar flux incident on a surface element whose normal vector is directed at the sun.

From (A.1) and (A.2),

$$\hat{x} \cdot \hat{s} = \sin \phi \cos i \cos \Omega t \cos nt + \sin \phi \sin \Omega t \sin nt + \sin i \cos \phi \cos \Omega t \quad , \quad (\text{A.4})$$

which may be written

$$\hat{x} \cdot \hat{s} \sim \sin \phi \cos(nt - \omega t) + i \cos \phi \cos \Omega t \quad (\text{A.5})$$

for $i \ll 1$ (which is well satisfied for Europa).

We now examine the case where $i < \phi < \frac{\pi}{2} - i$ (i.e., the region equatorward of the Arctic Circles). In this region, Equation (A.5) reveals that $\hat{x} \cdot \hat{s} > 0$ if

$$(nt)_{\min} \leq nt \leq (nt)_{\max} \quad , \quad (\text{A.6})$$

where

$$\begin{aligned} (nt)_{\min} &= \frac{-\pi}{2} \Omega t - i \cot \phi \cos \Omega t \\ (nt)_{\max} &= \frac{\pi}{2} + \Omega t + i \cot \phi \cos \Omega t \quad . \end{aligned} \quad (\text{A.7})$$

The diurnally averaged solar insolation is obtained by the integral

$$F_d = \frac{\pi F_{\odot}}{2\pi} \int_{(nt)_{\min}}^{(nt)_{\max}} (\hat{x} \cdot \hat{s}) d(nt) \quad , \quad (\text{A.8})$$

where Equations (A.7) and (A.5) are inserted for $(nt)_{\max}$, $(nt)_{\min}$, $\hat{x} \cdot \hat{s}$. The result of this integral is then averaged over one cycle of (Ωt) (i.e., one Jovian year) to give the annual average solar insolation F_A as a function of ϕ . The result is

$$F_A = \frac{1}{2\pi} \int_0^{2\pi} F_d d(\Omega t) \simeq (\pi F_{\odot}) \left(\frac{\sin \phi}{\pi} \right) + O(i^2) \quad . \quad (\text{A.9})$$

We now examine the case where $\phi \ll i$ (which will give the same result as for $\pi - \phi \ll i$). In this case, Equation (A.4) may be written

$$\hat{x} \cdot \hat{s} \simeq \phi \cos(nt - \Omega t) + i \cos \Omega t \quad , \quad (\text{A.10})$$

which is greater than zero for

$$(\Omega t)_{\min} \leq \Omega t \leq (\Omega t)_{\max} \quad , \quad (\text{A.11})$$

where

$$\begin{aligned} (\Omega t)_{\min} &\simeq \frac{-\pi}{2} - \frac{\phi}{i} \cos(nt - \Omega t) \\ (\Omega t)_{\max} &\simeq \frac{\pi}{2} + \frac{\phi}{i} \cos(nt - \Omega t) \end{aligned} \quad (\text{A.12})$$

for $\phi \ll i$.

In this limit the average of (A.10) over the diurnal period is unimportant; the zenith angle of the sun near the poles varies approximately only yearly. The annual average solar insolation is given by

$$F_A \simeq \frac{\pi F_{\odot}}{2\pi} \int_{(\Omega t)_{\min}}^{(\Omega t)_{\max}} (\hat{x} \cdot \hat{s}) d(\Omega t) \quad , \quad (\text{A.13})$$

where Equations (A.10) and (A.12) are inserted for $(\hat{x} \cdot \hat{s})$, $(\Omega t)_{\max}$, and $(\Omega t)_{\min}$. The result is

$$F_A \simeq \frac{i}{\pi} + O\left(\frac{\phi^2}{i}\right) \quad . \quad (\text{A.14})$$

In the models of ice thickness presented in this paper, we use

$$F_A \simeq (\pi F_{\odot}) \frac{(i^2 + \phi^2)^{1/2}}{\sqrt{2} \pi} \quad , \quad (\text{A.15})$$

which has the correct form of the second-order term $\left(O\left(\frac{\phi^2}{i}\right)\right)$ and matches Equation (A.9) when $\phi = i$.

To calculate the mean surface temperature we equate the fraction of the annual insolation that is absorbed to the heat flux radiated to space:

$$(1 - A)F_A = \sigma_s T_s^4 \quad , \quad (\text{A.16})$$

where $\sigma_s = 5.7 \times 10^{-5} \text{ erg cm}^{-2} \text{ sec}^{-1} \text{ K}^{-1}$ is the Stefan-Boltzmann constant, A is the albedo of the ice, and T_s is the average surface temperature.

Using Equations (A.9) and (A.15) with Equation (A.16), we calculate the surface temperature as

$$T_s = \left[\frac{(1-A)}{\sigma_s} (\pi F_\odot) \left(\frac{\sin \phi}{\pi} \right) \right]^{1/4}, \quad i < \phi < \pi - i \quad (\text{A.17})$$

$$T_s = \left[\frac{(1-A)}{\sigma_s} (\pi F_\odot) \frac{(i^2 + \phi^2)^{1/2}}{\sqrt{2} \pi} \right]^{1/4}, \quad \phi < i \quad (\text{A.18})$$

In the models in this paper we use $A = 0.5$. $\pi F_s \simeq 5 \times 10^4 \text{ erg cm}^{-2} \text{ sec}^{-1}$ is the solar flux at Jupiter's orbit. With these parameters, the surface temperature varies between $\sim 110 \text{ K}$ at the equator to $\sim 52 \text{ K}$ at the poles. The surface-averaged value is $\sim 100 \text{ K}$.

Appendix B: Tidal Strains in a Thin Shell

Peale and Cassen (1978) derived analytical expressions for tidal strains as a function of position in incompressible two-layer elastic bodies for which the rigidity in each layer is allowed to be different. Using their development we obtain the periodic tidal strains in a thin incompressible elastic shell that overlies a fluid (zero rigidity) synchronously rotating satellite in an elliptical orbit. These strains are applied in this paper to calculate the equilibrium thickness of an ice shell overlying a liquid water layer on Europa.

The tidal strains are derived from the displacement vector \vec{u} , which satisfies the equilibrium equation

$$\mu \nabla^2 \vec{u} = \vec{\nabla} P \quad (\text{B.1})$$

and the incompressibility condition

$$\vec{\nabla} \cdot \vec{u} = 0 \quad (\text{B.2})$$

$P \equiv p - \rho U$, where ρ is the density of the body (assumed homogeneous). U is the total disturbing potential including self-gravity of the deformation and p is the mean pressure due to the tidal distortion.

Peale and Cassen write a particular solution to (B.1) and (B.2) for a two-layer body as

$$\vec{u} = \sum_{+,-} \left[A^{\pm} r^2 \vec{\nabla} P^{\pm} + B^{\pm} \vec{r} P^{\pm} - \vec{\nabla} \left(\Phi^{\pm} + \vec{r} \cdot \vec{\nabla} \Phi^{\pm} \right) \right] \quad , \quad (\text{B.3})$$

where

$$\Phi^{\pm} = \Phi_o^{\pm} \left(\frac{r}{a} \right)^2 P_2(\cos S) \quad (\text{B.4})$$

$$\Phi^{-} = \Phi_o^{-} \left(\frac{r}{a} \right)^{-3} P_2(\cos S) \quad (\text{B.5})$$

$$P^{+} = P_o^{+} \left(\frac{r}{a} \right)^2 P_2(\cos S) \quad (\text{B.6})$$

$$P^- = P_o^- \left(\frac{r}{a}\right)^{-3} P_2(\cos S) \quad (\text{B.7})$$

$$A^+ = \frac{5}{42\mu} \quad (\text{B.8})$$

$$A^- = 0 \quad (\text{B.9})$$

$$B^+ = -\frac{2}{21\mu} \quad (\text{B.10})$$

$$B^- = \frac{1}{2\mu} \quad (\text{B.11})$$

The angle S is defined by $\cos S \equiv \frac{\vec{r} \cdot \vec{R}}{(rR)}$, where \vec{r} and \vec{R} are the position vectors (measured from the satellite's center) of a point with the satellite and the center of the parent planet, respectively. a and μ are the radius of the satellite and the rigidity of whichever layer is being considered, respectively. $P_2(\cos S)$ is the second (unnormalized) Legendre polynomial.

The boundary conditions which the solution must satisfy are that the components of the stress tensor σ_{ij} must satisfy

$$\sigma_{ij}n_j = 0 \quad (\text{B.12})$$

at the (deformed) surface of the satellite, where n_j are the components of the unit normal vector to the surface, and that both the stress and the displacement are continuous at the boundary that separates the two layers.

When the above boundary conditions are applied, and the rigidity of the inner layer is allowed to go to zero, Peale and Cassen find that a system of five equations in the quantities Φ_o^+ , Φ_o^- , P_o^+ , P_o^- (for the outer layer), and $\Delta a''$, the displacement at the surface, results (see Peale and Cassen, 1978, Equation (B.12)). When those equations are solved with the assumption that the ratio δ of the thickness of the outer layer (the ice shell in our case) to the radius of the satellite is

small, it is found that

$$\Phi_o^+ = - \left(\frac{4}{11} \right) \left[1 + \frac{4}{11} (1 - 15\mu') \delta \right] \left(\frac{M_p a^5}{M_s R^3} \right) \quad (\text{B.13})$$

$$\Phi_o^- = \left(\frac{37}{308} \right) \left[1 - \frac{24}{11} \left(\frac{3}{37} + \frac{5}{2} \mu' \right) \delta \right] \left(\frac{M_p a^5}{M_s R^3} \right) \quad (\text{B.14})$$

$$P_o^+ = - \left(\frac{60}{11} \right) \left[1 + \frac{3}{11} \left(\frac{3}{5} - 20\mu' \right) \delta \right] \left(\mu \frac{M_p a^3}{M_s R^3} \right) \quad (\text{B.15})$$

$$P_o^- = \left(\frac{40}{11} \right) \left[1 - \frac{24}{11} \left(\frac{1}{5} + \frac{5}{2} \mu' \right) \delta \right] \left(\mu \frac{M_p a^3}{M_s R^3} \right) \quad (\text{B.16})$$

where M_p and M_s are the masses of the satellite and the parent planet, respectively, and

$$\mu' = \frac{\mu}{\rho g a} \quad (\text{B.17})$$

where μ , ρ , and g are the rigidity of the shell, the density, and the surface gravity of the satellite.

μ' for Europa's shell is ~ 0.6 if the rigidity μ of the ice is $\sim 4 \times 10^{10}$ dynes cm^{-2} (a frequently quoted rigidity for ice). In the subsequent calculations, we will let $\delta \rightarrow 0$ in Equations (B.13)–(B.16) because it is clear from their form that the errors in the displacement field that are incurred by doing so are of $O(\delta)$, which is ~ 0.01 for a shell thickness of ~ 20 km.

The function $\frac{1}{R^3} P_2(\cos S)$ may be expressed as a series expansion in Legendre's associated functions and trigonometric functions of the orbital elements of a satellite (cf. Kaula, 1964). Such an expansion is in general quite complicated, but for a synchronously rotating satellite with completely damped physical librations and zero inclination it reduces to

$$\begin{aligned} \frac{1}{R^3} P_2(\cos S) = & \left(\frac{3}{4a^3} \right) P_{22}(\cos \phi) [3 \cos M \cos 2\lambda + 4 \sin M \sin 2\phi] \\ & - \left(\frac{3e}{2a^3} \right) P_{20}(\cos \phi) \cos M \end{aligned} \quad (\text{B.18})$$

when terms of order e^2 and higher are neglected. In Equation (B.18), e and M are the orbital eccentricity and the mean anomaly, respectively, and ϕ and λ are the colatitude and longitude of a point on the surface of the satellite, measured in the coordinate system where the axes of the minimum, intermediate, and maximum principal moments are directed along the x , y , and z axes, respectively.

The expressions (B.13)–(B.16) and (B.18) may be inserted into Equations (B.4)–(B.7) for the quantities Φ^+ , Φ^- , P^+ , and P^- . The results may then be inserted with (B.8)–(B.11) into Equation (B.3) to obtain the tidal displacement vector \vec{u} as a function of ϕ , λ , and M . If $t = 0$ when $M = 0$ (i.e. at periapse) M is simply

$$M = nt \tag{B.19}$$

The elements of the strain tensor ϵ_{ij} may be found from \vec{u} , using their defining relations in spherical coordinates (cf. Sokolnikov, 1956, Equations 48.17).

We write the results as follows:

$$\epsilon_{rr} = g_1 [\sin^2 \phi f(M, \lambda) - 2P_2(\cos \phi) \cos M] \tag{B.20}$$

$$\begin{aligned} \epsilon_{\phi\phi} = g_2 [2f(M, \lambda) \cos 2\phi + 6 \cos 2\phi \cos M] \\ + g_3 [\sin^2 \phi f(M, \lambda) - 2P_2(\cos \phi) \cos M] \end{aligned} \tag{B.21}$$

$$\begin{aligned} \epsilon_{\lambda\lambda} = g_2 [2(\cos^2 \phi - 2)f(M, \lambda) + 6 \cos^2 \phi \cos M] \\ + g_3 [\sin^2 \phi f(M, \lambda) - 2P_2(\cos \phi) \cos M] \end{aligned} \tag{B.22}$$

$$\epsilon_{\phi\lambda} = g_2 \cos \phi [8 \cos(2\lambda) \sin M - 6 \sin(2\lambda) \cos M] \tag{B.23}$$

$$\epsilon_{r\phi} = \epsilon_{r\lambda} = 0 \quad , \tag{B.24}$$

where

$$g_1 = - \left(\frac{60}{88} \right) (C_R \gamma e)$$

$$g_2 = \left(\frac{45}{88} \right) (C_R \gamma e)$$

$$g_3 = \left(\frac{165}{88} \right) (C_R \gamma e)$$

$$g_4 = - \left(\frac{120}{88} \right) (C_R \gamma e)$$

$$f(M, \lambda) = 3 \cos 2\lambda \cos M + 4 \sin 2\lambda \sin M \quad , \quad (\text{B.25})$$

and

$$\gamma = \frac{n^2 a^3}{GM_s} \quad (\text{B.26})$$

is the characteristic ratio of the magnitude of the rotational and tidal potentials to the magnitude of the potential due to self-gravity of the satellite. The factor C_R has been added in an ad hoc (though justifiable) manner to the expressions for the g_i to account for the fact that in this development it has assumed that the density of the entire satellite is uniform. As mentioned in the *Introduction*, Ross and Schubert (1987) have found that the amplitude of the tidal distortion of an ice shell on Europa is actually smaller by a factor of ~ 2 than is predicted by Peale and Cassen's model, because the self potential of the tidal bulge is dominated by the density of water rather than by Europa's average density. Thus, $C_R \simeq 0.5$. It may be verified that

$$\epsilon_{rr} + \epsilon_{\phi\phi} + \epsilon_{\lambda\lambda} = 0$$

as is necessary for an incompressible body. $\epsilon_{r\phi}$ and $\epsilon_{r\lambda}$ go to zero as $\delta \rightarrow 0$.

Note that the ϵ_{ij} do not depend on the rigidity of the shell. This is to be expected for $\delta \ll 1$, because a thin shell cannot affect the shape of the fluid hydrostatic surface on which it rests. Furthermore, because of the symmetry of the

tidal bulge, it is clear that volume elements lying along the principal-moment axes of the shell cannot be displaced horizontally during tidal flexing. To lowest order, the tidal displacements must be representable as second degree spherical harmonics. These constraints are sufficient to infer that the strains given by Equations (B.19)–(B.23) will apply to a thin, continuous shell of ice on Europa regardless of its rheology.

In the models of shell thickness presented in this paper, Equations (B.19)–(B.23) are used to obtain the quantity $\dot{\epsilon}_{ij}^2$. Although the time-averaged quantity $\overline{\dot{\epsilon}_{ij}^2}$ (used in the Maxwell model, Section 3) is expressible analytically, its form is very cumbersome and we do not display it here. The quantity $\overline{\dot{\epsilon}_{ij}^2}$ as a function of latitude and longitude on Europa is shown in Figure 1.

Acknowledgements

This work was supported by NASA Grant NAGW-185 of the Planetary Geophysics program.

References

- Cassen, P.M., Peale, S.J., and Reynolds, R.T. (1982). Structure and thermal evolution of the Galilean satellites. In *Satellites of Jupiter*, D. Morrison (ed.), University of Arizona Press, Tucson, pp. 93–128.
- Consolmagno, G.J. and Lewis, J.S. (1976). Structure and thermal models of icy Galilean satellites. In *Jupiter*, T. Gehrels (ed.), University of Arizona Press, Tucson, pp. 1035–1051.
- Danby, J.M.A. (1962). *Fundamentals of Celestial Mechanics*. The Macmillan Company, New York.
- Eirich, F.R. (1956). *Rheology: Theory and Applications*. Vol. I. Academic Press, New York.
- Goldreich, P. (1966). Final spin states of planets and satellites. *Ap. J.* **71**, 1–7.
- Greenberg, R. and Weidenschilling, S.J. (1984). How fast do the Galilean satellites spin? *Icarus* **58**, 186–196.
- Hobbs, P.V. (1974). *Ice Physics* Oxford University Press, London.
- Kaula, W.M. (1964). Tidal dissipation by solid friction and the resulting orbital evolution. *Rev. Geophys.* **2**, 661–685.
- Lambeck, K. (1980). *The Earth's Variable Rotation: Geophysical Causes and Consequences*. Cambridge University Press, Cambridge.
- Murase, T. and McBirney, A.R. (1973). Properties of some common igneous rocks and their melts at high temperatures. *Geol. Soc. Amer. Bull.* **84**, 3563–3592.

- Nye, J.F. (1957). The distribution of stress and velocity in glaciers and ice sheets. *Proc. Roy. Soc. London, Ser. A* **239**, 113–133.
- Ojakangas, G.W. and Stevenson, D.J. (1986). Episodic volcanism of tidally heated satellites with application to Io. *Icarus* **66**, 341–358.
- Ojakangas, G.W. and Stevenson, D.J. (1988). Polar wander of a synchronously rotating satellite with application to Europa. Submitted to *Icarus*.
- Paterson, W.S.B. (1981). *The Physics of Glaciers* Pergamon Press, Oxford, England.
- Peale, S.J. and Cassen, P. (1978). Contribution of tidal dissipation to lunar thermal history. *Icarus* **36**, 245–269.
- Pilcher, C.B., Ridgway, S.T., and McCord, T.B. (1972). Galilean satellites: Identification of water frost. *Science* **178**, 1087–1089.
- Ross, M.N. and Schubert, G. (1987). Tidal heating in an internal ocean model of Europa. *Nature* **325**, 133–134.
- Sabadini, R., Smith, B.K., and Yuen, D.A. (1987). Consequences of experimental transient rheology. *Geophys. Res. Lett.* **14**, 8116–819.
- Sacks, I.S. and Murase, T. (1983). *The Anelasticity of Peridotite and Partial Melt in the Asthenosphere*. Dept. Terrestrial Mag. Ann. Rep. 1982–1983.. Reprinted from *Carnegie Institution of Washington Year Book 82*, Washington, D.C., 509–512.

- Smith, J.C. and Born, G.H. (1976). Secular acceleration of Phobos and Q of Mars. *Icarus* **27**, 51–54.
- Sokolnikov, I.S. (1956). *Mathematical Theory of Elasticity, 2nd Ed.* New York.
- Squyres, S.W., Reynolds, R.T., Cassen, P., and Peale, S.J. (1983). Liquid water and active resurfacing on Europa. *Nature* **301**, 225–226.
- Thomas, P. and Schubert, G. (1987). Finite element models of non-Newtonian crater relaxation. *Proc. 17th LPSC. J. Geophys. Res.* **92**, 749–758.
- Turcotte, D.L. and Schubert, G. (1982). *Geodynamics.* Wiley, New York.

PAPER III**Polar Wander of a Synchronously Rotating
Satellite with Application to Europa**

Polar Wander of a Synchronously Rotating Satellite with Application to Europa

Gregory W. Ojakangas and David J. Stevenson

Division of Geological and Planetary Sciences

California Institute of Technology

Pasadena, California 91125

Submitted to: *Icarus*

May, 1988

Contribution number 4520 from the Division of Geological and Planetary Sciences,
California Institute of Technology, Pasadena, California 91125.

Abstract

An ice shell on Europa that is decoupled from the silicate core by a layer of liquid water has a thermal-equilibrium thickness profile that varies with position over its surface, because of spatial variations in the surface temperature and tidal dissipation within the ice (see previous paper). The second spherical harmonic degree components of these thickness variations and of any fossil rotational and tidal bulges present on the shell contribute to the inertia tensor of the body. The problem is that of a planetary elastic lithosphere that is topographically loaded from below. Following the development of Willemann and Turcotte (1981) we develop equations describing the variations in the inertia tensor of a body, which are caused by the addition of second harmonic degree topography to the base of the crust. Applied to the case of an ice shell on Europa, it is found for many choices of parameters that a state of thermal equilibrium for the shell will involve an orientation of Europa's principal axes of inertia (when the hydrostatic bulges are relaxed), which is unusual for a synchronously rotating satellite. Specifically, the intermediate and maximum principal moments are reversed. To reach the preferred orientation for synchronous satellites, a thermal equilibrium ice shell must execute a net reorientation of ninety degrees about the satellite-planet direction. We present a simple model of a rigid, synchronously rotating satellite in a circular orbit for which the difference between the intermediate and maximum principal moments is linear in time, passing through zero when $t = 0$. The model demonstrates that the expected reorientation is indeed dynamically favored.

We then consider a more realistic model, including the effects of various torques which act to couple the motions of the core, shell, and liquid water layer, as well as the effect of viscous dissipation which arises in the shell due to the predicted

polar wander. It is found that the Poincaré torque, gravitational coupling, and the torque due to viscous shear in the liquid water layer are unable to induce significant motion of the core during polar wander of the shell. However, the Poincaré torque exerted on the liquid water layer by the shell is believed to cause the liquid water layer to reorient in coincidence with the shell. The model suggests that viscous friction in the shell eliminates the possibility that polar wander will occur unless preexisting fractures (e.g., due to tidal stresses (Crawford and Stevenson, 1988)) extend from the surface to a depth where the ice behaves viscously on the polar wander time scale. If the temperature T_f at the base of the fractured region is as high as $\sim 140\text{--}145$ K, the model indicates that polar wander occurs on a time scale of $10^6\text{--}10^5$ y (shorter as T_f increases) after the sign of the difference between the maximum and intermediate principal moments reverses. In the absence of dissipation, polar wander would occur in $\sim \text{few} \times 10^3$ y. Polar wander must occur on a time scale significantly shorter than $\sim 10^7$ y, or the thickness profile of the ice will be in continuous equilibrium with its thermal environment regardless of its orientation, and the mechanism driving the polar wander will be virtually eliminated. It is likely that events of large scale polar wander occur episodically, separated in time by periods on the order of the time scale for thermal diffusion through the shell ($\sim 10^7$ y), although a state of slow, continuous drifting of the pole is also possible. The time scale of viscous flow of topography at the base of the ice is also near 10^7 y. If dissipation in the shell due to polar wander is a few orders of magnitude smaller than our simple model suggests, polar wander as described here is a much more effective means for fracturing the ice than is tidal flexing, and it may contribute to producing the observed global fracture systems in Europa's ice.

1. A Review of Polar Wander

The term “polar wander” refers to a secular motion of the surface of a planetary body with respect to its axis of rotation. True polar wander is to be distinguished from free precession and from the forced precession of a planet’s axis of rotation in space, due to torques exerted by the sun and other bodies on its rotational bulge. Both free precession and forced precession result in movements of the rotation axis with respect to the surface of the body, but these movements are very small and do not have secular components. All freely rotating bodies in which dissipation occurs will ultimately reside in the state of minimum total energy. Since the minimum energy for any freely rotating body involves rotation purely about the maximum principal axis of inertia, true polar wander of such a body must involve a change in the orientation of that axis with respect to the body. If the magnitude as well as the orientation of the maximum principal moment changes, polar wander must be accompanied by dissipation of energy.

The idea that the rotation axis of the earth may have drifted by large amounts over its surface during geologic time has been in existence at least since the nineteenth century (cf. Darwin, 1877). Equally old is the realization that the earth’s rotational bulge inhibits polar wander to the extent that it remains rigid during the reorientation process. If the earth’s rotational bulge were perfectly rigid, large scale polar wander would require the emplacement, somewhere on or within the earth, of a mass comparable to that contained in the rotational bulge — a girdle of mass some twenty kilometers high encircling the entire earth, with large latitudinal extent.

Darwin argued that that the earth’s rotational bulge was rigid, and therefore that substantial polar wander was implausible. Subsequently, it became widely

realized that the bulk of the interior of the earth could not possess substantial long-term strength because of the high degree of isostatic compensation of the earth's topographic features, inferred from the small magnitude of gravity anomalies and the absence of correlation of gravity anomalies with topography.

Although implicit in earlier work (cf. Milankovich, 1934), T. Gold clearly pointed out (Gold, 1955) that a truly fluid or "plastic" earth would reorient upon emplacement of an arbitrarily small disturbing mass, so that such a mass would be translated from its initial latitude to the equator. Goldreich and Toomre (1969) demonstrated that relatively slow motions of many small masses distributed over the surface or interior of such a fluid earth can cause relatively rapid motions of the principal axes with respect to the earth. In addition, they showed that the angle between the axis of the maximum principal moment and the angular momentum vector is preserved during such motions, when the motion of the axis of the maximum principal moment is slow compared to free precession. Recent work, based primarily on paleomagnetic data, indicates substantial amounts of polar wander of the earth have occurred on a geologic time scale (Gordon, 1987). While Gold was certainly correct in asserting that a fluid behavior for the bulk of the earth's interior greatly increases the potentiality for polar wander, the work of Vening Meinesz (1947) had already shown that the presence of an elastic lithosphere on a fluid planet with a rotational bulge provides a substantial hindrance to polar wander, since energy of elastic strain must be stored in such a lithosphere during any re-orientation. Munk and MacDonald (1960) presented a summary of the debate over the question of polar wander for the earth up until that time, as well as substantial additional work on the problem. They briefly considered the effects of an elastic lithosphere, which they parameterized as an equivalent surface tension. While such

an approach is instructive, it does not quantitatively reproduce the effects of an elastic lithosphere on polar wander.

It is now widely accepted that terrestrial planetary bodies have thin outer layers (or "lithospheres"), which behave elastically on geologic time scales, as well as interiors that behave fluidly on similar time scales. Two examples are the moon and Mars, both of which have large near-surface loads that have remained incompletely compensated over geologic time. In the case of the moon the load is associated with the mare or mascons, and in the case of Mars the best example is the Tharsis bulge. The incomplete compensation has been attributed to elastic support, implying the existence of an outer shell that behaves elastically on a geologic time scale (cf. Willemann and Turcotte, 1981).

In the light of the plate tectonic revolution, it is clear that a continuous elastic lithosphere does not exist on the earth. However, a planetary model consisting of a thin, continuous elastic lithosphere overlying a fluid interior may well be the most reasonable and simple one with which to investigate the possibility of polar wander of many planetary bodies.

Willemann (1984) derived quantitative results for the amount of polar wander that a freely rotating body of such a nature would experience after a disturbing mass of a given magnitude is emplaced at a given colatitude. In his model, the unstressed shape of the lithosphere is that of a hydrostatic fluid, i.e., the oblate ellipsoidal figure of a fluid in equilibrium with self-gravitational and rotational potentials. This is certainly appropriate if the planet cooled sufficiently for an outer layer to become elastic while it was rotating, or if all previous nonhydrostatic stresses had been effectively relieved by fractures that were subsequently annealed or cemented by intrusions. A small fraction of the original hydrostatic bulge remains fixed with

respect to the planet's surface as polar wander proceeds, while the greater portion responds in a fluid manner, remaining symmetric about the direction of the rotation vector. It is this (typically) small "fossil" rotational bulge, present because of the elastic nature of the lithosphere, which prohibits the disturbing mass from being translated all the way to the equator, as in Gold's model. Willemann calculates the amount of reorientation by diagonalizing the inertia tensor of the sum of the fossil bulge and the disturbing mass. The effect of the emplaced disturbing mass on the inertia tensor is reduced by a factor $(1 - C_w)$ (explained below), which takes into account the degree of isostatic compensation of a mass emplaced on an elastic lithosphere.

2. Introduction

The purpose of this paper is several-fold. First, we wish to point out an effect on the inertia tensor of a planetary body which Willemann appropriately ignores in his work, but which can be very important in some polar wandering scenarios. We will then describe one such scenario: that of a planet with an elastic lithosphere which is topographically loaded from below. We will describe how this scenario applies to the question of polar wander of Europa, caused by spatial variations in the thickness of an ice shell overlying a liquid water ocean on that moon. The possibility of such polar wander of Europa will be examined in three steps: first we will demonstrate that the combined effects of spatial variations in the thickness of such an ice shell and the fossil bulge of the ice shell on Europa's inertia tensor may result in an orientation of its principal moments which is unusual for a synchronously rotating satellite. Second, we will demonstrate that reorientation of such a body toward the usual orientation for synchronous satellites is favored from a dynamical

perspective by developing and solving equations of motion for a simple body whose inertia tensor evolves in time in the manner described in the first step.

Third, we will approach the problem more realistically by considering the dynamics of the three-component system on which this model of Europa depends: an ice shell and a silicate core, separated by a layer of liquid water. Various torques act to couple the motions of the core, the shell, and the liquid layer during polar wander of Europa. We present a model of polar wander of Europa's shell, in which it is assumed to reorient independently of the core, impeded only by dissipation within the shell itself. The liquid water layer is assumed to reorient in coincidence with the ice shell so that the shell and the liquid behave as a single entity. Using the results of our model, we justify these assumptions a posteriori in Appendix A by arguing that none of the coupling torques are able to induce appreciable motion of the core during polar wander of the shell but that the Poincaré torque exerted on the liquid layer by the shell probably causes the liquid layer to reorient in coincidence with the shell. Finally, we discuss the implications of the modeling presented here to the problem of fracturing Europa's ice.

3. The Iceberg Effect

The previously ignored effect alluded to above we will call simply the "iceberg effect", as it is best exemplified by the illustration of an ocean that is covered with icebergs compared to the same ocean when the icebergs have all melted (cf. Munk and MacDonald, 1960, Section 5.9). The iceberg-laden ocean contributes more to the inertia tensor, because the ice is slightly farther from the axis of rotation, on average, than the water from which it formed.

The manner in which the iceberg effect contributes to the problem of a

topographic load emplaced on an elastic lithosphere can be demonstrated by the following extreme cases. In the following examples, the mass represented by the topography t may be thought of as having been removed from near the poles (where its absence does not affect the polar moment of inertia) and emplaced near the equator.

When the rigidity of the lithosphere is very large (Figure 1), the load is rigidly supported without deflection of the lithosphere and the contribution of the emplaced mass to the polar moment of inertia of the planet is

$$\Delta I_{\text{lithosphere}}^{\text{rigid}} \sim R^4 \rho_c t, \quad (3.1)$$

where R is the radius of the top of the crust, ρ_c is the density of the crust (assumed to be the same as the density of the disturbing mass), ρ_m is the density of the mantle, t is the total thickness of the emplaced mass, and b_c is the thickness of the crust. It is assumed that $t \ll b_c \ll R$, for simplicity. It is also assumed that the areal extent of the topographic load is $\sim R^2$ (true for second degree loads).

In the limit where the lithosphere possesses no rigidity, the situation is as depicted in Figure 2. Now the topography t is distributed above and below the crust according to the principle of isostasy, i.e. (see Figure 2), $X_1 = \left(\frac{\Delta\rho}{\rho_m}\right)t$ and $X_2 = \left(\frac{\rho_c}{\rho_m}\right)t$. The contribution of the topography to the inertia tensor is much smaller than in the case of rigid support, but it is nonzero. Adding the effects of the topography protruding above and below the surrounding crust,

$$\Delta I_{\text{lithosphere}}^{\text{zero rigidity}} \sim \rho_c X_1 R^4 - \Delta\rho X_2 R^2 (R - b_c)^2 \approx \Delta\rho \frac{\rho_c}{\rho_m} R^4 t \left(\frac{2b_c}{R}\right). \quad (3.2)$$

The contribution of the topography t to the moment of inertia is smaller by a factor $\left(\frac{\Delta\rho}{\rho_m}\right) 2 \left(\frac{b_c}{R}\right)$ in the case of perfect isostatic compensation compared to the case of rigid support.

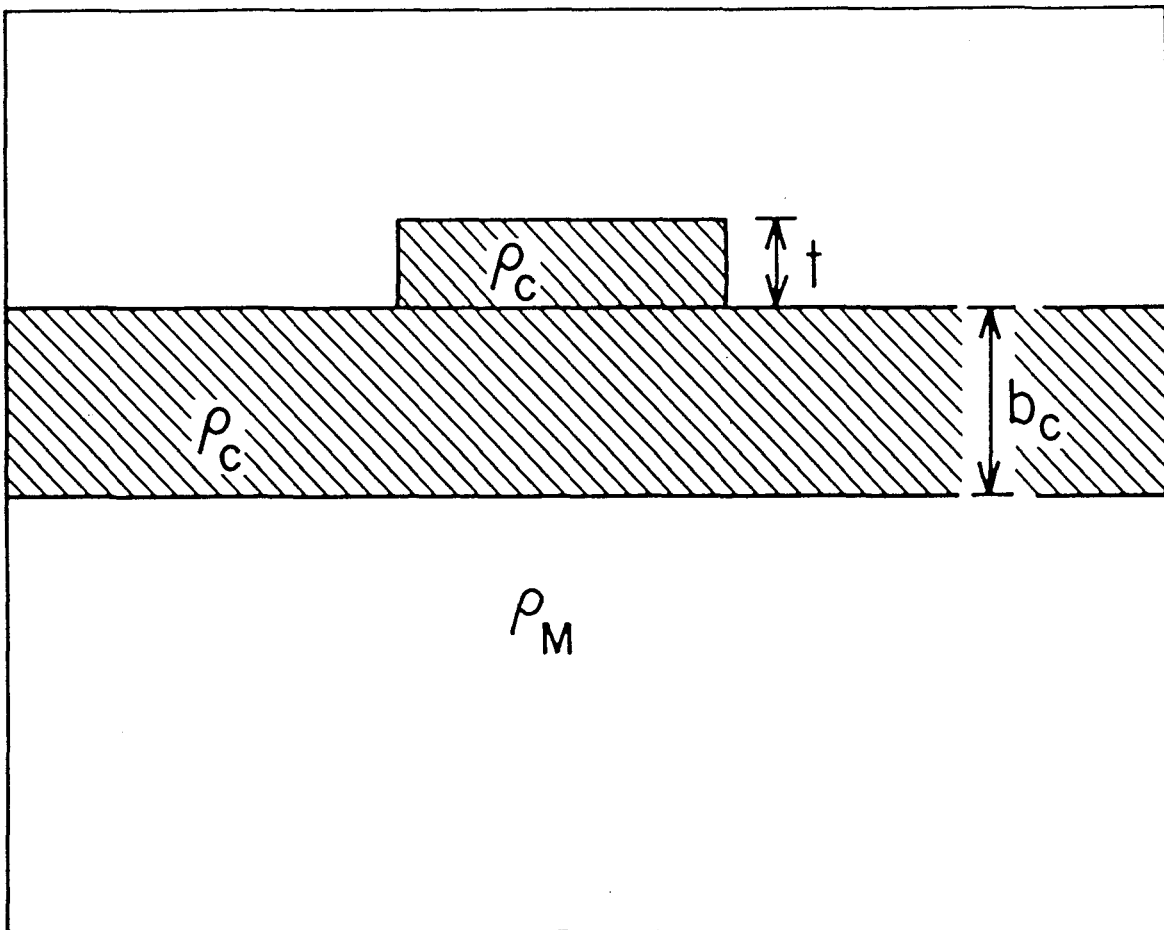


Figure 1. Loading of an elastic lithosphere from above by topography of thickness t , in the limit where the lithosphere possesses infinite rigidity.

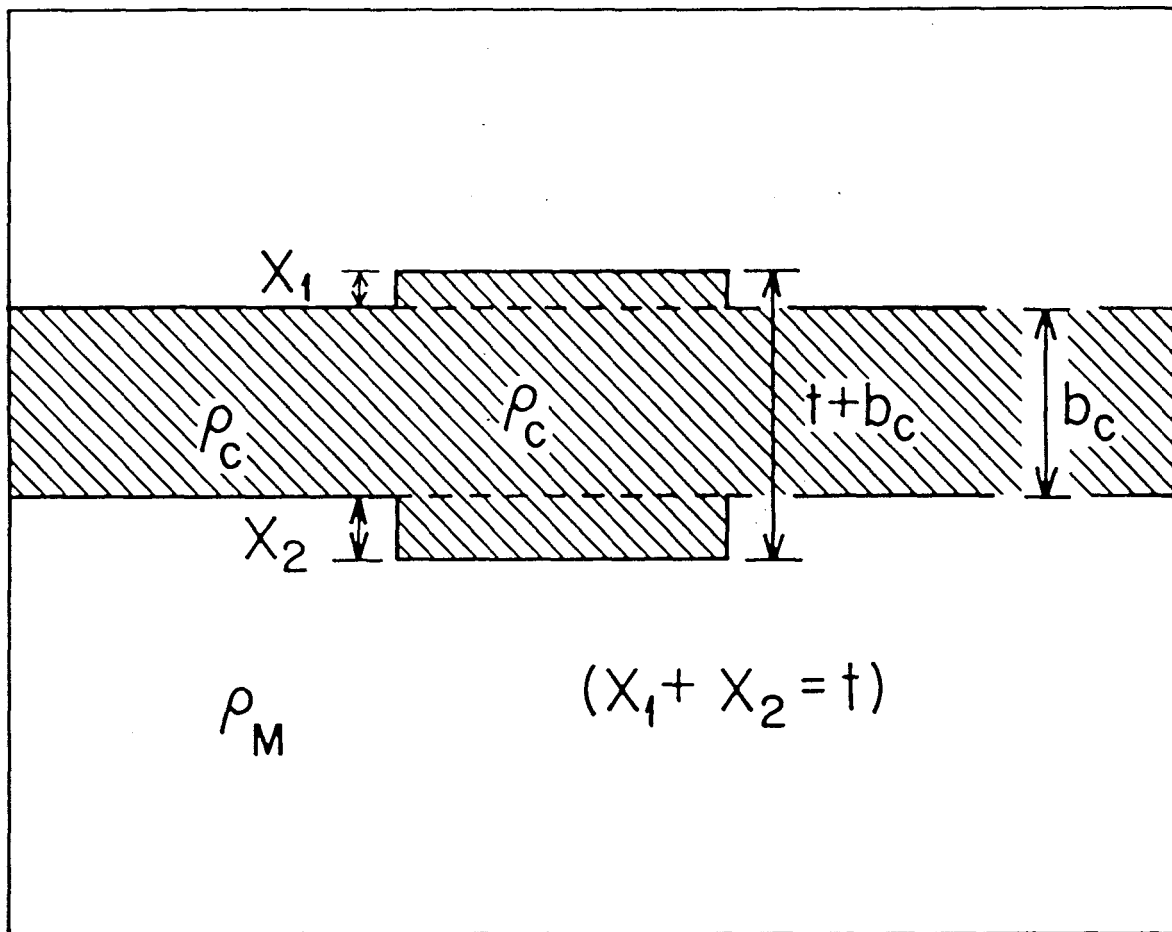


Figure 2. Response of a lithosphere to loading from either above or below, in the limit where the rigidity of the lithosphere goes to zero.

Now consider the case where topography of density ρ_c is added to the base of the crust rather than to the upper surface. Such a situation might occur upon emplacement of a deep-seated igneous intrusion or batholith. We will argue that this is the type of loading experienced by an ice shell overlying a water ocean on Europa, as the ice attempts to equilibrate to a changing thermal environment.

Figure 3 depicts the case where the rigidity of the lithosphere is very large. The topography is rigidly confined below the crust and the contribution of the emplaced mass to the inertia goes as

$$\Delta I \sim -\Delta\rho t R^2 (R - b_c)^2 \approx -R^4 \Delta\rho t \left[1 - 2 \frac{b_c}{R} \right]. \quad (3.3)$$

When the lithosphere has no rigidity, we again have the situation shown in Figure 2. To lowest order, the inertia contribution for the fluid case is smaller than for rigid support by a factor $\left(\frac{\rho_c}{\rho_m}\right) 2 \left(\frac{b_c}{R}\right)$.

Two important differences are evident in the case of bottom loading versus top loading: Firstly, the contribution of the added topography to the inertia (for bottom loading) must change sign (becoming positive) as the rigidity of the lithosphere goes to zero. Secondly, the iceberg effect is larger in comparison to rigid support by a factor of $\frac{\rho_c}{\Delta\rho}$ in the case of bottom loading. We shall see that when the rigidity of the lithosphere is finite and of a reasonable magnitude, the iceberg effect may dominate in some real problems.

3.1 Development with Finite Rigidity

Only the second degree spherical harmonic components of topography contribute to the inertia tensor. We now present the contribution of these components to the moment of inertia of a planet about the axis of the pole of the harmonics, when the rigidity of the lithosphere is finite and nonzero. We follow the development

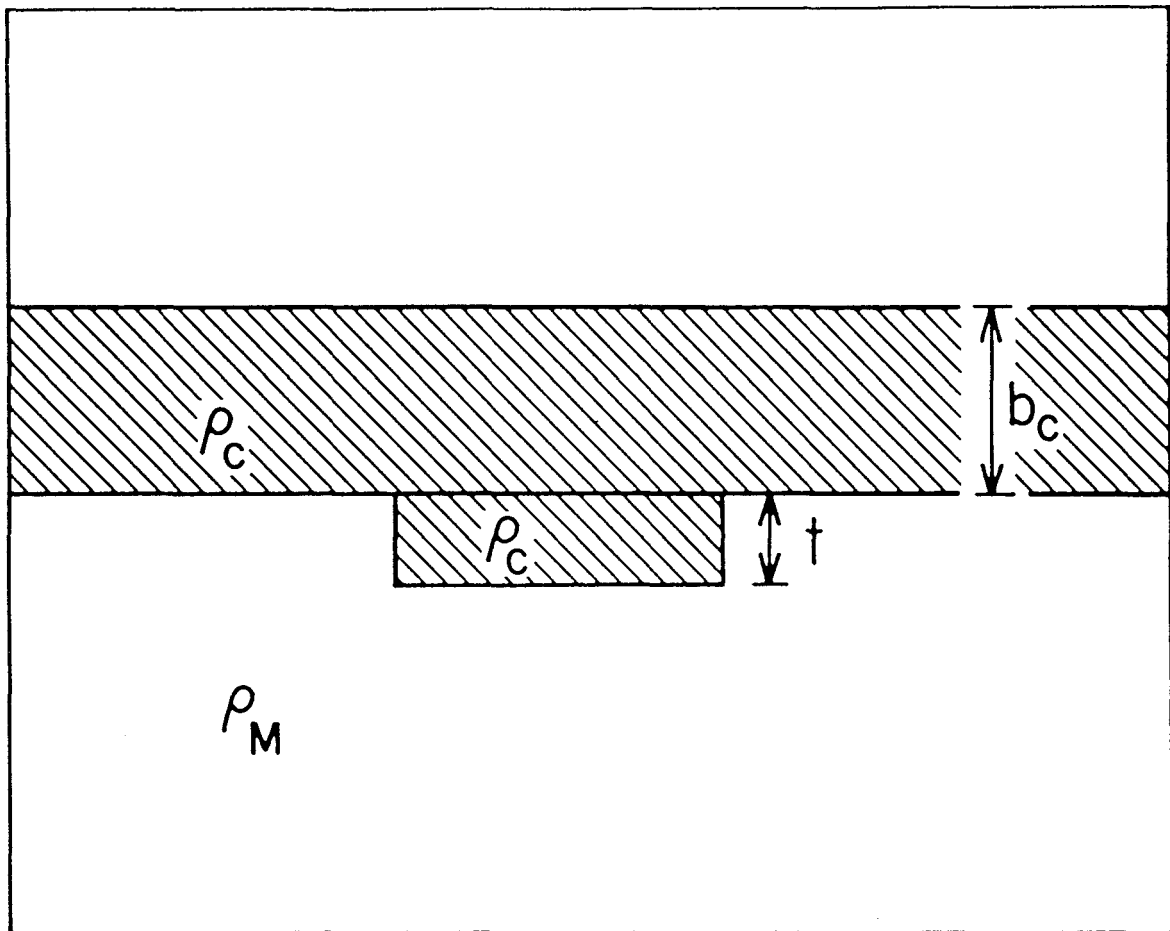


Figure 3. Loading of an elastic lithosphere from below by topography of thickness t , in the limit where the lithosphere possesses infinite rigidity.

of Turcotte et al. (1981).

Loading from Above

Consider the usual case of loading from above. The effect on the external gravity field of a second harmonic degree mass distribution h_{2M} of density ρ_c at the surface of the planet, and another, w_{2M} , of density $-(\rho_m - \rho_c)$ at the base of the crust is given by Jeffreys (1976), Equation 5.06.01:

$$U = \frac{-GM}{r} \left(\frac{a}{r}\right)^2 \frac{3}{5\bar{\rho}a} \left[h_{2M}\rho_c - \left(1 - \frac{b_c}{a}\right)^4 (\rho_m - \rho_c)w_{2M} \right] , \quad (3.4)$$

where G , M , $\bar{\rho}$, and a are the gravitational constant, the mass, the average density, and the average radius of the planetary body, respectively, and r is distance measured from the body's center. All other constants are as defined previously.

h_{2M} represents the amount of topography remaining after the addition of a column of mass of height

$$t_{2M} = h_{2M} + w_{2M} \quad (3.5)$$

to the surface, and w_{2M} represents the resulting displacement of the base of the crust. Turcotte et al. (1981) found that w_{2M} is related to h_{2M} by

$$(\rho_m - \rho_c)w_{2M} = \rho_c h_{2M} C , \quad (3.6)$$

where

$$C = \frac{1}{1 + \frac{\tau_o}{\Delta\rho \left(1 - \frac{3\rho_m}{5\bar{\rho}}\right)}} \quad (3.7)$$

$$\tau_o = 8 \left(\frac{1+\nu}{5+\nu}\right) \mu' \left(\frac{d}{a}\right) \bar{\rho} \quad \mu' = \frac{\mu}{\bar{\rho}ga} .$$

ν , μ , and d are the Poisson's ratio, rigidity, and thickness of the lithosphere, respectively, and g is the planet's surface gravity. $\Delta\rho$ is the density difference that would support the load in the absence of elasticity. In the case of loading from above, it is simply $\Delta\rho = \rho_m - \rho_c$. In obtaining the above expressions, only membrane stresses are assumed to be important; bending stresses have been ignored. Their effects are small compared to those of membrane stresses as long as $\left(\frac{d}{a}\right)^2 \ll 1$.

From Equations (3.4)–(3.7), the C_{2m} components of the gravity field due to the topography are seen to be

$$C_{2m} = Q_{2m} \left[\frac{(1 - C) + 4 \left(\frac{b_c}{c}\right) C}{1 + \frac{\rho_c}{\Delta\rho} C} \right], \quad (3.8)$$

where

$$Q_{2m} = \frac{3\rho_c t_{2m}}{5\bar{\rho}a} \quad (3.9)$$

is a convenient measure of the magnitude of the topographic load.

Equation (3.8) may be written more conveniently in Willemann's notation (Willemann, 1984) as

$$C_{2m} = Q_{2m} \left[(1 - C_w) + 4C_w \frac{b_c}{a} \frac{\Delta\rho}{\rho_m} \right], \quad (3.10)$$

where

$$C_w = \frac{1}{1 + \frac{\tau_a}{\rho_m \left[1 - \frac{3}{5} \frac{\rho_m}{\rho}\right]}}. \quad (3.11)$$

The C_{2m} may be related to the diagonal inertia tensor components about the polar axis of the harmonics by

$$I_{xx} = I' + Ma^2 \left(\frac{C_{20}}{3} - 2C_{22} \right) \quad (3.12)$$

$$I_{yy} = I' + Ma^2 \left(\frac{C_{20}}{3} + 2C_{22} \right) \quad (3.13)$$

$$I_{zz} = I' - \frac{2}{3} Ma^2 C_{20} \quad (3.14)$$

(cf. Lambeck, 1980), where I' is the average moment of inertia.

When the topography of interest is a localized disturbing mass as in Willemann's development (e.g., a "mountain"), its effect on the gravity field is easiest to describe in the coordinate system where the mass is at the pole of the harmonics. Then the only nonzero second degree component is C_{20} .

Equation (3.10) with $m = 0$ is identical to Equation (19) of Willemann (1984) except for the additional term due to the iceberg effect.

Loading from Below

Now we consider the case where the topography t_{2m} is added to the base of the crust. The external gravity field due to this topography is

$$U = \frac{-GM}{r} \left(\frac{a}{r} \right)^2 \frac{3}{5\bar{\rho}a} \sum_{m=1}^2 \left[\rho_c w_{2M} - \left(1 - \frac{b_c}{a} \right)^4 (\rho_m - \rho_c) h_{2M} \right] , \quad (3.15)$$

where h_{2m} is the amount of topography remaining after equilibrium is reached, and w_{2m} is the amount that the surface has risen in response to the load. Again, the total amount of topography added is $t_{2m} = h_{2m} + w_{2m}$. The equation analogous to (3.6) in this case is

$$\rho_c w_{2m} = (\rho_m - \rho_c) h_{2m} C , \quad (3.16)$$

where C is given by (3.7).

In this case, since the load is from below, the effective density that would “support” it in the absence of elasticity is simply $\Delta\rho = \rho_c$, the density of the resulting topographic response, w_{2M} , at the surface. Equations (3.5), (3.7), (3.15), and (3.16) now give

$$C_{2m} = Q_{2m} \left(\frac{\rho_m - \rho_c}{\rho_c} \right) \left[\frac{-(1 - C) + 4 \frac{b_c}{a}}{1 + \frac{(\rho_m - \rho_c)}{\rho_c} C} \right], \quad (3.17)$$

which may be written using Equation (3.11) as

$$C_{2m} = Q_{2m} \left(\frac{\rho_m - \rho_c}{\rho_c} \right) \left[-(1 - C_w) + 4 \frac{b_c}{a} \left(1 - \frac{(\rho_m - \rho_c)}{\rho_m} C_w \right) \right]. \quad (3.18)$$

Equations (3.12), (3.13), and (3.14) may again be used to convert C_{2m} to contributions to the inertia tensor.

Note that Equations (3.10) and (3.18) have the correct limits: When the rigidity of the lithosphere goes to zero, $C_w \rightarrow 1$ and the iceberg effect (Equation (3.2)) is obtained in both cases (once Equations (3.12)–(3.14) are used to convert the C_{2m} to an effect on the inertia). Similarly, when the rigidity becomes infinite, $C_w \rightarrow 0$ and the results given by Equations (3.1) and (3.4) for rigid support of loads are recovered. Also, when $\rho_m \rightarrow \rho_c$ there is no density contrast associated with the topography at the base of the crust, so that there is no load on the lithosphere for the case of loading from below, and consequently no effect on the inertia.

4. An Ice Shell on Europa: A Case of Loading from Below

The following discussion requires that Europa possess a substantial mantle of water overlying its silicate interior, a significant portion of which is liquid at depth. A brief summary of the debate over whether such a configuration is likely for Europa is given in the paper “Thermal State of an Ice Shell on Europa” (hereafter referred

to as “Paper 1”). There we conclude that when the temperature–dependence of the tidal dissipation within the ice is considered, a liquid layer will probably persist if it ever existed at all. Detailed calculations of plausible thickness profiles of such a shell are also presented in Paper 1. We demonstrate in this section that the likely spatial variations in the thickness of the shell add a component to Europa’s inertia tensor that may lead to an orientation of the principal axes which is unusual for a synchronous satellite. Enroute to that conclusion, we show how topographic loading of an elastic lithosphere from below applies to the case of an ice shell on Europa, the importance of the iceberg effect in the problem, and the manner in which a fossil bulge on the shell also contributes to the inertia tensor. The question of whether the inertia variations described here lead to polar wander is treated in the following sections. In Paper 1 we show how variations in tidal dissipation and solar insolation over the shell cause it to vary in thickness with both latitude and longitude in its equilibrium state. For purposes of illustration, imagine that at some time an unstressed ice shell existed over a liquid water ocean on Europa, but that the thickness of the shell differed substantially from the equilibrium profile (we will argue later that this may be the situation after an episode of polar wander on Europa). The ice at the base of the shell would then begin to melt in some regions and grow thicker in others, approaching the equilibrium profile in the characteristic time required for heat to diffuse through the ice (\lesssim a few times 10^7 years for a shell of thickness 20 km). Thus, topography would be added to the base of the ice, and this is a case of topographic loading of a crust (in this case, the ice shell) from below.

The importance of the iceberg effect in this problem can be appreciated by inserting the appropriate numbers into Equation (3.18), recalling that the first and

second terms in that expression represent elastic support and the iceberg effect, respectively. One important difference between the problem at hand and more standard problems of topographic loading (such as the Tharsis bulge on Mars) is that in this case the crust is thicker than the lithosphere. The crust may be identified with the entire ice shell. We define the lithosphere as that region of the shell that behaves elastically on the time scale during which the crust is loaded. The Maxwell time τ_M , defined as

$$\tau_M = \frac{\eta}{\mu} \quad , \quad (4.1)$$

where η is the dynamic viscosity and μ is the rigidity, is the characteristic time scale which separates elastic behavior from viscous behavior in materials possessing both elastic and viscous properties (cf. Eirich, 1956). Using a typical rheological law for the viscosity of ice, a rigidity of 4×10^{10} dynes cm^{-2} , and temperature profiles typical of those given in Paper 1, the Maxwell time of the ice is longer than the diffusion time through the shell for typically the outer ten percent of shell. From Paper 1, the average thickness of an ice shell on Europa is typically about 20 km. Therefore, 20 km and 2 km are representative values for the shell thickness, b_c , and the lithosphere thickness, d , respectively. When these values are inserted into Equation (3.18), with appropriate values for the density of water (ρ_m), the density of ice (ρ_c), the surface gravity, average density, and average radius of Europa, and values for the Poisson's ratio and rigidity of ice of 0.33 and 4×10^{10} dynes cm^{-2} , respectively, it is found that the term due to the iceberg effect is almost an order of magnitude larger than the term representing elastic support. Thus, the iceberg effect is more important than elastic support for an ice shell on Europa, and variations in ice thickness of the second spherical harmonic degree are accompanied by geoid anomalies of the same sign.

It is convenient to describe the inertia tensor of Europa in the right-handed coordinate system, fixed in the body, which, before polar wander, has its origin at the Europa's center, the X-axis directed toward Jupiter, and the Z-axis perpendicular to the orbit (i.e., along the usual rotation axis). Since the variations in ice thickness are due to tidal dissipation and solar insolation, both of which possess symmetry about all three coordinate planes in this coordinate system, the equilibrium thickness profile possesses these symmetries as well (see Paper 1). The second degree spherical harmonic components of the ice thickness profile contribute to the inertia tensor in the same manner as does a localized disturbing mass. However, because of the inherent triaxial symmetry, this contribution is equivalent to that of three pairs of disturbing masses, of the appropriate sizes, arranged initially at the poles, the sub- and anti-Jupiter points, and the apices of the satellite. Moreover, since Europa is a synchronously rotating body, its hydrostatic figure is distinctly triaxial, and therefore any fossil bulge on the lithosphere will be triaxial as well.

Another important difference from the case of a disturbing mass such as the Tharsis bulge on Mars is that in the problem at hand, the symmetry requires that the principal axes of inertia do not move with respect to the body's surface as a thermal equilibrium thickness profile is approached from, say, a state of constant ice thickness. Instability can occur only if the relative magnitudes of any pair of principal moments are reversed as equilibrium is approached. By contrast, Mars must have begun reorienting as soon as the growth of Tharsis was initiated, unless the infinitely improbable situation prevailed in which the bulge was grown exactly at the previous rotational pole.

The usual state of dynamic equilibrium for any satellite (if it exists) is one in which the body is synchronously rotating, with the minimum, intermediate, and

maximum moments of inertia aligned along the direction toward the parent planet, the tangent to the orbit, and the normal to the orbit, respectively (cf. Danby, 1962). Thus the orientation of Europa's principal axes of inertia will be unusual (suggesting the possibility of polar wander) if $I_{xx} > I_{zz}$, $I_{xx} > I_{yy}$, or $I_{yy} > I_{zz}$, in the coordinate system described previously. In order to determine whether any of these possibilities are likely to come about on Europa as a result of thermal evolution, Equations (3.12)–(3.14) may be used to relate the three possible unstable states to the gravity field. We thus obtain:

$$I_{xx} > I_{zz} \quad : \quad C_{20} - 2C_{22} > 0 \quad (4.2)$$

$$I_{xx} > I_{yy} \quad : \quad -4C_{22} > 0 \quad (4.3)$$

$$I_{yy} > I_{zz} \quad : \quad C_{20} + 2C_{22} > 0 \quad (4.4)$$

In the spirit of Willemann's development (Willemann, 1984) C_{20} and C_{22} may each be considered to consist of a component due to the presence of the fossil bulge, and a component due to the second degree variations in ice thickness. In Paper 1, the second degree components of ice thickness are given for each of the profiles presented. These may be translated into second degree components of the gravitational field using Equation (3.18). In addition to the effects of ice thickness, a thin continuous elastic shell of ice will possess a fossil bulge that contributes to the inertia and must be included in any calculation of the body's inertia tensor.

It will be noted that the presence of a fossil bulge tends to stabilize the system, since it has the form of a hydrostatic bulge with proportionately attenuated semi-major axes. A (rigid) body with a figure that is hydrostatic under the tidal and rotational potentials of a synchronously rotating satellite is, of course, stable.

By comparison with the semimajor axes of a fluid synchronously rotating moon of constant density as given by Jeffreys (1976) Equation (4.08.13), it is easily

seen that the surface of a synchronous hydrostatic moon may be written

$$r = a [1 + \epsilon_{20} Y_{20}(\phi) + \epsilon_{22} Y_{22}(\phi, \lambda)] \quad , \quad (4.5)$$

where

$$\begin{aligned} \epsilon_{20} &= \frac{-5}{6} h\gamma \\ \epsilon_{22} &= \frac{1}{4} h\gamma \end{aligned} \quad (4.6)$$

and Y_{2m} are the unnormalized spherical harmonic functions

$$\begin{aligned} Y_{20} &\equiv \frac{1}{2} (3 \cos^2 \phi - 1) \\ Y_{22} &\equiv 3 \sin^2 \phi \cos 2\lambda \quad . \end{aligned} \quad (4.7)$$

ϕ is colatitude measured from the rotational pole and λ is longitude measured from the subplanet point. h is the second degree Love number that relates the response of the surface to a second degree disturbing potential (cf. Munk and MacDonald, 1960).

The fossil bulge is the bulge that would remain if rotational and tidal potentials were removed. The ratio of the vertical deflection of an elastic lithosphere under the load of a second degree potential to the vertical deflection of a fluid planet under the same load is C_w (Willemann and Turcotte, 1981), as given by Equation (3.11). Therefore, if the rotational and tidal potentials were removed, the surface deformation written as in Equation (4.5) would be described by

$$\begin{aligned} \epsilon_{20}^{\text{fossil bulge}} &= \frac{-5}{6} h\gamma(1 - C_w) \\ \epsilon_{22}^{\text{fossil bulge}} &= \frac{1}{4} h\gamma(1 - C_w) \quad . \end{aligned} \quad (4.8)$$

The fossil bulge may be thought of as two topographic components, one at the surface and one at the base of the crust, both of which have magnitudes given

by Equation (4.8), with densities ρ_c and $(\rho_m - \rho_c)$, respectively. With this in mind, Equation (5.06.01) of Jeffreys (1976) may then be used to obtain the effect of the fossil bulge on the gravity field:

$$U = \frac{-GM}{r} \left(\frac{a}{r}\right)^2 \frac{3}{5\bar{\rho}a} \sum_{m=1}^2 \left[a\rho_c \epsilon_{2m} \right]_{\text{fossil bulge}} + \left(1 - \frac{b_c}{a}\right)^4 (\rho_m - \rho_c) a \epsilon_{2m} \left. \right]_{\text{fossil bulge}} \quad (4.9)$$

To lowest order, the second degree gravity components are therefore:

$$\begin{aligned} C_{20} \left. \right]_{\text{fossil bulge}} &= \frac{3}{5} \frac{\rho_m}{\bar{\rho}} \epsilon_{20} \left. \right]_{\text{fossil bulge}} = -\frac{1}{2} h\gamma \left(\frac{\rho_m}{\bar{\rho}}\right) (1 - C_w) \\ C_{22} \left. \right]_{\text{fossil bulge}} &= \frac{3}{5} \frac{\rho_m}{\bar{\rho}} \epsilon_{22} \left. \right]_{\text{fossil bulge}} = \frac{3}{20} h\gamma \left(\frac{\rho_m}{\bar{\rho}}\right) (1 - C_w) \quad . \end{aligned} \quad (4.10)$$

Because of large maxima in the ice thickness profiles at the sub- and anti-Jupiter points (cf. Figure 2 of Paper 1), the $\ell = 2$, $m = 2$ component of the ice thickness is always a positive quantity in the models presented in Paper 1, while the $\ell = 2$, $m = 0$ component is always negative. Since harmonic components of ice thickness have corresponding components of gravity of the same sign, it is evident from Equations (4.2) and (4.3) that the situations where $I_{xx} > I_{zz}$ or $I_{xx} > I_{yy}$ cannot occur as a result of variations in ice thickness, in the context of our models. However, for a wide range of reasonable parameters, we shall now see that I_{yy} is greater than I_{zz} for thickness profiles representing thermal equilibrium.

If the fossil bulge of the shell and the spatial variations in ice thickness are the only important rigid components of the inertia tensor, Equations (3.18) and (4.10) may be summed (to obtain the total C_{2m}) and inserted into Equation (4.4), giving a criterion which the thickness variations t_{20} and t_{22} must satisfy so that $I_{yy} > I_{zz}$:

$$\left[\frac{(t_{20} + 2t_{22})}{a} \right] \left(\frac{3(\rho_m - \rho_c)}{h\gamma\rho_m} \right)$$

$$\times \left[-1 + \frac{1}{2} \left(\frac{5 + \nu}{1 + \nu} \right) \left(\frac{\rho_c}{\bar{\rho}} \right) \left(1 - \frac{3}{5} \frac{\rho_m}{\bar{\rho}} \right) \left(\frac{\bar{\rho} g a}{\mu} \right) \left(\frac{b_c}{d} \right) \right] > 1 \quad (4.11)$$

Recall that for this problem, $\nu = 0.33$ is the Poisson's ratio of ice, $\rho_m = 1.0 \text{ g cm}^{-3}$ is the density of water, and $\rho_c = 0.92 \text{ g cm}^{-3}$ is the density of the ice. g , $\bar{\rho}$, a , and γ are taken to be 131 cm sec^{-2} , 3.03 g cm^{-3} , $1.56 \times 10^8 \text{ cm}$, and 5×10^{-4} for Europa, respectively. The Love number h for a homogeneous fluid body is $\frac{5}{2}$ (cf. Munk and MacDonald, 1960). However, Ross and Schubert (1987) have found that h is substantially smaller for an ice shell on Europa, since the self-potential of a second degree deformation at the surface of Europa is weighted strongly by the density of ice and water, which is much lower than the average density of the satellite. We use their value for h of 1.26.

With these parameters, the inequality (4.11) may be written

$$\left(\frac{t_{20} + 2t_{22}}{1 \text{ km}} \right) (0.243) \left[-1 + (0.75) \left(\frac{4 \times 10^{10} \text{ dyne cm}^{-2}}{\mu} \right) \left(\frac{b_c}{d} \right) \right] > 1 \quad (4.12)$$

where the rigidity μ of the ice, the average shell thickness b_c , and the lithosphere thickness d have been left as variables.

It should be noted that if large scale reorientation of the ice shell occurs, large membrane stresses will be imparted to the ice. Membrane stresses imparted to a continuous elastic shell as a result of a 90-degree reorientation are several times $\mu\gamma$, which is about 20 bars for Europa if $4 \times 10^{10} \text{ dynes cm}^{-2}$. Fracture of the ice (at least the ice near the surface) is very likely for stresses of this magnitude (cf. Crawford and Stevenson, 1988). It is important to note that since any fossil bulge is maintained by these stresses in the ice, the release of stress accompanying fracture would reduce or eliminate a fossil bulge and its contribution to the inertia tensor. If the ice is able to anneal or become effectively cemented by intruding warm ice upon fracturing, the system would effectively return to a state characterized by a

continuous, unstressed lithosphere with a non-equilibrium thickness profile, after a period of polar wander and subsequent fracture. In this manner, any “memory” of previous episodes of polar wander may be lost.

In Paper 1, several thermal models are presented for an ice shell on Europa, yielding theoretical estimates of t_{20} and t_{22} . Their magnitudes vary with model parameters such as the temperature-dependence of the dissipation and thermal conductivity within the ice, the type of rheology assumed for the ice, and the amount of heat flowing from the core. For most of the models, $t_{20} + 2t_{22}$ is a positive quantity with a magnitude of between 0.4 km and 1.2 km. Perhaps the most reasonable case considered in Paper 1 is that in which a generalized flow law, for which the strain rate is proportional to the third power of the stress, is assumed for the ice. The reader is referred to Paper 1 for details. For that model, $t_{20} + 2t_{22}$ is roughly 1 km.

Also from the thermal models of Paper 1, it is evident that the average shell thickness is roughly an order of magnitude larger than the average lithosphere thickness, which, as noted previously, is the region of the shell that behaves elastically on the time scale of the loading. Thus the ratio $\left(\frac{b_f}{d}\right)$ may be taken to be ~ 10 , although it is possibly as small as ~ 4 . Measurements of the rigidity μ of polycrystalline ice range from 1.1×10^9 dynes cm^{-2} to 4.1×10^{10} dynes cm^{-2} (Hobbs, 1974), although the most reliable estimates are closer to the upper limit.

The values of $t_{20} + 2t_{22}$ from Paper 1 should be taken only as crude estimates, as many assumptions are made (see Paper 1) and there are uncertainties in many parameters. However, it is evident from the values discussed here that the inequality (4.12) is satisfied for a wide range of parameters. For example, if $\left(\frac{b_f}{d}\right)$ is ~ 10 , μ is $\sim 4 \times 10^{10}$ dynes cm^{-2} and $t_{20} + 2t_{22}$ is ~ 1 km, it is satisfied by a factor of

~ 1.6 . (4.12) is more difficult to satisfy as $\left(\frac{b_c}{d}\right)$ decreases, and easier to satisfy as μ decreases. If $\left(\frac{b_c}{d}\right) \sim 4$ and $\mu \sim 4 \times 10^{10}$ dynes cm^{-2} (the most difficult case to satisfy), $t_{20} + 2t_{22}$ must be $\gtrsim 2.1$ km for (4.12) to be satisfied, while if $\mu \sim 1.1 \times 10^9$ dynes cm^{-2} and $\left(\frac{b_c}{d}\right) \sim 10$ (the easiest case), $t_{20} + 2t_{22}$ need only be ~ 0.02 km.

The fossil bulge may be effectively eliminated if (as will be discussed later) the outer region of the shell represented by d is continuously being fractured by the cyclic tidal stress so that it cannot anneal. If such were the case, $I_{yy} > I_{zz}$ if $t_{20} + 2t_{22} > 0$.

We have yet to investigate what reorientation, if any, Europa would experience as a result of the inertia variations described in this section. An obvious question, to be discussed in the section *Coupling and Damping*, is whether the rocky core of Europa will reorient with the ice shell if polar wander takes place. If the core were constrained to reorient in coincidence with the shell, any fossil bulge existing on the core would contribute an additional stabilizing influence on the inertia tensor, reducing the probability that $I_{yy} > I_{zz}$ in thermal equilibrium. For example, with a core rigidity of 6.5×10^{11} dynes cm^{-2} , a lithosphere on the core will have to be less than ~ 200 m in thickness if $t_{20} + 2t_{22}$ for the shell is ~ 1 km, in order to have $I_{yy} > I_{zz}$ for the composite (core plus shell) system.

The earth's core is believed to move very nearly in coincidence with its mantle, during the precession of the equinoxes, because of the influence of a torque known as the Poincaré or inertial torque (Rochester, 1976). This torque arises because of the hydrodynamical pressure distribution at the core/mantle interface when the axis of figure of the core departs from its axis of rotation. Although such a torque is present in the problem of core/mantle coupling on Europa, it is shown

in Appendix A that it is unable to induce coincident motion of the core and shell, as are torques due to frictional and gravitational coupling. However, we also argue in Appendix A that the Poincaré torque probably *does* induce coincident motion of the liquid water layer with the shell during polar wander of the shell.

It will be argued that the ice shell (plus the liquid layer) of Europa may therefore reorient independently of the silicate core. In that case, the relevant inertia tensor is that of the ice shell plus the liquid layer, and a fossil bulge on the core does not contribute to the instability criterion.

It is clear from the above discussion that for many possible models of Europa's structure, the presence of thermal equilibrium ice thickness profiles may imply that I_{yy} is greater than I_{zz} , in the relevant inertia tensor. Since this would be an unusual orientation for the principal axes of a synchronously rotating satellite, a state of thermal equilibrium for Europa may not represent a state of dynamic equilibrium. The implication is, therefore, that as thermal equilibrium is approached, Europa may become dynamically unstable and reorient to obtain the preferred state for synchronously rotating satellites. If I_{yy} becomes greater than I_{zz} as suggested, the net reorientation required to do so would be accomplished most directly by a rotation of 90 degrees about the axis that passes through the sub- and antiJupiter points, so that polar ice is brought to the apices, and ice near the apices is brought to the poles.

However, reorientation of Europa is not assured by merely showing that the moment about the tangent to the orbit exceeds the moment about the rotation axis in thermal equilibrium. It must be demonstrated that the expected polar wander is not dynamically inhibited. That is the purpose of the following section.

5. Polar Wander of a Rigid Synchronously Rotating Body

We now wish to investigate the dynamical evolution of a body that is initially synchronously rotating, whose inertia tensor evolves toward thermal equilibrium as we have proposed in the previous section. The simplest model with which to do so is that of a rigid body in a circular orbit, for which the difference between the intermediate and maximum moments is linear in time.

Consider a body whose principal moments of inertia are

$$\begin{aligned} I_1 &= I_o \left(1 + \frac{t}{\tau} \right) \\ I_2 &= I_o \\ I_3 &= I_o(1 - \epsilon) \quad , \end{aligned} \tag{5.1}$$

where t is time, τ and ϵ are constants, and $\frac{t}{\tau} > -\epsilon$. Thus when $-\epsilon\tau < t < 0$, $I_3 < I_1 < I_2$, but as t passes through zero, I_1 becomes the maximum principal moment and $I_3 < I_2 < I_1$. The terms $I_o \left(\frac{t}{\tau} \right)$ and $I_o\epsilon$ represent inertia components due to ice thickness variations and the fossil bulges, respectively. The axes associated with I_1 , I_2 , and I_3 correspond to the axes fixed in the frame of the body, which are initially aligned along the tangent to the orbit, the rotation vector, and the direction to the planet, respectively. We denote these axes by x_1 , x_2 , and x_3 . We shall see that this unconventional choice of axes is convenient in the following development.

It should be noted that it is actually physically impossible to change the magnitude of one principal moment without changing at least one of the other two. This is immediately evident from inspection of Equations (3.12)–(3.14). Thus, in general, both I_o and ϵ in Equations (5.1) must be functions of time. However, the important dynamics arises as a result of the change of sign of the principal moment difference $I_1 - I_2$, so that we may ignore the time-dependence of ϵ and/or I_o .

In order to derive equations of motion for the body we must first link a coordinate system that is nonrotating in inertial space to the x_i coordinate system fixed in the body, through a series of rotations. Let the nonrotating coordinate system be defined as x'_i , with the origin at the center of mass of the satellite and the x_3' -axis directed along the normal to the orbit. The directions of the x_1' and x_2' -axes are arbitrary.

Because the body is in a circular orbit, its rotation about its center of mass is independent of its position in the orbit. The constant radial acceleration of the x'_i origin is balanced by the central force of the planet. We first rotate counterclockwise by an angle $n(t - t_o)$ about the x_3' -axis, to a coordinate system x''_i that is rotating with the mean motion n such that the x_1'' and x_2'' axes are directed opposite to the orbital velocity of the satellite and directly away from the parent planet, respectively (see Figure 4). We then perform the standard Euler angle rotations to arrive at the body coordinate system, x_i : a rotation by an angle φ about the x_3'' axis, followed by a rotation by an angle θ' about the x_1''' -axis, followed by a rotation by an angle ψ about the x_3'''' -axis. These rotations are shown in Figure 5.

Thus, a vector \vec{x}'' in the x''_i coordinate system may be transformed to the x_i coordinate system by the matrix multiplication $\vec{x} = A\vec{x}''$, where

$$A \equiv \begin{bmatrix} \cos \psi & \sin \psi & 0 \\ -\sin \psi & \cos \psi & 0 \\ 0 & 0 & 1 \end{bmatrix} \begin{bmatrix} 1 & 0 & 0 \\ 0 & \cos \theta' & \sin \theta' \\ 0 & -\sin \theta' & \cos \theta' \end{bmatrix} \begin{bmatrix} \cos \varphi & \sin \varphi & 0 \\ -\sin \varphi & \cos \varphi & 0 \\ 0 & 0 & 1 \end{bmatrix} . \quad (5.2)$$

Within the framework of the above transformations, purely synchronous rotation, with the principal axes oriented in the usual sense for synchronous satellites is the state where $\theta' = \frac{\pi}{2}$, and $\varphi = \psi = \dot{\theta}' = \dot{\psi} = \dot{\varphi} = 0$, when $t < 0$. When $t > 0$, the

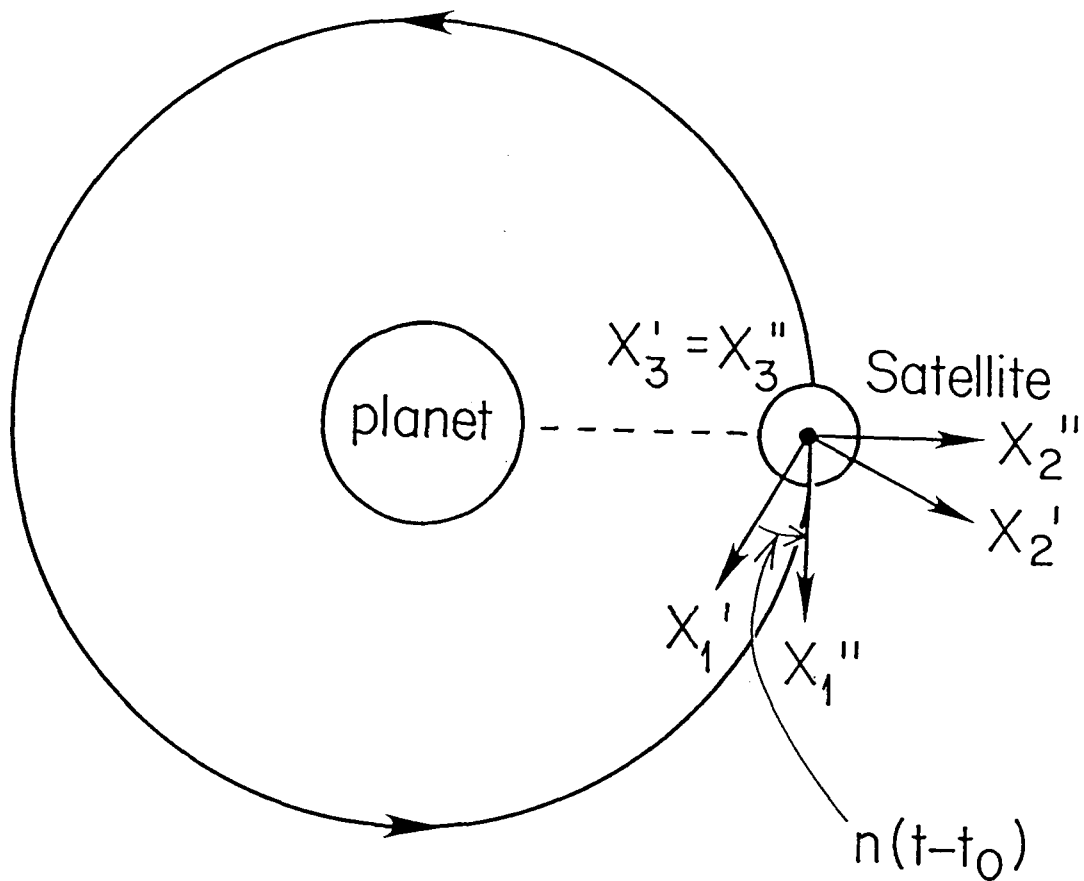


Figure 4. Rotation from the nonrotating x_i' coordinate system to the x_i'' coordinate system that rotates synchronously with the mean motion, n , about the x_3' -axis. The x_1'' and x_2'' axes are directed opposite to the orbital velocity and directly away from the planet, respectively.

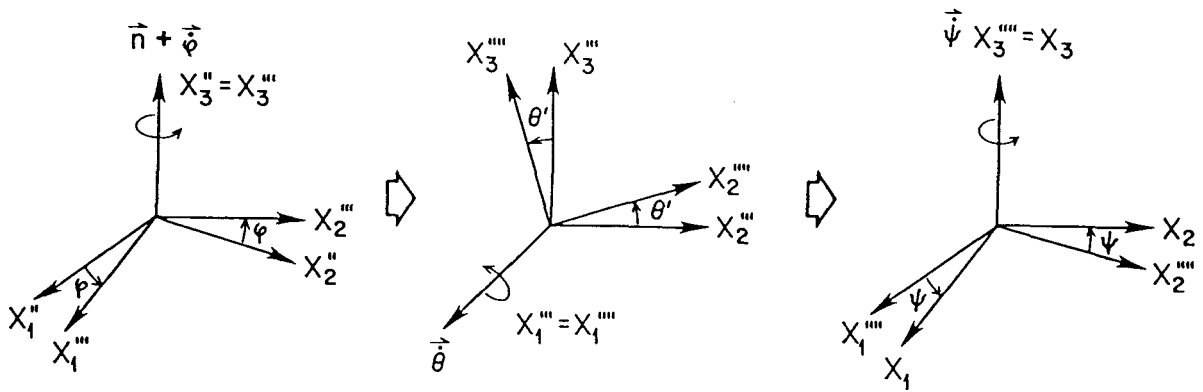


Figure 5. The Euler angle rotations that relate the x_i'' coordinate system to the x_i coordinate system, fixed in the body.

usual state is the same as above, but with $\psi = \frac{\pi}{2}$. Now it is evident why our choice of body axes (see Equations (5.1)) is convenient: the most direct path toward the usual orientation for a synchronous satellite as t passes through $t = 0$ is simply a 90-degree rotation in the coordinate ψ .

The direction cosines of the body axes x_1 , x_2 , and x_3 , with respect to the direction toward the planet, are defined as λ_1 , λ_2 , and λ_3 , respectively. They are

$$\begin{bmatrix} \lambda_1 \\ \lambda_2 \\ \lambda_3 \end{bmatrix} = A \begin{bmatrix} 0 \\ -1 \\ 0 \end{bmatrix} = \begin{bmatrix} -\cos \psi \sin \varphi - \sin \theta \cos \varphi \sin \psi \\ \sin \psi \sin \varphi - \sin \theta \cos \varphi \cos \psi \\ \cos \theta \cos \varphi \end{bmatrix}, \quad (5.3)$$

where

$$\theta \equiv \frac{\pi}{2} - \theta' \quad . \quad (5.4)$$

The total angular velocity, written in the x_i coordinate system is easily found to be

$$\begin{bmatrix} \omega_1 \\ \omega_2 \\ \omega_3 \end{bmatrix} = \begin{bmatrix} (n + \dot{\varphi}) \sin \psi \cos \theta - \dot{\theta} \cos \psi \\ (n + \dot{\varphi}) \cos \psi \cos \theta + \dot{\theta} \sin \psi \\ (n + \dot{\varphi}) \sin \theta + \dot{\psi} \end{bmatrix} \quad . \quad (5.5)$$

Euler's equations of motion for a body in a circular orbit subjected to the tidal torque are (cf. Danby, 1962)

$$\frac{d}{dt}(I_1 \omega_1) = (I_2 - I_3) \omega_2 \omega_3 - 3n^2(I_2 - I_3) \lambda_2 \lambda_3 \quad (5.6)$$

$$\frac{d}{dt}(I_2 \omega_2) = (I_3 - I_1) \omega_1 \omega_3 - 3n^2(I_3 - I_1) \lambda_1 \lambda_3 \quad (5.7)$$

$$\frac{d}{dt}(I_3 \omega_3) = (I_1 - I_2) \omega_1 \omega_2 - 3n^2(I_1 - I_2) \lambda_1 \lambda_2 \quad , \quad (5.8)$$

where

$$n^2 = \frac{GM_p}{R^3} \quad (5.9)$$

is the mean motion, M_p is the mass of the parent planet, G is the gravitational constant, and R is the semimajor axis of the orbit.

Multiplying Equation (5.6) by $\sin \psi$ and Equation (5.7) by $\cos \psi$ and adding the results, the equation

$$\begin{aligned} \ddot{\varphi} \cos \theta = & -\omega_o^2 \sin \varphi \cos \varphi \cos \theta \\ & + \dot{\theta} [2(n + \dot{\varphi}) \sin \theta - \alpha] + \frac{t}{\tau} \cos \psi \left\{ \left[\dot{\theta} \cos \psi - (n + \dot{\varphi}) \sin \psi \cos \theta \right] \alpha \right. \\ & \left. - 3n^2 \cos \varphi \cos \theta [\cos \psi \sin \varphi + \sin \theta \cos \varphi \sin \psi] \right\} \end{aligned} \quad (5.10)$$

is obtained, where

$$\alpha \equiv \frac{I_3 \omega_3}{I_o} = (1 - \epsilon) [(n + \dot{\varphi}) \sin \theta + \dot{\psi}] \quad (5.11)$$

$$\omega_o = \sqrt{3n^2 \epsilon} \quad , \quad (5.12)$$

and terms involving products and squares of $\left(\frac{t}{\tau}\right)$ and ϵ have been neglected. Similarly, multiplying Equation (5.6) by $-\cos \psi$ and Equation (5.7) by $\sin \psi$ and adding, the equation

$$\begin{aligned} \ddot{\theta} = & n\alpha \cos \theta - [n^2 + \omega_o^2 \cos^2 \varphi] \frac{1}{2} \sin 2\theta - \dot{\varphi} \cos \theta [(2n + \dot{\varphi}) \sin \theta - \alpha] \\ & + \frac{t}{\tau} \sin \psi \times \left\{ \left[\dot{\theta} \cos \psi - (n + \dot{\varphi}) \sin \psi \cos \theta \right] \alpha \right. \\ & \left. - 3n^2 \cos \theta \cos \varphi [\cos \psi \sin \varphi + \sin \theta \cos \varphi \sin \psi] \right\} \end{aligned} \quad (5.13)$$

is obtained.

Equation (5.8) may now be re-written

$$\begin{aligned} \dot{\alpha} = & \left(\frac{t}{\tau}\right) \left\{ [(n + \dot{\varphi})^2 - \dot{\theta}^2] \frac{1}{2} \sin 2\psi - \dot{\theta}(n + \dot{\varphi}) \cos 2\psi \right\} + 3n^2 \\ & \times \left(\frac{t}{\tau}\right) [\cos \psi \sin \varphi + \sin \theta \cos \varphi \sin \psi] [\sin \psi \sin \varphi - \sin \theta \cos \varphi \cos \psi] \quad . \end{aligned} \quad (5.14)$$

If it is further assumed that $\theta \ll 1$ and $\phi \ll 1$ (to be verified later), Equations (5.10), (5.13), and (5.14) become

$$\ddot{\varphi} = -\omega_o^2 \varphi + \dot{\theta}[2n\theta - \alpha] + \left(\frac{t}{\tau}\right) \cos \psi [-n\alpha \sin \psi - 3n^2(\varphi \cos \psi + \theta \sin \psi)] \quad (5.15)$$

$$\ddot{\theta} = n\alpha - (n^2 + \omega_o^2) \theta - \dot{\varphi}(2n\theta - \alpha) + \left(\frac{t}{\tau}\right) \sin \psi [-n\alpha \sin \psi - 3n^2(\varphi \cos \psi + \theta \sin \psi)] \quad (5.16)$$

$$\dot{\alpha} = \left(\frac{t}{\tau}\right) \left[\frac{1}{2} (n^2 + 2n\dot{\varphi}) \sin 2\psi - n\dot{\theta} \cos 2\psi \right], \quad (5.17)$$

when terms of higher order than squares and products of ϵ , $\frac{t}{\tau}$, θ , ϕ , and the derivatives of θ , ϕ , and ψ are ignored.

A solution to Equations (5.15)–(5.17) is easily affected in the limit where $\left(\frac{t}{\tau}\right)$ is very small (the meaning of “very small” will soon become evident). Clearly if $\left(\frac{t}{\tau}\right)$ is small enough (see Equation (5.17)), α may be treated as a constant in Equations (5.15) and (5.16).

To first order, Equation (5.16) then gives

$$\theta \simeq \left(\frac{n\alpha}{n^2 + \omega_o^2} \right) + \epsilon_\theta e^{i\omega_\theta t} \quad (5.18)$$

$$\omega_\theta = \sqrt{n^2 + \omega_o^2}$$

and Equation (5.15) gives

$$\varphi \simeq \epsilon_\varphi e^{i\omega_\varphi t}, \quad (5.19)$$

where ϵ_θ and ϵ_φ are arbitrary constants of integration representing oscillations about the mean state. When $\theta = 0$, Equation (5.19) describes the well known phenomenon of physical libration (cf. Danby, 1962). Averaging Equations (5.18) and (5.19) over short period oscillations and combining with equation (5.11), it is easily seen that

$$\bar{\theta} \simeq \frac{\dot{\psi}}{4\epsilon n} \simeq \frac{n\alpha}{n^2 + \omega_o^2} \quad (5.20)$$

Ignoring $\dot{\phi}$, $\dot{\theta}$, and $\dot{\psi}$ relative to n , and ignoring ϵ relative to unity, the time derivative of Equation (5.20) may be inserted into equation (5.17) to give

$$\ddot{\psi} \simeq 2\epsilon \left(\frac{t}{\tau}\right) n^2 \sin 2\psi \quad . \quad (5.21)$$

Equation (5.21) is the crucial Equation describing polar wander as the inertia tensor evolves. It is the equation of a pendulum under the influence of a time variable gravitational acceleration where 2ψ corresponds to the angle between the arm of the pendulum and the direction of gravity. As t passes through zero, the direction of gravity reverses, and 2ψ passes from a state of stability about $2\psi = 0$ to a state of stability about $2\psi = \pm\pi$.

When $\sin 2\psi$ is small, an approximate solution of Equation (5.21) may be found by the WKB approach as long as $|t|$ is not too small (cf. Mathews and Walker, 1970). As in the standard WKB solution, the amplitude of oscillations in ψ increases as $t \rightarrow 0$, while the frequency decreases. A sketch of a solution to equation (5.21) is shown in Figure 6.

An idea of the form of the solution to the equations may be obtained by setting $\left(\frac{t}{\tau}\right)$ equal to some effective constant value, $\left(\frac{t_o}{\tau}\right)$, when $t > 0$. This is a sensible approximation to examine since the mechanisms which cause the inertia tensor to evolve are altered once reorientation begins (see Section 6.2). Then Equation (5.21) may be solved exactly.

If $\dot{\psi} \simeq 0$ when $\psi \simeq 0$, Equation (5.21) may be integrated once to obtain

$$\dot{\psi} \simeq 2n \left[\epsilon \frac{t_o}{\tau} \right]^{1/2} \sin \psi \quad . \quad (5.22)$$

Then Equation (5.20) gives

$$\bar{\theta} \simeq \frac{1}{2} \left(\frac{t_o/\tau}{\epsilon} \right)^{1/2} \sin \psi \quad . \quad (5.23)$$

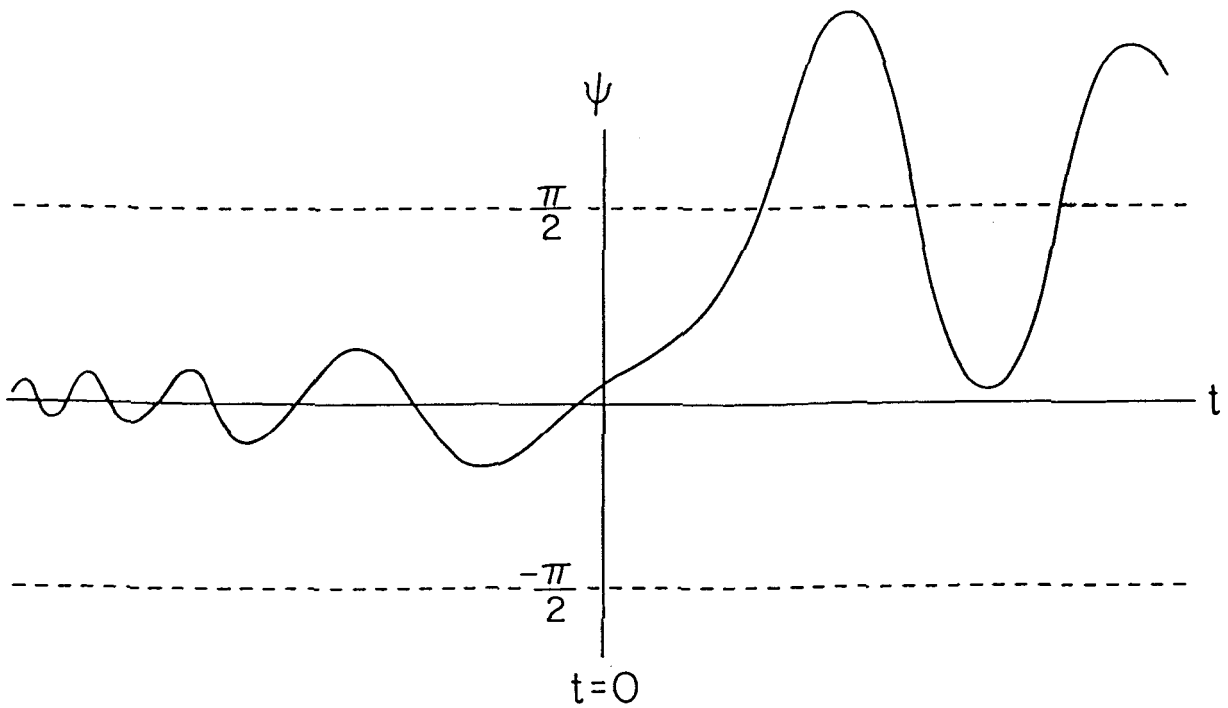


Figure 6. The form of the solution to Equation (5.21) with no damping. ψ may oscillate about $\pm\frac{\pi}{2}$ when time $t > 0$, depending on the values of ψ and $\dot{\psi}$ at $t = 0$. Circulation of ψ is also possible, but is unlikely for any real body because of the presence of damping.

Iteration of Equation (5.15) reveals that φ has a second order component that varies with ψ as well:

$$\bar{\varphi} \simeq -\frac{1}{2} \left(\frac{t_o/\tau}{\epsilon} \right)^{3/2} \sin^2 \psi \cos \psi \quad . \quad (5.24)$$

Note that $\bar{\varphi}$ is smaller than $\bar{\theta}$ by $\sim \left(\frac{t_o/\tau}{\epsilon} \right)$.

Equations (5.23) and (5.24) reveal that the approximation assumed earlier of $\theta, \varphi \ll 1$ is valid as long as

$$\left(\frac{t}{\tau} \right)^{1/2} \ll \epsilon^{1/2} \quad . \quad (5.25)$$

An obvious criterion for the validity of Equation (5.18) is that $\bar{\theta}$ and $\bar{\varphi}$ do not change by a substantial fraction during one oscillation period of their oscillating components. With Equations (5.18) through (5.24), it can be seen that this requirement implies only that $\left(\frac{t}{\tau} \right)^{1/2} \ll 1$. Thus, Equation (5.25) is a more stringent requirement than the criterion for $\alpha \approx \text{constant}$ in Equations (5.15) and (5.16), and it is sufficient for the validity of the approximations made thus far. Note that because of the requirement given by Equation (5.25), Equation (5.21) does not imply that $\vec{\psi} = 0$ if $\epsilon = 0$; the equation is not valid in that limit.

When φ and θ are small, they may be visualized as a pair of Cartesian coordinates defining the orientation of the x_3 axis with respect to the direction to the planet as shown in Figure 7. The plane of the (φ, θ) coordinate system is oriented perpendicular to the line passing through the centers of the parent planet and the satellite, with its origin at the point on the surface of the satellite that intersects the line. The φ and θ axes are directed opposite to the orbital velocity, and along the orbit normal, respectively. The ordered pair (φ, θ) then describes the positions of the intersection of the x_3 -axis with this plane, in units of the satellite's radius, while the value of ψ describes rotation of the satellite around the x_3 -axis.

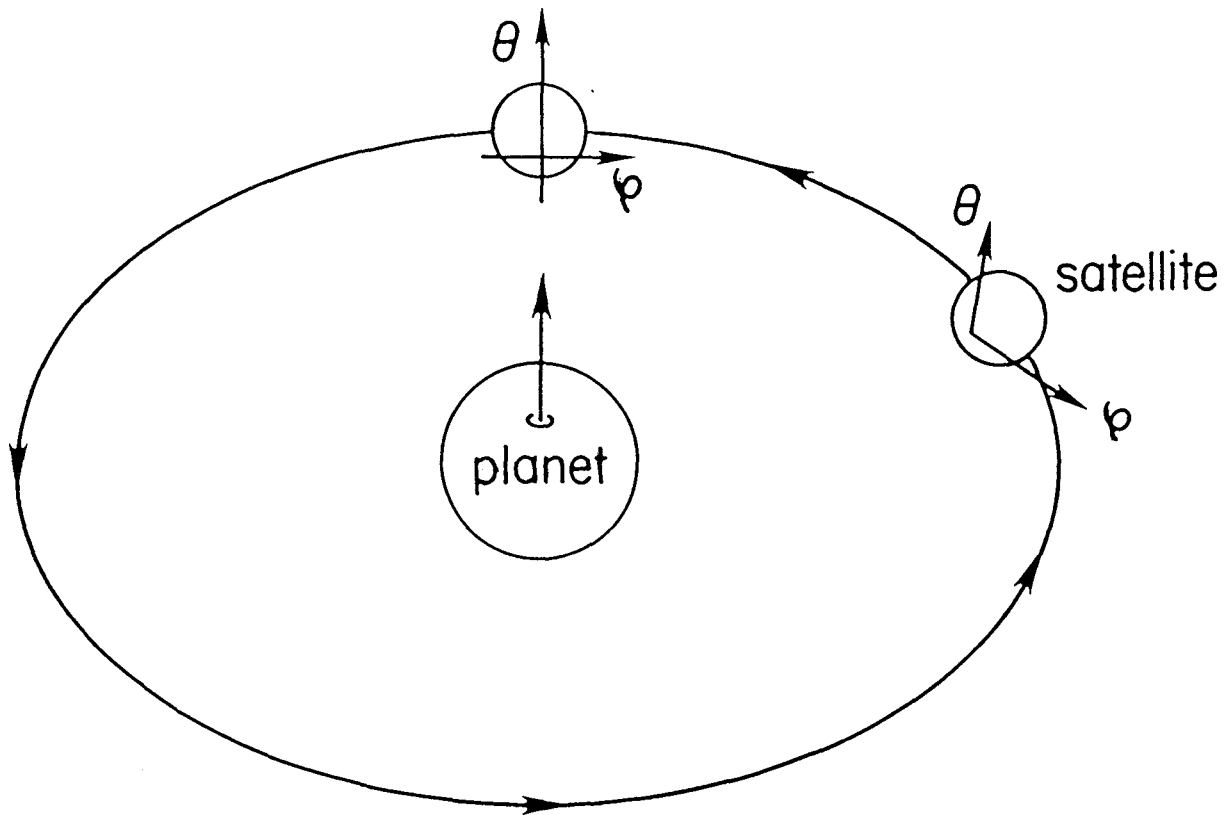


Figure 7. Visualization of the ordered pair (φ, θ) as Cartesian coordinates describing the orientation of the x_3 body axis. See text for description.

The solutions (5.22) through (5.24) can be visualized clearly with the above visual aid. When t becomes positive, the quantity 2ψ “falls” from zero toward $\pm\pi$, just as a pendulum for which the direction of gravity has reversed. As ψ accelerates, the x_3 -axis tips out of the plane of the orbit in accordance with the evolution of $\bar{\theta}$ as given by Equation (5.23), reaching a maximum absolute value as ψ passes through the new potential minimum of the pendulum at $\psi = \pm\frac{\pi}{2}$. At the same time the x_3 -axis lags behind the subplanet point by an amount given by $\bar{\varphi}$, Equation (5.24).

These dynamics are intuitively understandable. As t becomes positive, the maximum principal moment of inertia, about which the body is rotating, becomes the intermediate moment. A freely rotating body will not rotate in a stable manner about the axis of its intermediate moment of inertia, but rather if the rotation vector is initially coincident with that axis, it will make large excursions from it on the time scale of free precession (cf. Goldstein, 1970). However, in this problem the tidal torque inhibits the growth of the angle between the x_3 -axis and the satellite-planet direction so that excursions from the intermediate axis must tend toward the axis of the maximum moment. At constant angular momentum, a body must reduce its spin-rate as it approaches a state of rotation about the axis of the maximum principal moment. Such a reduction in spin implies the growth of a negative value of $\bar{\varphi}$. A negative $\bar{\varphi}$ is predicted from the equations (Equation (5.24)), but the tidal torque “spins-up” the body very effectively so that $\bar{\varphi}$ remains very small. An important difference between this problem and the problem of polar wander of a freely rotating body is that in this case the total kinetic energy of the body as well as its angular momentum are actually greater after polar wander than before, because of the ability of the tidal torque to “spin-up” the satellite.

Without dissipation, large oscillations in ψ about $\psi = \pm\frac{\pi}{2}$ will continue

indefinitely. The time required for ψ to evolve from a value near zero to a value near $\pm\frac{\pi}{2}$ depends on the initial values of ψ and $\dot{\psi}$. A rough estimate of the time scale, T , may be obtained from Equation (5.21) by identifying the coefficient of $\sin 2\psi$ with the square of a characteristic angular velocity of ψ ; and assuming $t \sim T$:

$$T \sim \left(\frac{\tau}{n^2 \epsilon} \right)^{1/3} . \quad (5.26)$$

The time scale given by (5.26) may be recognized as the geometric mean of the free precession time scale for a symmetric top whose principal moments of inertia differ by a fraction ϵ and the same time scale for a symmetric top whose moments differ by a fraction $\sim \frac{t}{\tau}$.

Since no motion will occur at all if $\dot{\psi} = \psi = 0$ when $t > 0$ (i.e. if the pendulum is precisely balanced at the top of its support), it is useful to estimate the dependence of the polar wander time scale on the value of ψ when t passes through $t = 0$. If we approximate Equation (5.21) and its solution by $\ddot{\psi} \sim \left[n^2 \epsilon_s \left(\frac{t}{\tau} \right) \right] \psi$ and $\psi \sim \psi_o \cosh \left[n \left(\epsilon \frac{t}{\tau} \right)^{1/2} t \right]$, respectively (assuming that $\dot{\psi} \sim \psi \sim 0$ when $t = 0$), the characteristic time for ψ to grow to \sim unity is seen to be

$$T \sim \left[\frac{\tau}{n^2 \epsilon_s} \right]^{1/3} (-\ln \psi_o)^{1/3} , \quad (5.27)$$

where ψ_o is the value of ψ when $t = 0$. The dependence of T on ψ_o is clearly extremely weak. For example, the time scale given by (5.27) is longer than that given by (5.26) by more than an order of magnitude only if $\psi_o \lesssim \exp[-10^3]$ radians.

The model presented here does not explicitly include dissipation and as such cannot be expected to simulate reality. Its purpose is to demonstrate that large scale reorientation can be expected to occur for a synchronous satellite if the axis of the intermediate moment becomes the axis of the maximum moment. The motion is not dynamically inhibited.

In the following sections, the mechanism of polar wander described here will be made more realistic by addressing the question of the degree of coupling of the motions of the core and the shell, and anelastic damping of the motions.

6. A More Realistic Model for Europa

A comprehensive investigation of polar wander of Europa must address and quantify two classes of physical phenomena that are crucial to an understanding of the extent and form of the polar wander: mechanisms of coupling between the core, the shell, and the layer of liquid water (or “ocean”), as well as mechanisms of damping of angular motion. Several torques exist that act to couple the motions of the core, shell, and liquid layer. We will consider the inertial or Poincaré torque, gravitational coupling, and coupling due to viscous or turbulent shear within the liquid layer. Coupling and damping of the motions of the core and shell are not entirely separate issues. While the Poincaré and gravitational coupling torques are conservative in nature, the viscous and turbulent coupling are dissipative and therefore contribute to damping of motion. Also, any polar wander experienced by a *nonrigid* body will invoke time-dependent strains, and hence dissipation within it. An effective torque results which will tend to damp its angular motion. Such damping must be included in calculations of reorientation of Europa’s core and shell.

We will begin by assuming that the shell is able to reorient independently of the core, impeded only by anelastic friction within the shell itself. The layer of liquid water is assumed to reorient in coincidence with the shell, so that the ice and liquid water may be treated as a single entity. Given the motion of the shell (plus liquid) which results from this assumption, we show in Appendix A that

the coupling torques mentioned above are incapable of inducing significant angular reorientations of the core during polar wander of the shell, but that the Poincaré torque exerted on the liquid layer by the ice shell probably does cause the liquid to reorient in coincidence with the shell. The above assumptions are thus verified a posteriori.

In Section 6.1 we estimate the damping torque which results from dissipation occurring in the shell during polar wander. In Section 6.2 we incorporate this torque into the equations of motion of the shell and describe the solution. In Section 6.3 we discuss the implications of the results of Section 6.2 on the history and surface morphology of Europa.

6.1 Dissipation in the Shell during Polar Wander

Because a thin ice shell must conform very nearly to the hydrostatic surface of the underlying ocean throughout any reorientation event, strains are necessarily imparted to the shell during polar wander. Work must be expended on the shell in order to impose these strains. This required work in turn implies the existence of effective torques which impede polar wander of the shell and which must be included in the equations of motion.

If the ice shell behaves as a viscoelastic medium, the large variation in temperature through the shell will induce a spectrum of viscoelastic behavior within it during polar wander — the cold, near-surface ice, where the Maxwell time τ_M is longer than the time scale τ_{pw} over which polar wander takes place, will respond elastically to imposed strains, while warmer ice near the shell-ocean interface (where $\tau_{pw} \gg \tau_M$) behaves viscously. However, even if the ice behaves as a simple Maxwell medium, the equations describing the stresses and strain rates within it during polar wander are very difficult to solve. We therefore have chosen to approximate

the shell by an outer layer which responds elastically throughout any reorientation event, underlain by a layer which responds viscously on the same time scale. We define the boundary between the two layers as the surface within the shell where $\tau_M = \tau_{pw}$.

The work necessary to impart the required strains to the outer, elastic layer of the shell is simply energy of elastic strain. It can be shown that this elastic strain energy is implicitly accounted for by including (as we have) the kinetic energy of the fossil bulge on the shell in the equations of motion (see Section 4). We may therefore direct our attention solely to the work required to produce the strains associated with polar wander in the viscous layer of the shell. This work is simply viscous dissipation.

It is useful to visualize polar wander of the shell in the x''_i coordinate system, defined in Section 5, which is rotating with the mean motion, \vec{n} . In this coordinate system, the shell is motionless if it is synchronously rotating, and any motion may be equated with polar wander. The coordinate axes of the x''_i coordinate system coincide with the semimajor axes of a synchronously rotating fluid.

As mentioned above, a thin shell must conform very nearly to the hydrostatic surface of the underlying ocean throughout any reorientation event. By visualizing a reorientation of the shell by an angle of 90 degrees about one of the x''_i coordinate axes, it is therefore clear that during such a reorientation, a characteristic chord within the shell experiences a net strain of the order γ , since meridional and equatorial great circles on the surface of a synchronously rotating fluid differ in length by fractions of this order (see Equations (4.5) and (4.6)). The characteristic volumetric strain ϵ caused by an arbitrary rotation ζ about one of the x''_i axes is therefore of order $\epsilon \sim \gamma\zeta$, and the characteristic viscous stress caused by this strain

is $\sigma \sim \eta \dot{\epsilon} \sim \eta \gamma \dot{\zeta}$ where η is the viscosity of a volume element in the viscous layer. Since the dissipation rate per unit volume in a viscous medium is $q = \overline{\sigma_{ij} \dot{\epsilon}_{ij}}$ where σ_{ij} and $\dot{\epsilon}_{ij}$ are the elements of the stress and strain rate tensors, respectively,

$$q \sim \eta \gamma^2 \dot{\zeta}^2 . \quad (6.1)$$

We take the viscosity, η , in (6.1) to be the steady state creep viscosity for polycrystalline ice, which obeys an Arrhenius relationship:

$$\eta = \eta_o \exp \left[\ell \left(\frac{T_m}{T} - 1 \right) \right] , \quad (6.2)$$

where T_m , η_o , and ℓ are the melting point temperature, the viscosity at the melting point, and a constant $\ell \approx 24$, respectively (cf. Hobbs, 1974).

Because the viscosity given by Equation (6.2) is a very strongly increasing function of temperature, the total dissipation rate W in the viscous layer is dominated by the dissipation in the shallowest, most viscous region of the layer. Because (by definition) $\tau_M \equiv \frac{\eta}{\mu} \sim \tau_{pw}$ at the depth, the viscosity there is

$$\eta_{\max} \sim \mu \tau_{pw} \sim \frac{\mu}{\dot{\zeta}} . \quad (6.3)$$

The thickness Δb of the region of the shell in which the viscosity is within an order of magnitude of η_{\max} is roughly

$$\Delta b \sim \left(\frac{-d \log_{10} \eta}{dT} \right)^{-1} \left(\frac{dz}{dT} \right) , \quad (6.4)$$

where $\frac{d \log_{10} \eta}{dT}$ and $\frac{dz}{dT}$ are evaluated at the depth where $\eta = \eta_{\max}$. We approximate the temperature gradient $\frac{dz}{dT}$ crudely by

$$\frac{dz}{dT} \simeq \left[\frac{b_c}{T_m - T_s} \right] , \quad (6.5)$$

where T_m and T_s are the melting point temperature of ice and a characteristic temperature at the surface of the shell, respectively. Using Equation (6.2) for the viscosity, $\frac{-d \log_{10} \eta}{dT}$ may be evaluated at the temperature where $\eta = \eta_{\max}$, giving

$$\frac{-d \log_{10} \eta}{dT} = \frac{\ell}{T_m \ln 10} \left[1 - \frac{1}{\ell} \ln \left(\frac{\dot{\zeta} \eta_o}{\mu} \right) \right]^2 \sim \frac{\ell}{T_m} \quad (6.6)$$

We will ignore the factor $\frac{[1 - (1/\ell) \ln(\dot{\zeta} \eta_o / \mu)]^2}{\ln 10}$ since it has a value of \sim unity for typical values of $\ell \approx 24$, $\eta_o \sim 10^{14}$ Poise, 10^9 dynes $\text{cm}^{-2} \leq \mu \leq 4 \times 10^{10}$ dynes cm^{-2} , and for a very broad range of $\dot{\zeta}$. For example, the factor varies between ~ 1.2 and ~ 2.1 as $\frac{1}{\dot{\zeta}}$ varies between $\sim 10^3$ y and $\sim 10^7$ y, for $\mu \sim 4 \times 10^{10}$ dynes cm^{-2} .

The total viscous dissipation in the shell may now be estimated by multiplying the volume of the layer in which $\eta \sim \eta_{\max}$ by the volumetric dissipation rate $q \sim \eta_{\max} \gamma^2 \dot{\zeta}^2$ within that layer, i.e.

$$W \sim (4\pi a^2 \Delta b) \eta_{\max} \gamma^2 \dot{\zeta}^2 \quad (6.7)$$

where a is the radius of the shell. Using Equations (6.1) and (6.3)–(6.6), Equation (6.7) may be written

$$W \sim C_v |\dot{\zeta}|$$

$$C_v \sim \frac{4\pi a^2 b_c}{\ell} \left(\frac{T_m}{T_m - T_s} \right) \mu \gamma^2 \quad (6.8)$$

The general reorientation rate of the shell in the x_i'' coordinate system is simply $(\vec{\omega} - \vec{n})$ where $\vec{\omega}$ and \vec{n} are the components of the total angular velocity of the shell and of the x_i'' coordinate system itself, written in the x_i'' coordinate system. The components of $(\vec{\omega} - \vec{n})$ along each of the x_i'' axes contribute to the total dissipation rate. The general formula for the dissipation is complicated but a

reasonable approximation is

$$W = \frac{[C_1(\omega_1 - n_1)^2 + C_2(\omega_2 - n_2)^2 + C_3(\omega_3 - n_3)^2]}{|\vec{\omega} - \vec{n}|}, \quad (6.9)$$

where ω_i and n_i are the components of $\vec{\omega}$ and \vec{n} along each of the x_i'' axes, and the C_i are each of order C_v as given by Equation (6.8).

None of the C_i are equal, because the semimajor axis differences of a synchronously rotating fluid are unequal. The dissipation W implies the existence of damping terms in the equations of motion for the shell. These may be found by noting that W is a Rayleigh dissipation function (Goldstein, 1970). The dissipative torque $\vec{\Gamma}_v$ on the shell thus has components

$$\Gamma_{vi} = -\frac{\partial W}{\partial \omega_i} \simeq -\frac{\left[2C_i(\omega_i - n_i) - W \frac{(\omega_i - n_i)}{|\vec{\omega} - \vec{n}|}\right]}{|\vec{\omega} - \vec{n}|} \quad (6.10)$$

along the x_i'' coordinate axes. For computational simplicity, we shall assume that $C_1 = C_2 = C_3 = C_v$ in the equations of motion of the shell (Section 6.2). Then Equation (6.10) becomes

$$\vec{\Gamma}_v = \begin{cases} -C_v \frac{(\vec{\omega} - \vec{n})}{|\vec{\omega} - \vec{n}|} & \vec{\omega} \neq \vec{n} \\ 0 & \vec{\omega} = \vec{n} \end{cases}, \quad (6.11)$$

i.e., the torque due to viscous dissipation during polar wander is assumed to be of constant magnitude, directed opposite to the vector $(\vec{\omega} - \vec{n})$ as long as $(\vec{\omega} - \vec{n}) \neq 0$. If $\vec{\omega} - \vec{n} = 0$ there is no polar wander and clearly no torque due to viscous friction in the ice. Equation (6.11) has an unusual form for a torque arising from dissipation since it is not proportional to an angular velocity. The reason is as follows: as described above, most of the dissipation occurs in the most viscous ice, near the upper boundary of the viscous layer, where the characteristic time scale of the strain is equal to the Maxwell time. If the value of ζ is reduced, the upper boundary of the

viscous layer moves closer to the outer surface of the shell, where the local viscosity and the Maxwell time of the ice are proportionately longer (note from Equation (6.3) that $\eta_{\max} \propto 1/\dot{\zeta}$). Because of this effect, the total dissipation rate in the ice depends effectively on only one factor of $\dot{\zeta}$, and the resulting torque is independent of $\dot{\zeta}$. This approximation is not strictly correct if $\dot{\zeta}$ is not roughly constant, but we employ it for simplicity.

In the following section we will demonstrate that the torque given by Equation (6.8) is so large that it virtually eliminates the possibility of polar wander of a continuous ice shell (due to the mechanism described in this paper).

However, if fractures or zones of weakness exist in the ice which extend to a depth exceeding that where the Maxwell time of the ice is comparable to the polar wander time scale, the form of the damping torque may be significantly altered and its magnitude greatly reduced, because the strain in the ice above that level may be largely accommodated by the fractures themselves rather than by net extension of continuous volume elements. Thus the upper boundary of the layer in which viscous dissipation occurs will be limited by the base of the fractured region, and the maximum viscosity in the layer (and hence the total amount of viscous dissipation) will be limited by the viscosity at that depth. As will be discussed in the following section, polar wander must take place on a time scale significantly shorter than the time scale for thermal diffusion through the ice shell ($\sim 10^7$ y) or the mechanism which drives the polar wander will be effectively eliminated. In the following section we conservatively adopt a few $\times 10^6$ y as the approximate maximum time scale on which polar wander can occur. In order that the damping torque is reduced as described above, we therefore require that zones of weakness or fractures in the ice extend to a depth where $\tau_M \lesssim \text{few} \times 10^6$ y. If $\eta_o \sim 10^{14}$

Poise, and $\mu \sim 4 \times 10^{10}$ dynes cm^{-2} , the Arrhenius relation (6.2) and Equation (4.1) indicate that the temperature at which $\tau_M \sim 2 \times 10^6$ y is about 135 K. Crawford and Stevenson (1988) predict that current tidal flexing of a decoupled ice shell on Europa may create fractures extending downward from the surface of the ice to a depth of ~ 1 kilometer. Using a typical temperature gradient of ~ 10 K km^{-1} and a surface temperature of ~ 100 K (see Paper 1) a temperature of 135 K is reached at a depth of ~ 3.5 km, significantly deeper than the ~ 1 km fractures predicted by Crawford and Stevenson. However, zones of weakness due to previous tidal fractures may extend to much greater depths if Europa's orbital eccentricity was several times larger in the recent past as suggested by Ojakangas and Stevenson (1986). Also, the presence of a low conductivity regolith on Europa's surface may increase the temperature at the base of the fractured region by several tens of degrees, allowing it to considerably exceed 135 K. If the temperature at the base of the fractures or zones of weakness is ~ 145 K, the Maxwell time is only $\sim 10^5$ y.

To estimate the total viscous dissipation rate, W_f , if τ_M at the base of the fractured region is less than the polar wander time scale, we follow a development identical to that which led to Equation (6.8). In this case,

$$W_f \sim (4\pi a^2 \Delta b_f) \eta_f \gamma^2 \dot{\zeta}^2, \quad (6.12)$$

where η_f is the viscosity of the ice at the base of the fractured region, and Δb_f is the thickness of the region of the ice in which the viscosity is within an order of magnitude of η_f . The magnitude of η_f is found by evaluating $\eta(T_f)$ using Equation (6.2), where T_f is the temperature at the base of the fractured region, which we

approximate as

$$T_f \simeq T_s + (T_m - T_s) \left(\frac{z_f}{b_c} \right) , \quad (6.13)$$

where z_f is the depth of the base of the fractured region. Δb_c is found from Equation (6.4), where $\frac{d \log_{10} \eta}{dT}$ is evaluated at $T = T_f$:

$$\frac{d \log_{10} \eta}{dT} = - \frac{\ell(T_m/T_f)^2}{T_m \ln 10} . \quad (6.14)$$

Using Equations (6.2), (6.4), (6.5), and (6.14), equation (6.12) may now be written

$$W_f \sim C_f \zeta^2$$

$$C_f \sim 4\pi a^2 b_c \left(\frac{\ln 10}{\ell} \right) \left(\frac{T_m}{T_m - T_s} \right) \left(\frac{T_f}{T_m} \right)^2 \eta_o \exp \left[\ell \left(\frac{T_m}{T_f} - 1 \right) \right] \gamma^2 . \quad (6.15)$$

As described in the development which led to Equation (6.9), the general reorientation rate of the shell in the x_i'' coordinate system is $(\vec{\omega} - \vec{n})$, and the components of $(\vec{\omega} - \vec{n})$ along each of the x_i'' axes contribute to the total dissipation rate. Thus the generalization of Equation (6.15) to the case of arbitrary $(\vec{\omega} - \vec{n})$ is

$$W_f = C_{f1}(\omega_1 - n_1)^2 + C_{f2}(\omega_2 - n_2)^2 + C_{f3}(\omega_3 - n_3)^2 , \quad (6.16)$$

where the C_{fi} are each of the order of C_f as given by Equation (6.15) but none of them are equal, and the $(\omega_i - n_i)$ are the components of $(\vec{\omega} - \vec{n})$ along the x_i'' axes.

The dissipative torque due to W_f has components

$$\Gamma_{fi} = \frac{-\partial W_f}{\partial \omega_i} = -2C_{fi}(\omega_i - n_i) \quad (6.17)$$

along the x_i'' axes. For simplicity we will assume $C_{f1} = C_{f2} = C_{f3} = C_f$ in the equations of motion of the shell, so that (6.17) becomes simply

$$\vec{\Gamma}_f = -2C_f(\vec{\omega} - \vec{n}) . \quad (6.18)$$

We believe that this assumption does not significantly change the solution of the equations of motion described in the following section.

6.2 Polar Wander of the Shell

We now derive equations of motion for the shell of Europa assuming that the only important torque (other than the tidal torque) affecting its motion is that due to viscous dissipation within the shell itself, as derived in section (6.1). As mentioned previously, we justify this assumption a posteriori in Appendix A using the solution of the equations derived here. There we argue that the Poincaré torque (among others) is unable to induce significant polar wander of the silicate core during reorientation of the shell. This is a significant result because the Poincaré torque is thought to be responsible for the nearly coincident motion of the Earth's core and mantle during the precession of the equinoxes. However, we also argue in Appendix A that it is likely that the Poincaré torque *does* cause the liquid water layer to reorient in coincidence with the ice shell. Therefore we shall refer hereafter to the sum of the ice shell and the liquid water layer collectively as “the shell” for simplicity.

The largest principal moment differences in the inertia tensor of the shell are due to the hydrostatic response of its surface to the tidal and rotational potentials. However, as long as any motion of the shell with respect to the x_i'' coordinate system (i.e. polar wander) occurs on a time scale which is long compared to the rotation period and the characteristic relaxation time of the hydrostatic bulge, that bulge will remain fixed in the x_i'' -coordinate system and will not contribute to the dynamics of the system. The time scale for relaxation of the hydrostatic bulge on the shell is essentially the gravity wave travel time in the ocean (a few hours), since the ocean is effectively inviscid and the overlying thin shell is almost elastic on this time scale and cannot significantly affect the shape of its surface.

A bulge which is stationary in the x_i'' coordinate system during reorientation

of the shell will propagate in a coordinate system which is fixed with respect to it. The propagation of such a bulge implies that a nonzero angular momentum will exist with respect to the frame of the shell during its motion. In problems concerning the dynamics of non-rigid bodies, this momentum is known as relative angular momentum, and must in general be included in the equations of motion (Munk and MacDonald, 1960). However, the ratio of the rate of change of the relative angular momentum to the term in the equations of motion which drives polar wander (which is a measure of its importance in the equations of motion) is

$$\sim \frac{\gamma}{\left(\frac{t}{\tau}\right)} \left(\frac{\tau_{\text{rot}}}{\tau_{pw}}\right)^2$$

where τ_{rot} and τ_{pw} are the rotation period and the time scale on which the polar wander occurs, respectively. Even if τ_{pw} is as small as $\sim 10^3$ years, and $\frac{t}{\tau} \sim 10^{-6}$ (which we shall argue is \sim the upper limit of its possible values), this ratio is $\sim 10^{-8}$. The relative angular momentum is therefore utterly negligible. We conclude from the above discussion that if any large-scale polar wander experienced by the shell occurs on a time scale which is long compared to the rotation period, the components of the inertia tensor due to the hydrostatic tidal and rotational bulges as well as the relative angular momentum due to the motion of those bulges over the shell may be ignored in the equations of motion.

We first investigate the likelihood of polar wander if the shell is not pervasively fractured to a significant depth (see previous section). The equations of motion for the shell are obtained directly from the Euler Equations (5.6)–(5.8) of section 5. Since the Euler equations describe the components of the total rate of change of angular momentum directed along each of the principal axes of the shell, we simply add to each of them the appropriate component of the torque given by

Equation (6.11), projected along the appropriate principal axes of the shell. The equations of motion are thus

$$\frac{d}{dt}(I_1\omega_1) = (I_2 - I_3)\omega_2\omega_3 - 3n^2(I_2 - I_3)\lambda_2\lambda_3 - \frac{C_v}{|\vec{\omega} - \vec{n}|}(\omega_1 - n_1) \quad (6.19)$$

$$\frac{d}{dt}(I_2\omega_2) = (I_3 - I_1)\omega_1\omega_3 - 3n^2(I_3 - I_1)\lambda_1\lambda_3 - \frac{C_v}{|\vec{\omega} - \vec{n}|}(\omega_2 - n_2) \quad (6.20)$$

$$\frac{d}{dt}(I_3\omega_3) = (I_1 - I_2)\omega_1\omega_2 - 3n^2(I_1 - I_2)\lambda_1\lambda_2 - \frac{C_v}{|\vec{\omega} - \vec{n}|}(\omega_3 - n_3) \quad , \quad (6.21)$$

where $(\omega_i - n_i)$ are the components of $(\vec{\omega} - \vec{n})$ directed along the axes of the body coordinate system x_i as defined in Section 5:

$$(\omega_1 - n_1) = \dot{\varphi} \sin \psi \cos \theta - \dot{\theta} \cos \psi \quad (6.22)$$

$$(\omega_2 - n_2) = \dot{\varphi} \cos \psi \cos \theta + \dot{\theta} \sin \psi \quad (6.23)$$

$$(\omega_3 - n_3) = \dot{\varphi} \sin \theta + \dot{\psi} \quad , \quad (6.24)$$

and the other parameters are as defined in Sections 5 and 6.1.

Now several operations are performed to cast Equations (6.19)–(6.21) in a more useful form: The moments of inertia I_i are replaced by the expressions of Equation (5.1), and the λ_i , ω_i , and $(\omega_i - n_i)$ are replaced by Equations (5.3), (5.5), and (6.22)–(6.24), respectively. The product of $\sin \psi$ with Equation (6.19) is added to the product of $\cos \psi$ with Equation (6.20) to obtain Equation (6.25), and the product of $-\cos \psi$ with Equation (6.19) is added to the product of $\sin \psi$ with Equation (6.20) to obtain Equation (6.26). Equation (6.27) is obtained directly from equation (6.21). The resulting equations are divided by I_o . Finally, it is assumed that $\left(\frac{t}{\tau}\right) \ll \epsilon$, $\varphi \ll \theta \ll 1$, $\dot{\theta} \ll n$, $\dot{\varphi} \ll n$, $\dot{\varphi}\theta \ll \dot{\psi} \ll n\theta$ so that when such terms appear together, the smaller is neglected. These assumptions may be verified a posteriori.

The resulting equations of motion may be written as follows:

$$\ddot{\varphi} = -3n^2\epsilon\varphi + n\theta\dot{\theta} - 2n^2\theta\left(\frac{t}{\tau}\right)\sin 2\psi - \frac{1}{I_o}\frac{C_v}{|\vec{\omega} - \vec{n}|}\dot{\varphi} \quad (6.25)$$

$$\ddot{\theta} = n\dot{\psi} - 4n^2\epsilon\theta - \frac{1}{I_o}\frac{C_v}{|\vec{\omega} - \vec{n}|}\dot{\theta} \quad (6.26)$$

$$n\dot{\theta} = \frac{1}{2}\left(\frac{t}{\tau}\right)n^2\sin 2\psi - \frac{1}{I_o}\frac{C_v}{|\vec{\omega} - \vec{n}|}\dot{\psi} \quad (6.27)$$

Because $|\vec{\omega} - \vec{n}| \approx \dot{\psi}$ in the solution to the (undamped) equations of motion of Section 5, we expect that if polar wander occurs at all, $\dot{\psi}$ will be the dominant component of $|\vec{\omega} - \vec{n}|$ in the solution of Equations (6.25)–(6.27), which include the damping torque described in Section 6.1. Also from the development of Section 5, we may identify the right-hand side of Equation (6.27) as the important quantity driving polar wander. If the right-hand side of Equation (6.27) is a positive quantity, the shell will experience polar wander. This criterion may now be written

$$\sin 2\psi \gtrsim \frac{2C_v}{\left(\frac{t}{\tau}\right)n^2I_o} \quad (6.28)$$

I_o is taken to be the moment of inertia of a thin spherical shell,

$$I_o \simeq \frac{8\pi}{3}\rho b_o a^4 \quad , \quad (6.29)$$

where ρ , b_o , and a are the density, average thickness, and radius of the shell, respectively. Using Equations (6.8) and (6.29), the criterion (6.28) may be written

$$\sin 2\psi \gtrsim \left(\frac{\mu}{4 \times 10^{10} \text{ dynes cm}^{-2}}\right) \left[\frac{10^{-5}}{(t/\tau)}\right] \quad (6.30)$$

when values of b_o and ρ are taken to be ~ 100 km and ~ 1 g cm $^{-3}$, respectively, and other parameter values are as stated previously.

The quantity $\left(\frac{t}{\tau}\right)$ for a shell which is not coupled to the core of Europa is essentially

$$\frac{t}{\tau} = \frac{(I_{yy} - I_{zz})}{I_o} \quad , \quad (6.31)$$

where I_{yy} and I_{zz} are as defined by Equations (3.13) and (3.14), and the C_{2m} are those portions of the total C_{2m} which are due to ice thickness variations and the fossil bulge on the shell. Using Equations (3.9), (3.18), and (4.10), the equilibrium value of $\left(\frac{t}{\tau}\right)$ may thus be written

$$\left(\frac{t}{\tau}\right)_{\text{equil}} \simeq (10^{-5}) \left[\left(\frac{t_{20} + 2t_{22}}{1 \text{ km}} \right) - 0.6 \left(\frac{\mu}{4 \times 10^{10} \text{ dynes cm}^{-2}} \right) \left(\frac{d}{2 \text{ km}} \right) \right] \quad (6.32)$$

for a shell (ice plus ocean) of ~ 100 km thickness, $b_c \sim 20$ km, and other parameters as discussed in Section 4.

Similarly, the quantity ϵ is essentially

$$\epsilon = \frac{(I_{zz} - I_{xx})}{I_o} \quad (6.33)$$

where I_{xx} and I_{zz} are as defined by Equations (3.12) and (3.14), and the C_{2m} are those portions due to a fossil bulge on the shell (see equation (4.10)) and ice thickness variations. Using Equations (3.9), (3.12), (3.14), and (4.10), (6.33) may be written

$$\epsilon \simeq 2 \times 10^{-5} \left[\left(\frac{d}{2 \text{ km}} \right) \left(\frac{\mu}{4 \times 10^{10} \text{ dynes cm}^{-2}} \right) + (0.5) \left(\frac{-t_{20} + 2t_{22}}{1 \text{ km}} \right) \right] , \quad (6.34)$$

for a shell with a thickness of ~ 100 km, and other parameters as discussed in section 4.

At this point it is necessary to discuss in some detail the value which $\left(\frac{t}{\tau}\right)$ is likely to attain.

Since $(t_{20} + 2t_{22})$ may become as large as ~ 1 km if the ice thickness approaches its thermal equilibrium profile (see section 4 and Paper 1), Equation (6.32) appears to indicate that $\frac{t}{\tau}$ may approach values on the order of $\sim 10^{-5}$. However, a thermal equilibrium ice thickness profile can only be achieved on a time scale which

approaches the time required for an element of heat to diffuse through the entire ice shell. As the following discussion indicates, polar wander must occur on a time scale significantly shorter than this diffusion time, or the mechanism driving the polar wander is effectively eliminated.

The evolution of the thickness profile of the ice shell is driven by spatial variations in the distribution of tidal heating within the ice and the temperature at the surface of the ice (see Paper 1), both of which are functions of latitude and longitude *measured in a coordinate system which is synchronously rotating* (e.g., the x_i'' coordinate system described in Section 5 or the X, Y, Z coordinate system in which the gravitational harmonics are computed (Section 4)). Since $\frac{t}{\tau}$ represents a fraction of the inertia tensor measured *in the frame of the shell*, it is clear that its growth will be affected by reorientation of the shell with respect to a synchronously rotating coordinate system. In the extreme case where reorientation occurs on a time scale longer than the thermal diffusion time for the entire thickness of the ice shell ($\sim 10^7$ years), the inertia tensor of the shell would become effectively fixed in the synchronously rotating coordinate system, regardless of the motion of the shell. Furthermore, the form of such an inertia tensor would correspond to a pendulum which is continually balanced directly above its support so that the driving mechanism for the polar wander would be effectively eliminated. If reorientation occurs on a shorter time scale, however, the evolution of the thickness profile will remain effectively unaltered by polar wander of the shell for the period of time which is required for the effects of an altered surface temperature and local tidal dissipation rate to diffuse toward the base of the ice (where increments to the ice thickness are accrued). The effects of a changing surface temperature cannot reach the base of the ice until the thermal diffusion time for the shell's entire thickness

has elapsed. However, the effect of the spatial distribution of tidal dissipation on ice thickness is in general more important in determining the value of $t_{20} + 2t_{22}$ than the effect of variations of surface temperature (see Paper 1).

Since most of the tidal dissipation is probably concentrated in the lowermost ~ 1 km or so of the ice, the base of the ice will begin to respond to its changing thermal environment within about 10^5 years (the diffusion time through ~ 1 km of ice) after substantial polar wander begins. However, large-scale changes in the amount of heat flowing upward from the base of the ice (and hence the rate at which $\left(\frac{t}{\tau}\right)$ grows), cannot occur without alteration of the temperature gradient of a substantial portion of the ice above the level where the dissipation is concentrated. Therefore, we conclude that $\left(\frac{t}{\tau}\right)$ will continue to grow throughout the period during which the polar wander occurs, if the time scale of the polar wander is significantly smaller than 10^7 y.

The equilibrium value of $\left(\frac{t}{\tau}\right)$ given by Equation (6.32) indicates that the principal moments of the shell may change by a fraction $\sim 10^{-5}$ in $\sim 10^7$ years (the thermal diffusion time through a 20 km-thick ice shell) if the thermal-equilibrium value of $t_{20} + 2t_{22}$ is ~ 1 km. Therefore, the parameter $\tau \sim 10^{12}$ years.

The actual response of the time evolution of the thickness profile to reorientation is clearly complicated. We (somewhat arbitrarily) assume that $\left(\frac{t}{\tau}\right)$ will cease to grow when $t \gtrsim 2 \times 10^6$ years, if substantial reorientation has occurred by that time. Thus if $\tau \sim 10^{12}$ years, $\frac{t}{\tau}$ cannot exceed a value of $\sim \text{few} \times 10^{-6}$.

From the above discussion it is evident that $t_{20} + 2t_{22}$ cannot attain its thermal equilibrium value if polar wander is to occur. Polar wander must occur on a time scale less than the diffusion time through the ice.

Therefore it is inappropriate to insert values of $\frac{t}{\tau}$ larger than $\sim \text{few} \times 10^{-6}$

in Equation (6.30). Note also from Equations (6.32) and (6.34) that for values of $\frac{t}{\tau} \lesssim 10^{-6}$, the requirement that $\frac{t}{\tau} \ll \epsilon$ is satisfied for $\mu \sim 4 \times 10^{10}$ dynes cm^{-2} and $d \sim 2$ km.

Now it is clear from the criterion (6.30) that ψ must have an initial value of $\gtrsim 10$ degrees in order for polar wander of the shell to be initiated, even if μ is as small as the lower limit given by Hobbs (1974) of $\sim 10^9$ dynes cm^{-2} and $\left(\frac{t}{\tau}\right)$ is as large as $\sim 10^{-6}$. The authors know of no reasonable mechanism capable of inducing such large initial values of ψ . For illustration, to produce an off-diagonal element of the inertia tensor of the shell of a magnitude corresponding to a value of ψ of $\sim 10^\circ$ by an impacting body, one would require an impact in mid-latitudes of a 3 g cm^{-3} object ~ 300 km in radius.

We therefore claim that it is virtually impossible for polar wander of the shell to be initiated if the shell is not pervasively fractured to a significant depth. Using the analogy (described in Section 5) of the angle 2ψ to a pendulum, it is as though the pendulum, which becomes balanced at the top of its support as t becomes positive, is immersed in a substance which produces a large, constant frictional force opposing its motion whenever $\dot{\psi} \neq 0$. The pendulum is thus "stuck" at the top of its support, where the effect of gravity on its motion is very small.

We now examine the case (see Section 6.1) where the ice shell is pervasively fractured due to tidal stresses, to a depth where the local Maxwell time is less than $\sim \text{few} \times 10^6$ y, the maximum time scale on which polar wander can occur. In this case, as described in Section 6.1, the torque to viscous dissipation in the shell during polar wander has a significantly smaller magnitude, and a form which we approximate by Equation (6.18). The development of the equations of motion is identical to that which led to Equations (6.25)–(6.27), when the torque given by

Equation (6.11) is replaced by Equation (6.18). We write the resulting equations as follows:

$$\ddot{\varphi} = -3n^2\epsilon\varphi + n\theta\dot{\theta} - 2n^2\theta\left(\frac{t}{\tau}\right)\sin 2\psi - \left(\frac{C_f}{I_o}\right)\dot{\varphi} \quad (6.35)$$

$$\ddot{\theta} = n\dot{\psi} - 4n^2\epsilon\theta - \left(\frac{C_f}{I_o}\right)\dot{\theta} \quad (6.36)$$

$$n\dot{\theta} = \frac{1}{2}\left(\frac{t}{\tau}\right)n^2\sin 2\psi - \left(\frac{C_f}{I_o}\right)\dot{\psi} \quad , \quad (6.37)$$

where C_f is given by Equation (6.15). The solution of Equations (6.35)–(6.37) is found as follows: we first assume that the terms $\ddot{\theta}$ and $\left(\frac{C_f}{I_o}\right)\dot{\theta}$ in Equation (6.36) are insignificant compared to the others (verifiable a posteriori). Thus Equation (6.36) gives

$$\theta \simeq \frac{\dot{\psi}}{4n\epsilon} \quad (6.38)$$

(as was also found in the dissipationless case described in Section 5). Differentiating Equation (6.38) with respect to time and inserting the result for $\dot{\theta}$ on the left-hand side of Equation (6.37), the following decoupled equation describing the evolution of ψ is found:

$$\ddot{\psi} \simeq 2\left(\frac{t}{\tau}\right)\epsilon n^2\sin 2\psi - 4\epsilon\left(\frac{C_f}{I_o}\dot{\psi}\right) \quad . \quad (6.39)$$

Equation (6.39) is the equation of a simple damped pendulum, for which the direction of gravity reverses as $\left(\frac{t}{\tau}\right)$ passes through zero. By analogy to the equation of the damped simple harmonic oscillator, it is easy to show that the solution to Equation (6.39) is overdamped if the square of the coefficient multiplying $\dot{\psi}$ is much greater than the coefficient multiplying $\sin 2\psi$. Using Equations (6.15) and (6.29), this criterion may be written

$$\left(\frac{t/\tau}{\epsilon}\right)(10^{-6}) \ll 1 \quad (6.40)$$

for $T_f \sim 145$ K for $T_s \sim 100$ K, $\eta_o \sim 10^{14}$ Poise, and other parameter values as given previously. Thus the system is clearly in the overdamped regime for reasonable choices of parameters. The inertial term $\ddot{\psi}$ may therefore be ignored in Equation (6.39), so that

$$\dot{\psi} = \frac{1}{2} \left[\frac{\left(\frac{t}{\tau}\right) n^2 I_o}{C_f} \right] \sin 2\psi \quad , \quad (6.41)$$

which may be integrated, yielding

$$\tan \psi = (\tan \psi_o) \exp \left(\frac{t}{\tau_f} \right)^2 \quad (6.42)$$

$$\tau_f = \left[\frac{C_f \tau}{n^2 I_o} \right]^{\frac{1}{2}} \quad ,$$

where ψ_o is the value of ψ when t passes through zero, and τ_f is the characteristic time scale of the polar wander. Figure 8 shows $\psi(t)$ as given by Equation (6.42). The time required for large scale polar wander to occur is very weakly dependent on ψ_o , as may be seen by solving equation (6.42) for the value of t when ψ reaches 45° :

$$t(\psi = 45^\circ) = [-\ln(\tan \psi_o)]^{\frac{1}{2}} \tau_f \quad . \quad (6.43)$$

For example, Equation (6.43) indicates that the time scale for large scale polar wander is more than an order of magnitude larger than τ_f only if $\psi_o \lesssim 10^{-11}$ radians. Small effective values of ψ_o are inevitable due to irregularities in ice albedo (leading to irregularities in ice thickness), small impacting bodies, etc. Thus if polar wander is favored, it is very easily initiated and occurs on a time scale comparable to τ_f , virtually regardless of the value of ψ_o .

However, as discussed earlier, τ_f must be significantly shorter than the time scale for diffusion of heat through the shell ($\sim 10^7$ y). τ_f depends on the temperature, T_f , at the base of the fractured region. In Figure 9, τ_f is plotted as a function

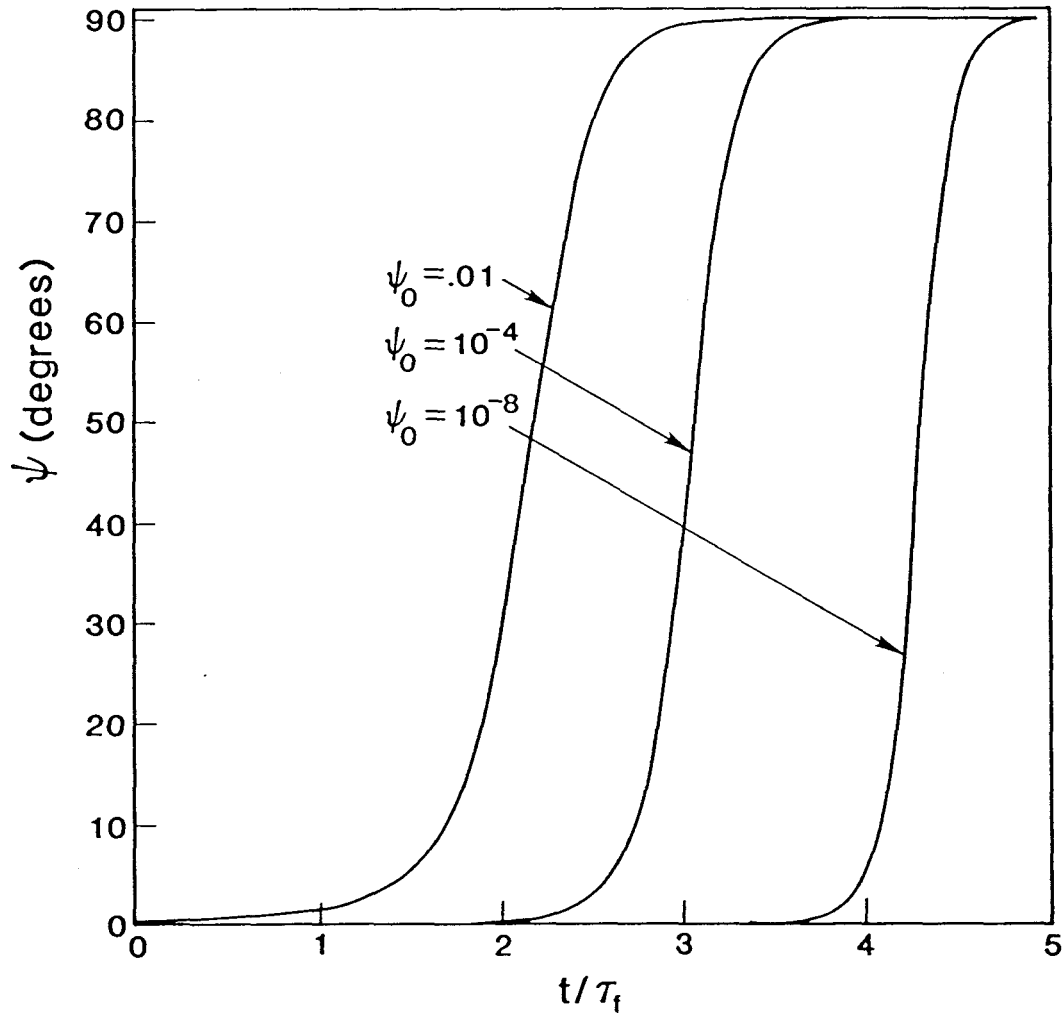


Figure 8. The polar wander tip-angle ψ as a function of time as given by Equation (6.42). Curves are labeled by ψ_0 , the initial value of ψ . Time is in units of τ_f . Note the weak dependence of the time required for polar wander on ψ_0 .

of T_f , using Equations (6.15), (6.29), and (6.42). The Maxwell time at the base of the fractured region is also plotted as a function of T_f in Figure 9, using equation (6.2) in the definition of the Maxwell time, $\tau_M \equiv \frac{\eta}{\mu}$. In order for the dissipative torque to be roughly described by Equation (6.18) it is necessary for the Maxwell time at the base of the fractured region to be significantly smaller than τ_f (see section 6.1). Figure 9 demonstrates that this requirement is satisfied for our choices of parameters, at all values of T_f . Note that if $T_f \lesssim 140$ K, τ_f exceeds $\sim \text{few} \times 10^6$ y and polar wander probably does not occur, for the reasons discussed in section 6.1.

It is instructive to compare τ_f to the time scale for undamped polar wander given by Equation (5.26). If $\epsilon \sim 10^{-5}$ (see Equation (6.34)) and $\tau \sim 10^{12}$ y (see above) Equation (5.26) gives $T \sim 5 \times 10^3$ years. Thus if polar wander were uninhibited by dissipation within the shell, it would occur in only $\sim 5 \times 10^3$ years. This is therefore a lower limit to the actual polar wander time scale.

The evolution of θ during polar wander is found immediately from equations (6.38) and (6.41):

$$\theta \simeq \frac{1}{8} \left(\frac{t/\tau}{\epsilon} \right) \left(\frac{nI_o}{C_f} \right) \sin 2\psi \quad , \quad (6.44)$$

where the time behavior of ψ is given by Equation (6.42).

Inserting Equation (6.44) into Equation (6.35), it may now be seen that the first and third terms dominate on the right-hand side of (6.35), so that

$$\varphi \simeq -\frac{2}{3} \left(\frac{t/\tau}{\epsilon} \right) \theta \sin 2\psi \simeq -\frac{1}{12} \left(\frac{t/\tau}{\epsilon} \right)^2 \left(\frac{nI_o}{C_f} \right) [\sin 2\psi]^2 \quad . \quad (6.45)$$

Equations (6.42), (6.44), and (6.45) completely describe the solution to lowest order of the equations of motion (6.35)–(6.37).

Using $T_f \sim 145$ K, and other parameter values as stated previously, Equations

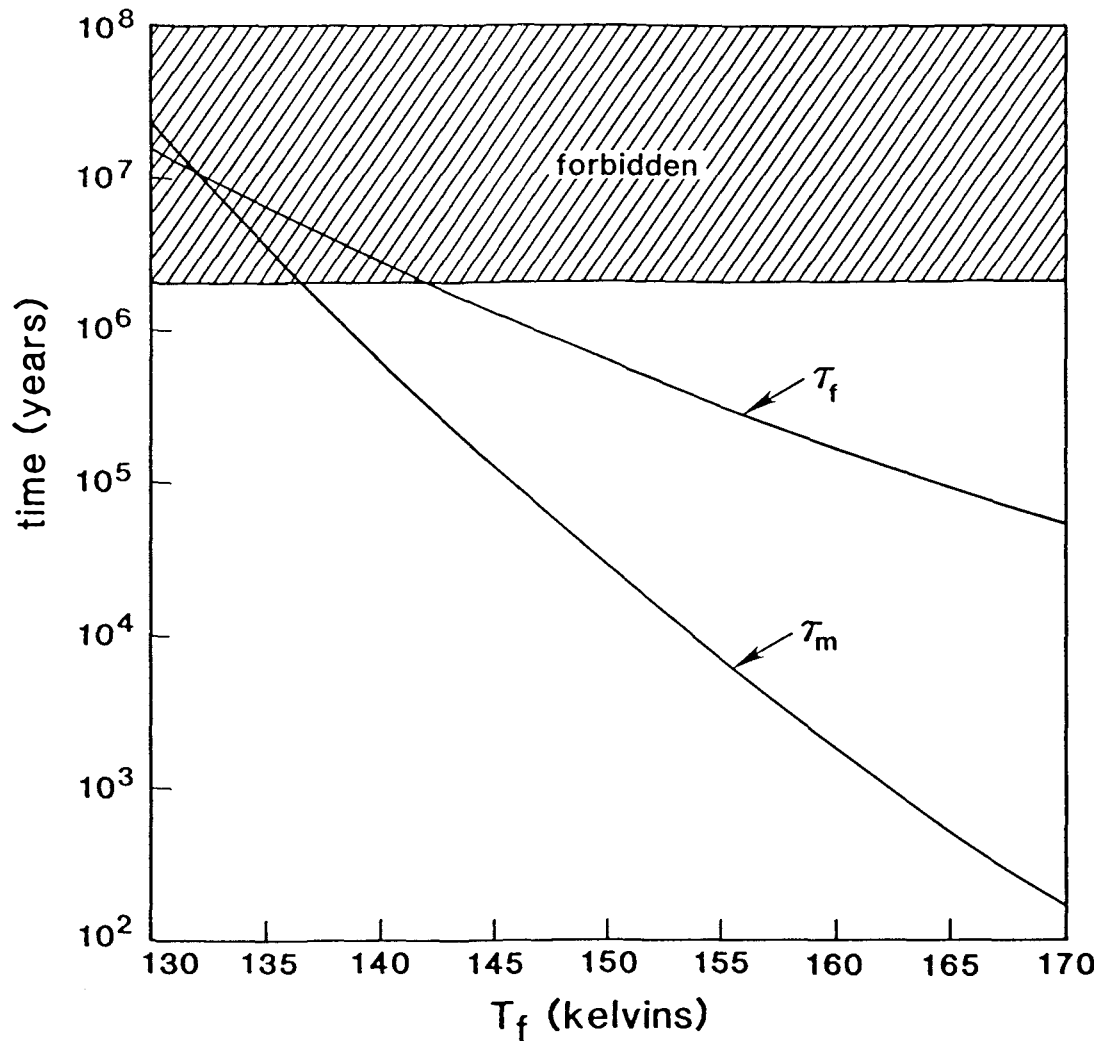


Figure 9. The time scale τ_f and the Maxwell time τ_M at the base of the fractured region, plotted as functions of T_f . τ_M must be less than τ_f , and τ_f must be less than $\sim 2 \times 10^6$ years or the mechanism driving polar wander is eliminated by thermal diffusion (see text).

tions (6.44) and (6.45) may be written

$$\theta \simeq 1.2 \times 10^{-4} \left(\frac{t/\tau}{\epsilon} \right) \sin 2\psi \quad (6.46)$$

$$\varphi \simeq -8 \times 10^{-5} \left(\frac{t/\tau}{\epsilon} \right)^2 [\sin 2\psi]^2 \quad (6.47)$$

Thus θ and φ remain very small while ψ evolves from \sim zero to $\frac{\pi}{2}$. It may now be readily verified that $\varphi \ll \theta \ll 1$, $\dot{\theta} \ll n$, $\dot{\varphi} \ll n$, and $\dot{\varphi}\theta \ll \dot{\psi} \ll n\theta$ (as was assumed when simplifying the equations of motion to obtain Equations (6.35)–(6.37)), as long as $\left(\frac{t}{\tau}\right) \ll \epsilon$. Because the ice is assumed in this development to be pervasively fractured to a depth where the Maxwell time is less than τ_f , any fossil bulge on the shell due to elastic behavior of the outer regions of the ice must be set to zero, because strains in the elastic portion of the shell are accommodated by the fractures (see Section 6.1). Thus, when evaluating $\frac{t}{\tau}$ and ϵ using Equations (6.32) and (6.34), only the terms which are proportional to the ice thickness components, t_{2m} , should be retained. The criterion $\frac{t}{\tau} \ll \epsilon$ may then be written

$$\left(\frac{t/\tau}{\epsilon} \right) \approx \frac{1}{2} \left[\frac{t_{20} + 2t_{22}}{-t_{20} + 2t_{22}} \right] \ll 1 \quad (6.48)$$

In Table I of Paper 1, values of the quantities $4t_{22}$ and $t_{20} + 2t_{22}$ are tabulated for four examples of plausible thermal equilibrium thickness profiles for a decoupled ice shell. Three of the examples have $t_{20} + 2t_{22} > 0$, so that polar wander is possible. In the first such example the ice is assumed to behave as a Maxwell medium and a uniform heatflow of $10 \text{ erg cm}^{-2} \text{ s}^{-1}$ is assumed to flow into the ice from the core. In the second example the ice is assumed to behave according to the generalized Glen's flow law with a flow law exponent of $n_G = 3$, and in the third example a generalized flow law is also assumed, with a more extreme value of $n_G = 5$ (see Paper 1 for other details). For these three examples the values which

$\left(\frac{t/\tau}{\epsilon}\right)$ would have in thermal equilibrium may be derived from Table I of Paper 1, giving ~ 0.05 , ~ 0.2 , and ~ 0.3 , respectively. Thus, if thermal equilibrium were reached, the criterion (6.48) would be only marginally satisfied. However, we have argued that polar wander can only occur if $\frac{t}{\tau}$ remains substantially smaller than its thermal equilibrium value throughout the period during which polar wander takes place. While $\frac{t}{\tau}$ must evolve from negative to positive values as the thickness profile approaches thermal equilibrium, it may be easily shown that the thermal equilibrium value of the principal moment difference represented by ϵ when $\psi = 0$ (before polar wander) is not markedly different from the thermal-equilibrium value of ϵ when $\psi = \frac{\pi}{2}$ (after polar wander). Using Equations (3.9), (3.12)–(3.14), and (3.18), the former and latter may be seen to be proportional to the thermal equilibrium values of $-t_{20} + 2t_{22}$ and $4t_{22}$, respectively. These quantities are of the same sign. The average difference between them, derived from Table I of Paper 1, is only $\sim 30\%$, and is as small as $\sim 9\%$ for the case of the Maxwell rheology (with the nonzero core heatflow). For the Maxwell model of Table I with zero core heatflow, it is only $\sim 2\%$ (although polar wander is not likely for that model). Because the thermal equilibrium value of ϵ does not depend strongly on the orientation of the shell, it is therefore likely that ϵ may remain close to that value throughout the history of the shell. Since $\left(\frac{t}{\tau}\right)$ must be significantly smaller than its thermal equilibrium value during polar wander, the criterion given by (6.48) may therefore be well satisfied. In any case, we expect that the solution for the shell's motion given by (6.42), (6.44), and (6.45) will be roughly correct even if the inequality (6.48) is not strong.

6.3 Discussion

Several additional points bear mentioning:

As indicated in Figure 9, polar wander of a shell which is pervasively fractured (from the surface downward) may occur on a time scale $\tau_f \sim 10^5\text{--}10^6$ y if the temperature at the base of the fractured region, T_f , exceeds 140 K. Shorter time scales are possible if T_f is higher still. However, as discussed in Section 6.2, typical temperature gradients make shorter time scales unlikely. Thus the lower limit to τ_f is somewhat uncertain, although for very large values of T_f it must be limited by the time scale for undamped polar wander of $\sim \text{few} \times 10^3$ y given by Equation (5.26). An upper limit is given by the fact that polar wander must occur on a time scale significantly shorter than the time required for diffusion of heat through the ice, $\sim 10^7$ y (see Section 6.2).

Another important time scale which polar wander must not approach is the time scale on which topography at the base of the shell will exhibit viscous flow. Viscous flow will occur because of the horizontal pressure variation within the ice, despite the presence of isostasy. Such flow will, of course, tend to eliminate the t_{2m} and hence the mechanism which drives the polar wander. The time scale for viscous flow is found in Appendix B to be on the order of $10^6\text{--}10^7$ years. Since this is similar to the thermal diffusion time for the shell, it therefore imposes no significant additional constraint on the range of time scales on which polar wander may occur.

It is likely that large scale polar wander of the shell occurs episodically: a state of thermal equilibrium for the shell is approached on a time scale of $\sim 10^7$ years (the thermal diffusion time scale). At some point during this approach to thermal equilibrium (when the orientations of the maximum and intermediate principal axes interchange), the shell becomes dynamically unstable and reorients toward the preferred orientation for synchronous satellites on the time scale τ_f . The shell then

begins to approach the thermal-equilibrium thickness profile as determined by its new orientation, and the process repeats itself. However, it is possible that the shell actually exhibits a continuous drifting motion on the thermal diffusion time scale of $\sim 10^7$ y, always remaining in a condition of slight thermal and orientational disequilibrium. Such a state probably can only occur if the time scale τ_f is comparable to the thermal diffusion time.

In Section (6.2) it is argued that polar wander cannot occur unless the strain imposed during reorientation is accommodated by fractures which extend from the surface to a depth such that they penetrate the layer which responds viscously on the polar wander time scale. The results of Crawford and Stevenson (1988) are called upon as support for the conjecture that such fractures may exist due to the influence of the eccentricity tide. However, the results of Crawford and Stevenson also suggest that the eccentricity tide may induce fractures extending upward from the base of the shell, as far as $\sim 92\%$ of the shell's thickness (if volatiles exist in solution within the liquid water layer, the fractures may even reach the surface). If pervasive fractures extend both downward from the surface and upward from the base of the shell, it is possible that viscous deformation during polar wander may be largely eliminated by motion along fractures. It is then possible that the polar wander proceeds relatively unhindered by viscous dissipation. Perhaps only a much smaller "effective" viscosity of the fractured ice contributes to the damping process. The polar wander time scale may then approach the time scale for undamped polar wander (Equation (5.26)) of $\sim 10^3$ y. However, if the viscosity and rigidity at the base of the shell have reasonable values of $\sim 10^{14}$ Poise and 4×10^{10} dynes cm^{-2} , respectively, the Maxwell time at the base of the ice is ~ 40 minutes, ~ 100 times shorter than the frequency of the tidal forcing (~ 3.5 days). Therefore, the ice at

the base of the shell may behave viscously on the tidal time scale and fractures extending upward from the base of the shell may not be produced.

As discussed in section (6.2), the simple model presented in this paper seems to indicate that polar wander of Europa's ice shell (by the mechanism described in this paper) is an unlikely cause of the extensive fractures of the satellite's surface which were observed in the Voyager images: unless extensive surface fractures exist as a result of another mechanism (e.g., the eccentricity tide) the polar wander process is so severely limited by viscous friction that it cannot occur. However, it is possible that the simple rheology employed in our calculations does not realistically describe the behavior of Europa's ice. If the actual dissipation within the ice resulting from polar wander is significantly smaller than our calculations suggest, large scale polar wander may occur without substantial preexisting fractures. If this is the case, polar wander would provide a very effective mechanism for fracturing the shell, as the stresses imparted to the elastic lithosphere during polar wander are $\sim \frac{1}{e} \sim 100$ times larger than the stresses imposed by the eccentricity tide (e is Europa's orbital eccentricity).

As discussed in Appendix A, a rotating fluid confined within an ellipsoidal cavity will have a torque known as the Poincaré torque exerted upon it by the cavity whenever the axis of symmetry of the cavity departs from the axis of rotation of the fluid. In Appendix A it is argued that the Poincaré torque exerted on the layer of liquid water by the ice shell probably causes the liquid to reorient in coincidence with the ice during polar wander, but that the Poincaré torque exerted on the silicate core by the overlying liquid is unable to induce significant motion of the core during polar wander. This result is noteworthy because the Poincaré torque is believed to be responsible for the very nearly coincident motion exhibited by the earth's

fluid core and its mantle during the precession of the equinoxes (cf. Rochester, 1976). The important distinctions between these very different problems may be described as follows: The Poincaré torque is large only if the axis of symmetry of the cavity departs from the rotation axis of the fluid contained within it by a large angle. In the case of the liquid layer and the ice shell on Europa, the axis of rotation of the fluid and the shell (as well as the core) always have very nearly the same direction in inertial space, but the lower surface of the shell (the “containing cavity”) has a large nonspherical permanent component to its surface due to the ice thickness variations, which departs from the rotation axis by a large angle ($\approx \psi$) as polar wander proceeds. Therefore the liquid layer is strongly coupled to the shell during polar wander. The Poincaré torque cannot be minimized by alignment of the rotation axis of the liquid with the symmetry axis of the cavity because angular momentum must be conserved. In the case of coupling between the core and the overlying liquid, the “cavity” (the surface of the core) is surrounded by the liquid. Since the rotation axis of the liquid (in coincidence with the ice) departs from its initial direction by an angle of only $\sim \frac{\dot{\psi}}{n}$ during polar wander ($\sim 10^{-7}$ to 10^{-8} radians for $\tau_{pw} \sim \frac{1}{\psi} \sim 10^5$ y to 10^6 y) the angle between the rotation axis and the symmetry axis of the core is always very small, so that the Poincaré torque is ineffective and the core cannot participate in the polar wander. In the case of the forced precession of the earth, the axis of figure of the containing cavity (the mantle) is essentially the mantle’s rotation axis, which exhibits large motions in inertial space on the precession time scale. In that case, the Poincaré torque is large unless the rotation axis of the fluid core closely follows that of the mantle. Since the torques due to the sun and the moon acting on the rotational bulges of the core and mantle are present in that case, the Poincaré torque can be minimized

by alignment of the rotation vectors.

The difference in the effectiveness of the Poincaré torque in core–mantle coupling on the earth and core–ocean coupling on Europa may be stated as follows: The characteristic rate of change of the angular momentum of the shell of Europa during polar wander is $\sim I_o n^2 \left(\frac{t}{\tau}\right)$, while the magnitude of the Poincaré torque acting on the core is $\sim \rho_{\text{water}} a^5 n^2 \gamma \chi$, where χ is the angle between the angular velocity vectors of the core and the overlying liquid. Comparing the above quantities, it is seen that the Poincaré torque is unable to couple the motion of the core to that of the overlying liquid if

$$10^{-3} \left(\frac{10^5 \text{ years}}{\tau_{pw}} \right) \left(\frac{10^{-6}}{\frac{t}{\tau}} \right) \ll 1 \quad , \quad (\text{A.6})$$

where τ_{pw} is the time scale on which the polar wander occurs, and $\chi \sim \frac{\dot{\psi}}{n} \sim \frac{\tau_{rot}}{\tau_{pw}}$, where $\tau_{rot} \sim \frac{1}{n}$ is the rotation period (see Appendix A). Except for a short period near $t = 0$, this inequality is well satisfied throughout the period during which the polar wander occurs. By contrast, the criterion that must be satisfied if the Poincaré torque is to be unimportant for the case of forced precession is

$$\left(\frac{\tau_{rot}/\tau_{pw}}{\gamma} \right) \gg 1 \quad , \quad (\text{6.49})$$

where τ_{prec} is the time scale of forced precession (cf. Lamb, 1932). For the forced precession of the earth, the left hand side of (6.49) is $\sim 10^5$ times *smaller* than unity. The Poincaré torque is thus very important in that problem.

Another question to be addressed is whether the topography at the base of the ice shell which drives the polar wander may melt as a result of friction with the underlying water during the polar wander process. The result depends on whether the kinetic energy (measured with respect to the core) acquired by a parcel of ice

during polar wander exceeds the latent heat of melting for the parcel. Since the kinetic energy per gram is $\sim \left(\frac{a}{\tau_{pw}}\right)^2$ and the latent heat is $\sim 10^9$ erg/g, the kinetic energy may be seen to be smaller than the latent heat by $\sim 10^{13}$ even if τ_{pw} is as short as $\sim 10^3$ years. Furthermore, the relative motion in our model is confined to a boundary layer at the core-ocean interface, and we expect relative motion at the base of the ice to be slight. The topography clearly cannot melt as a result of relative motion at the ice-ocean interface.

The total energy dissipated in the ice shell due to polar wander may be seen by integration of equation (6.15) to be on the order of

$$\int_0^{\tau_f} C_f \dot{\psi}^2 dt \sim \frac{C_f}{\tau_f} \sim n \left(\frac{I_o C_f}{\tau} \right)^{\frac{1}{2}} . \quad (6.50)$$

Using Equations (6.15), (6.29), and (6.42), equation (6.50) gives a total energy of $\sim 10^{25}$ ergs for $T_f \sim 145$ K and other parameter values as quoted in Section 6.1. This amounts to an average heatflow of $\sim 10^{-5}$ erg cm $^{-2}$ sec $^{-1}$ if the polar wander occurs in $\sim 10^5$ years. Since typical heatflows due to tidal dissipation in the ice are ~ 10 erg cm $^{-2}$ sec $^{-1}$ (see Paper 1), the heatflow caused by polar wander is negligible by comparison.

It should be noted that all of the dissipation which occurs throughout the time evolution of the ice thickness profile is not explicitly included in the damping mechanisms described in this paper. A significant dissipation is implied by the fact that the inertia tensor in our model is assumed to evolve in time in a manner which is independent of the orientation of the shell with respect to the rotational and tidal potential fields. In general, an arbitrary quasistatic redistribution of elements of mass within a spatially varying potential field will involve dissipation of energy. The magnitude of this energy in the problem described in this paper is $\lesssim \left(\frac{t}{\tau}\right) I_o n^2$,

which is $\sim 10^{24}$ erg if $\left(\frac{t}{\tau}\right)$ remains $\lesssim 10^{-6}$. This energy has been ignored in this development by ignoring terms of the form $\dot{I}_i\omega_i$ in the Euler equations of motion.

7. Conclusions

If Europa's structure consists of an elastic ice shell separated from a silicate core by a layer of liquid water, the variations in surface temperature over the shell, and tidal dissipation within it, will cause its thickness to vary with latitude and longitude in its thermal equilibrium state (Paper 1). The second degree components of these thickness variations contribute to the satellite's inertia tensor, as does the presence of a fossil rotational and tidal bulge. Since the thickness variations are accrued at the base of the ice shell, the problem is one where an elastic lithosphere is loaded from below. Following the approach used by Willemann and Turcotte (1981), we have developed equations that describe the effect on a body's inertia tensor of second-harmonic-degree topography that is added to the base of an elastic lithosphere on a planetary body. Analysis of the inertia tensor which Europa would have if its shell were in thermal equilibrium indicates that for many choices of parameters, such a state would involve an orientation of Europa's principal axes which is unusual for synchronously rotating satellites. Specifically, the axes of the intermediate and maximum principal moments are interchanged. To reach the preferred orientation, a thermal-equilibrium ice shell must execute a net reorientation of ninety degrees about the satellite-planet direction.

We have presented a simple model of a rigid, synchronously rotating satellite in a circular orbit for which the difference between the intermediate and maximum moments is linear in time, passing through zero when $t = 0$. The simple model indicates that the expected reorientation is indeed dynamically favored, accompanied

by a small transient tilt of the x_3 body axis (which normally is coincident with the satellite–planet direction) out of the plane of the orbit, and a small transient lag of the same axis behind the satellite–planet direction.

In order to determine more realistically the form which polar wander of an ice shell would take, we have considered a more realistic model which includes the effects of various torques which act to couple the motions of the core, shell, and liquid water layer, and the effect of viscous dissipation occurring in the shell as a result of polar wander. The coupling torques considered include the Poincaré torque, gravitational coupling, and the torque due to viscous or turbulent shear in the liquid water layer. None of these torques are found to be capable of inducing significant motion of the silicate core during polar wander of the shell. However, the Poincaré torque acting across the shell–ocean boundary may be shown to have precisely the magnitude and direction which is necessary to induce coincident motion of the liquid water layer and the shell (see Appendix A). We therefore assume that the liquid water layer and the ice shell move as a single, rigid entity. Such “rigid body” behavior of a liquid confined within an ellipsoidal cavity has been shown by Lamb (1932) to be a valid solution of the fluid dynamical equations of motion for a similar system. Relative motion between the silicate core and the overlying water is assumed to be confined to a boundary layer at the base of the ocean. It is found that viscous dissipation arising in the shell as a result of reorientation virtually eliminates the possibility that polar wander may occur, unless fractures (e.g., due to tidal stresses) extend from the surface of the shell to a depth where the ice behaves viscously on the polar wander time scale (i.e. a few kilometers or alternatively ~ 1 km if an insulating regolith exists which elevates the near–surface temperature by a few tens of Kelvins). Fractures extending to ~ 1 km depth due to

tidal stresses are predicted by Crawford and Stevenson (1988). If the temperature T_f at the base of the fractured region is between 140–145 K, polar wander occurs on a time scale of 10^6 – 10^5 years (decreasing as T_f increases) after the sign of the difference between the intermediate and maximum principal moments reverses. In the absence of dissipation within the ice, polar wander would occur on a time scale of $\sim \text{few} \times 10^3$ years. The friction which results in the liquid layer between the shell and the core due to polar wander of the shell, is turbulent unless the length scale of turbulence is $\lesssim 1$ km. Polar wander must occur in a time that is significantly less than the thermal diffusion time for the shell, $\sim 10^7$ y, or the thickness profile of the shell will respond to its new thermal environment, and the mechanism driving the polar wander will be virtually eliminated. Viscous flow of the topography at the base of the ice will also occur on a time scale near 10^7 y. Since the tidal dissipation is probably concentrated in the lower few km of the ice, the time evolution of the thickness profile will actually begin to be affected by its new orientation in the diffusion time for the lower few km of the ice, $\sim 10^5$ y, although substantial changes in the evolution of $\left(\frac{t}{\tau}\right)$ cannot occur until a significantly longer time has elapsed. We adopt 2×10^6 years as a conservative upper limit to the polar wander time scale. The simple model presented here suggests that large scale polar wander cannot occur unless extensive surface fractures already exist. However, if the dissipation in an unfractured shell arising from polar wander is in reality a few orders of magnitude smaller than our simple model suggests, polar wander would be a very effective mechanism for fracturing the shell, since stresses imparted during polar wander are $\sim \frac{1}{e} \sim 100$ times larger than those due to the eccentricity tide. Polar wander may play a role in the production of the extensive crack-like lineaments on Europa's surface.

Appendix A: The Coupling Torques

The purpose of this appendix is to describe the various torques which act to couple the motions of the silicate core, the liquid water layer, and the shell, during polar wander of the shell, and to estimate their effectiveness in doing so. We will discuss the well known Poincaré torque, gravitational coupling torques, and the torque due to viscous or turbulent friction within the liquid water layer. Although we will argue that none of these torques are capable of inducing appreciable motion of the silicate core during reorientation of the shell, we shall see that the Poincaré torque is unique in that it may cause the liquid water layer to reorient in coincidence with the shell. We will begin in section A.1 by arguing that the ocean reorients in coincidence with the shell during polar wander. Then in section A.2 we will discuss the extent to which the various torques are able to couple the motion of the core with that of the composite shell–ocean entity.

A.1 Shell–Ocean Coupling

A uniformly rotating fluid, confined within an ellipsoidal cavity will have a net torque exerted upon it, by the wall of the cavity, whenever the axis of rotation of the fluid departs from the axis of figure of the cavity. This torque is known as the Poincaré or inertial torque, and its value may be found by integrating over the surface of the contained fluid:

$$\vec{\Gamma}_P = - \int_S P [\vec{r} \times \hat{n}] dS \quad , \quad (\text{A.1})$$

where \hat{n} is the outward–directed unit normal vector of the surface, P is the pressure in the fluid at the surface, dS is an element of the surface area, and \vec{r} is the radius vector of the surface element from the center of the body (cf. Rochester, 1976).

For fluids with nonzero viscosity, Equation (A.1) is valid as long as the difference between the equatorial and polar radii of the cavity's surface significantly exceeds the thickness of the viscous or turbulent boundary layer which separates the interior from the cavity's surface. This criterion will be discussed later in this section. We wish to consider the Poincaré torque which is exerted on the liquid water layer by the ice shell during polar wander of the shell. However, as we will soon discuss, that problem is complicated by nonrigid behavior of the shell, effects due to self gravity, and the presence of the silicate core.

Therefore it is instructive to first discuss the simpler problem of a non-self-gravitating satellite consisting of a fluid confined within a rotating rigid elliptical cavity of characteristic ellipticity ϵ . We let the cavity rotate uniformly about an axis which departs from its minimum semimajor axis (i.e. its axis of maximum principal moment of inertia) by a large angle, and we wish to estimate the magnitude of the Poincaré torque exerted by the cavity on the fluid it contains. The cavity and the fluid are assumed to be in very nearly synchronous rotation, orbiting a parent planet under the influence of the tidal potential of the planet.

To evaluate Equation (A.1) it is necessary to know the pressure field within the fluid as well as the shape of the cavity. Only nonspherically symmetric components of the pressure field in the fluid can exert a net torque on the interface between the fluid and the cavity. The largest departures of the pressure field in the fluid from spherical symmetry are due to the tidal and rotational potentials. The sum of these potentials within the fluid may be written

$$U = -\frac{1}{2}\omega^2 r^2 \sin^2 \phi - \left(\frac{GM r^2}{R^3}\right) P_2(\cos S) \quad , \quad (\text{A.2})$$

where M , ω , R , r , ϕ , and S are the mass of the parent planet, the spin rate of the fluid, the body's orbital radius, the magnitude of the radius vector \vec{r} directed

from the center of the body to a point within the fluid, colatitude measured from the rotation pole of the fluid, and the angle between the vector joining the centers of the satellite and the parent planet and the vector \vec{r} , respectively. Because the fluid is in nearly synchronous rotation, both the tidal and rotational potentials are of order $\sim n^2 a^2$, where n and a are the mean motion and the average radius of the cavity. The portion ΔP of the pressure field within a uniformly rotating liquid layer of constant density ρ due to a potential U is

$$\Delta P = \rho U \quad (\text{A.3})$$

(cf. Jeffreys, 1976), aside from possibly an additive constant.

Because of the symmetry of the pressure field induced by the potential (A.2), the Poincaré torque vanishes only when the maximum semimajor axis (minimum axis of inertia) of the cavity is coincident with the axis separating the centers of the satellite and the planet, and the axes of rotation of the fluid and the cavity both coincide with the normal to the orbital plane. When the angles between any of the above pair or trio of axes are large, the order of magnitude of the Poincaré torque (A.1) acting on the fluid (with density ρ) may be estimated as follows: The characteristic magnitudes of the quantities $(\vec{r} \times \hat{n})$ and ΔP are $|\vec{r} \times \hat{n}| \sim a\epsilon$ and $\Delta P \sim \rho n^2 a^2$. Since the area of the surface of the cavity is $\approx 4\pi a^2$, the integral (A.1) has a characteristic magnitude $|\vec{\Gamma}_p| \sim \rho a^5 \omega^2 \epsilon$. We wish to demonstrate that the Poincaré torque is of the correct order of magnitude which is required to force the fluid, assuming it rotates as a rigid entity, to rotate with the same rotation vector as the cavity, even if the cavity is not rotating about one of its semimajor axes, and its maximum semimajor axis is not coincident with the satellite–planet direction.

It has been shown by Lamb (1932) that a rotating fluid confined within a

rigid ellipsoidal cavity may rotate effectively as a rigid entity in coincidence with the cavity in response to imposed motions (e.g., precession) of the cavity. We make no attempt to solve the fluid dynamical equations of motion for the system described here. We will simply assume that if the fluid reorients, it will do so effectively as a coherent, rigid entity.

With this in mind, assume that the cavity is rotating about an axis which is not a semimajor axis of its ellipsoidal figure, and also assume that the fluid shares the same rotation vector, $\vec{\omega}$, as the cavity. Since the shape of the fluid is dictated by that of the cavity, it is thus rotating about a nonprincipal axis of inertia, and its angular momentum must possess a component perpendicular to $\vec{\omega}$ of magnitude $\sim I_c \epsilon \omega$, which precesses about $\vec{\omega}$ at an angular rate $\sim \omega$ (cf. Goldstein, 1970). $I_c \sim \rho a^5$ is the characteristic moment of inertia of the fluid. Thus the angular momentum of the fluid is changing at a rate $\sim \rho a^5 \epsilon \omega^2$, which can only be true if a torque of the same magnitude is exerted on the fluid. Note that this magnitude is the same as that of the Poincaré torque.

In addition, a net torque due to the tidal potential is exerted on the nonspherical portion of the fluid whenever its orientation, as dictated by the orientation of the cavity, is such that none of its semimajor axes are coincident with the satellite-planet direction. The magnitude of this torque is of the order of the product of the nonspherical portion of the mass ($\sim \rho a^3 \epsilon$) multiplied by the magnitude of the tidal potential ($\sim \frac{GM}{R^3} a^2 \sim n^2 a^2$), or $\sim \rho a^5 n^2 \epsilon$. Note that this torque is also of the same magnitude as the Poincaré torque.

It is now evident that the Poincaré torque due to the tidal and rotational potentials is of the same order of magnitude as the torque which would be required to induce the fluid (if it behaves as a rigid body) to share the same rotation vector

and orientation as that of the cavity.

If the Poincaré torque is calculated precisely using Equations (A.2) and (A.3) in Equation (A.1), it can be shown, in fact, that it is of *exactly* the correct magnitude and direction which is required to induce coincident motion of the fluid and the cavity. We feel, however, that such a demonstration is inappropriately complicated to reproduce here.

We now wish to consider the coupling of the ice shell on Europa with an underlying layer of liquid water during polar wander of the shell. In the following discussion we will ignore the silicate core and assume that liquid water extends to Europa's center. The interface between the ice shell and the liquid water layer may be approximated by a spherical surface of radius $\sim a \approx 1550$ km to which is added three relatively small second harmonic degree bulges: a "fossil" bulge (see Section 4) of characteristic height $\sim \gamma a(1 - C_w) \sim 5$ m (for an unfractured shell with $\mu \sim 4 \times 10^{10}$ dynes cm^{-2} and $d \sim 2$ km), a "bulge" due to nonuniform ice thickness of order $\sim \frac{\rho_{\text{ice}}}{\rho_{\text{water}}} t_{2m} \sim 1$ km, and a hydrostatic bulge of characteristic height $\sim \gamma a \sim 1$ km. The hydrostatic bulge also has a small diurnal periodic component, which we will ignore, of order $\sim \gamma a e \sim 10$ m, where e is Europa's orbital eccentricity. The hydrostatic bulge represents the response of the ice shell to the tidal and rotational potentials and therefore possesses their symmetry. That bulge therefore remains very nearly fixed in the x_i'' coordinate system during polar wander as long as $n \gg \tau_{pw}^{-1}$, while both the fossil bulge and the bulge due to ice thickness variations remain fixed in the frame of shell as polar wander takes place. However, the fossil bulge is $\sim 10^2$ times smaller than that due to the ice thickness variations and in any case must be eliminated by pervasive fracturing if polar wander of the shell is to occur at all (see Section 6.2). We therefore approximate the shell-

ocean interface as a sum of the hydrostatic bulge and the bulge due to ice thickness variations. We define the characteristic ellipticities of these deformations as ϵ_h and ϵ_s , respectively.

Because the bulge ϵ_s remains fixed in the body from the shell, it is analogous to the ellipticity of the cavity in the non-self-gravitating system discussed above. The pressure induced by the tidal and rotational potentials exerts a torque on this bulge which is of exactly the correct magnitude and direction to allow the fluid to move in coincidence with the shell during polar wander. However, with the addition of self gravity and the nonrigid component ϵ_h to the shape of the shell-ocean interface, two additional effects arise: the mass contained in the hydrostatic bulge produces an additional potential due to self-gravity which increases the potential given by (A.2) by a factor $(1 + k_2)$ where k_2 is the second degree potential Love number (cf. Munk and MacDonald, 1960). This causes an additional component of the Poincaré torque of magnitude $k_2 \vec{\Gamma}_p$. Also, the second harmonic degree components of the mass contained in the ice shell produce a pressure component in the ocean which exerts a net torque across the surface component ϵ_h . However, these two additional torques may be shown to be of exactly equal magnitude and opposite direction, so that the problem reduces to that of the simple nongravitating, rigid system discussed above.

It is now clear that the Poincaré torque acting across the nonspherical component of the shell-ocean interface represented by ϵ_s is of the correct magnitude which is required to induce coincident motion of the ocean and the shell during polar wander. However, as mentioned earlier, this torque is only effective if the thickness Δ of the boundary layer between the ice and the liquid is significantly smaller than the difference between the equatorial and polar radii of the cavity,

$a\epsilon_s \sim 1$ km. If the relative motion across the boundary layer is laminar in nature and a geostrophic balance exists within it,

$$\Delta \approx \left(\frac{\nu}{n}\right)^{1/2}, \quad (\text{A.4})$$

where $\nu \sim 10^{-2} \text{ cm}^2 \text{ s}^{-1}$ is the kinematic viscosity of water and $n \approx 2 \times 10^{-5} \text{ s}^{-1}$ is the rotation frequency (cf. Greenspan, 1968). Then $\Delta \sim 10$ cm and the criterion $\Delta \ll a\epsilon_s$ for validity of the Poincaré torque is well satisfied. However, if the Reynolds number

$$\text{Re} = \frac{u\ell}{\nu} \gg 300 \quad (\text{A.5})$$

(Jeffreys, 1976) motion within the boundary layer will be turbulent and Δ will not be given by Equation (A.4). u is the characteristic velocity difference between the ice and the liquid just below the boundary layer, and ℓ is the characteristic length scale of the turbulence. The magnitude of the Reynolds number is difficult to estimate because the correct values of u and ℓ are uncertain. Although we expect the Poincaré torque to induce coincident motion of the fluid and the ice, some relative motion, however slight, must occur between them. If ℓ is comparable to the radius of the satellite, a , the Reynolds number criterion implies that motion will be turbulent if $u \gg 10^{-4} \left(\frac{a}{10^5 \text{ years}}\right)$. Because we expect polar wander to occur on a time scale of 10^5 – 10^6 y and we expect nearly coincident motion of the liquid and the shell, it thus seems plausible that the boundary layer is laminar in nature. If the boundary layer is turbulent, its thickness may be estimated by replacing the kinematic viscosity by the eddy viscosity, ν_{eddy} , in Equation (A.4). ν_{eddy} is roughly given by the product of the characteristic velocity of the turbulent eddies, u_{eddy} , and the length scale ℓ of the turbulence. The correct value of ν_{eddy} is uncertain. However, if the turbulence is caused by shear induced by the polar wander, ν_{eddy}

is certainly no larger than the product of the maximum values of u_{eddy} and ℓ , i.e., $\nu_{\text{eddy}})_{\text{max}} \leq \left(\frac{a}{\tau_{pw}}\right) a \sim 8 \times 10^3 \left(\frac{10^5 \text{ years}}{\tau_{pw}}\right) \text{ cm}^2/\text{sec}$. Therefore, $\Delta_{\text{max}} \lesssim \left(\frac{\nu_{\text{eddy}})_{\text{max}}}{n}\right)^{1/2} \sim 10^4 \text{ cm}$. Thus, even if the flow in the boundary layer between the ice and the liquid is turbulent, Δ may still be considerably less than $a\epsilon_s$, in which case the Poincaré torque is probably effective in causing the liquid layer to follow the motion of the ice. Alternatively, it is possible that the boundary layer is turbulent because of convection in the liquid layer. In that case, the boundary layer thickness is independent of the details of polar wander and may be larger than the above limit, perhaps exceeding $a\epsilon_s$. If $\Delta > a\epsilon_s$, so that the liquid layer is essentially uncoupled to the ice, polar wander of the shell will occur on a shorter time scale than we estimate in this paper, because the characteristic inertia of the shell, I_o , will be smaller (see Section 6). However, because the total mass of ice plus liquid water is at most ~ 5 times larger than the mass of ice alone, our results would not be greatly changed if $\Delta > a\epsilon_s$.

In light of the results discussed above, we believe that a liquid water layer beneath the ice shell on Europa may reorient in coincidence with the shell during polar wander of the shell, and we therefore refer to the composite shell–ocean entity as “the shell” in the text of this paper. We do not believe that the presence of the silicate core will affect this qualitative result.

A.2 Core–Shell Coupling

We now wish to discuss the various torques which act to couple the motions of the core and the shell during polar wander of the shell, and their effectiveness in doing so.

We have argued in Section A.1 that in a reorientation of the ice shell as

described in Section 6.2, the liquid layer will reorient in coincidence with the shell so that the shell and the liquid layer may be treated as a single entity. The shear due to any relative motion between the core and this ocean-shell entity will then be effectively confined to a boundary layer at the base of the ocean. We are therefore concerned here with torques exerted between the core and the shell-ocean entity. We will consider the Poincaré torque, gravitational coupling and the torque due to viscous or turbulent shear in the boundary layer between the base of the ocean and the core.

We shall argue that none of these torques are capable of inducing significant polar wander of the core by estimating the ratio of their magnitudes to the characteristic rate of change of the angular momentum of the shell during polar wander. If these ratios are small compared to unity (as we shall see is true), the shell is able to reorient independently of the core.

We begin by discussing the Poincaré torque acting on the surface of the core. Equation (A.1) may be used to estimate the magnitude of this torque, even though the ellipsoidal cavity is in this case surrounded by the fluid.

We assume that any reorientation of the silicate core of Europa will occur on a time scale which is long compared to the Maxwell time of the bulk of its interior, and the Rayleigh-Taylor time scale $\tau_{RT} \sim \frac{4\pi\nu}{g\lambda}$ (cf. Turcotte and Schubert, 1982), where ν and g are the kinematic viscosity of the core and its surface gravity, and λ is a lengthscale which in this case is comparable to the radius of the satellite $\sim a$. Then the shape of the core will remain very nearly the hydrostatic shape of a fluid under the tidal and rotational potentials. If the viscosity of the bulk of the core is $\lesssim 10^{21}$ Poise, a value characteristic of the earth's mantle (Garland, 1979), and the rigidity of the core is $\approx 6 \times 10^{11}$ dynes cm^{-2} , the above assumption

is valid if the motion of the core occurs on a time scale significantly longer than $\sim 10^4$ years. The surface of the core will in fact depart from the fluid shape due to fossil rotational and tidal bulges which will exist if a continuous elastic lithosphere is present on the core. Though fossil bulges will be much smaller than the fluid bulges, nonzero components of the torque given by Equation (A.1) will arise due to their presence. These components may be treated separately and will be considered shortly. We now estimate the portion of the inertial torque which exists in the absence of nonfluid behavior of the core.

With this in mind, we now consider both the silicate core and the overlying water layer to be fluids. The two fluids are prohibited from mixing by their enormous viscosity contrast ($\gtrsim 23$ orders of magnitude) as well as their substantial contrast in density. The portion of the pressure field in the ocean due to the tidal potential, and the response of the surface of the core to the tidal potential possess the same symmetry. Therefore, there can be no net torque between the ocean and the core due to the tidal potential. We may therefore ignore the presence of the tidal potential in estimating this portion of the inertial torque, and treat the surface of the core and the pressure field in the ocean as though their only departures from spherical symmetry are in response to their rotational potentials.

The Poincaré torque exists because of the variation over the surface of the core of the rotationally-induced pressure exerted by the overlying water. We will ignore the deflection of the surface of the core due to this imposed pressure. Any errors incurred by doing so will not effect the qualitative results of this analysis. Such a deflection can only reduce the calculated torque. We will see that even with this overestimate, the Poincaré torque is unimportant in this problem.

The shell and core must remain in very nearly synchronous rotation through-

out any reorientation event, so that the angle between their rotation vectors χ must remain very small. By evaluating the Poincaré torque (A.1) at the core-ocean interface due to the rotational potential in the ocean assuming the core and shell are in nearly synchronous rotation, it can easily be seen that its magnitude is $\Gamma_p \sim \rho_{\text{water}} a_c^5 n^2 \epsilon_h \chi$, where $\epsilon_h \sim \gamma$ is the ellipticity of the hydrostatic bulge on the core, and a_c is the mean radius of the core, $a_c \sim a$. The largest departure of the shell's rotation vector from the mean motion is $\sim \dot{\psi}$, so that $\chi \sim \frac{\dot{\psi}}{n}$. Given the motion of the shell described in Section 6.2, the characteristic magnitude of the rate of change of the angular momentum of the shell (in inertial space) may be calculated to be $\dot{L}_s \sim I_o n^2 \left(\frac{t}{\tau}\right)$. The Poincaré torque is unimportant if $\frac{\Gamma_p}{\dot{L}_s} \ll 1$, which may now be written

$$10^{-3} \left(\frac{10^5 \text{ years}}{\tau_{pw}} \right) \left(\frac{10^{-6}}{\left(\frac{t}{\tau}\right)} \right) \ll 1 \quad , \quad (\text{A.6})$$

using a total thickness of ice and ocean of ~ 100 km, $\dot{\psi} \sim \frac{1}{\tau_{pw}}$ where τ_{pw} is the polar wander time scale, and other parameters appropriate to Europa. Since typically $\tau_{pw} \sim 10^5$ – 10^6 years (if polar wander occurs at all) and $\left(\frac{t}{\tau}\right) \lesssim 10^{-6}$ during polar wander (see Section 6.2), this torque is clearly unimportant throughout at least most of the period during which polar wander takes place.

In the above development it is implicitly assumed that the pressure field is hydrostatic, with the entire core undergoing the same “rigid body” (i.e. constant vorticity) motion. If the spin vectors of the core and shell differ substantially in direction and magnitude, this will not be true, and the criterion (A.6) is incorrect. However, because the rotation rates of the core and shell are very nearly equal, and χ is very small (true because $\tau_{pw} \gg 1/n$), hydrostatic equilibrium is very nearly maintained and the criterion (A.6) is meaningful.

An additional component of the Poincaré torque exists if a “fossil” rotational and/or tidal bulge is present on the silicate core. The ellipticity of this bulge is of magnitude $\epsilon_f \sim (1 - C_w)\gamma$ where C_w may be found by inserting parameters relevant to the silicate core into Equation (3.11). $(1 - C_w)$ has a value of $\sim 0.05 \left(\frac{\mu_c}{6 \times 10^{11} \text{ dynes cm}^{-2}} \right) \left(\frac{d_c}{2 \text{ km}} \right)$ for the core, where μ_c and d_c are the rigidity of the core and the thickness of its lithosphere, respectively. The magnitude of the Poincaré torque Γ_f due to the pressure induced by the tidal and rotational potentials acting on the fossil bulge is $\Gamma_f \sim (1 - C_w)\rho a_c^5 \gamma n^2 \theta_f$, where θ_f is the angle between the rotation axis of the ocean and the minimum semimajor axis of the fossil bulge. This torque is unimportant if $\frac{\Gamma_f}{L_s} \ll 1$, which may be written

$$10^2 \left(\frac{\mu_c}{6 \times 10^{11} \text{ dynes cm}^{-2}} \right) \left(\frac{d_c}{2 \text{ km}} \right) \left(\frac{10^{-6}}{\frac{t}{\tau}} \right) \theta_f \ll 1 \quad . \quad (\text{A.7})$$

It is thus clear that for reasonable values of μ_c and d_c the torque is only unimportant if $\theta_f \ll 10^{-2} \left(\frac{t/\tau}{10^{-6}} \right)$. However, the torque Γ_f acts in a manner so as to maintain alignment between the rotation axis of the ocean and the minimum semimajor axis of the fossil bulge. Since the latter axis will be aligned with the normal to the orbit (because that is its minimum energy state) before an episode of polar wander occurs, and because the rotation vector of the ocean departs from this axis by an angle of only $\sim \frac{\dot{\psi}}{n} \sim 10^{-8} \left(\frac{10^5 \text{ y}}{\tau_{pw}} \right)$ there exists no mechanism of inducing a value of θ_f larger than $\sim 10^{-8}$. Therefore this torque is also unimportant in coupling the motions of the core and the shell.

The gravitational potential field in the ocean also has second degree components of the order $\sim \left(\frac{n^2 a^2}{\gamma} \right) \left(\frac{t}{\tau} \right) \left(\frac{I_o}{M a^2} \right)$ due to the sum of the thickness variations of the nearly isostatically compensated ice shell and the underlying liquid water which conforms to the shell. These components of gravity produce pressure varia-

tions which exert a torque on the core when integrated over the surface of the core's fossil bulge. This torque has a magnitude Γ_G where $\Gamma_G \sim I_o n^2 \left(\frac{t}{r}\right) (1 - C_w) \Big|_{\text{silicate core}}$ when the x_3 body axis of the shell departs from the minimum semimajor axis of the fossil bulge on the core by a large angle. This torque is thus unimportant if

$$\frac{\Gamma_G}{\dot{L}_s} \sim (1 - C_w) \Big|_{\text{silicate core}} \sim 0.05 \left(\frac{\mu_c}{6 \times 10^{11} \text{ dynes cm}^{-2}} \right) \left(\frac{d_c}{2 \text{ km}} \right) \ll 1 \quad (\text{A.8})$$

which is clearly true for reasonable choices of μ_c and d_c .

In a manner analogous to the problem of shell-ocean coupling, two additional torques act on the core which exactly cancel one another: A pressure component present in the ocean due to the gravitational potential of its the fossil bulge exerts a torque on the core when integrated over the surface of its hydrostatic bulge, and a pressure component due to the gravitational potential of the hydrostatic bulge in the fluid (present because its shape must conform to that of the hydrostatic bulge on the core) exerts a net torque on the core when integrated over its fossil bulge. Both of these torques are of magnitude $\sim \Gamma_f$.

We now consider one additional torque which acts to couple the motions of the core and the shell during polar wander: If relative motion occurs between the core and the shell, a torque due to viscous or turbulent friction will exist between them, directed along the difference of their angular velocities. If the friction is of a laminar and viscous nature, the torque acting on the shell may be written

$$\vec{\Gamma}_{\text{viscous}} = C_K (\vec{\omega}_{\text{core}} - \vec{\omega}_{\text{shell}}) \quad , \quad (\text{A.9})$$

where

$$C_K \sim \rho \nu \left(\frac{a}{\Delta} \right) a^3 \quad (\text{A.10})$$

and

$$\Delta \simeq \left(\frac{\nu}{n} \right)^{1/2} \quad (\text{A.11})$$

is the thickness of the Ekman boundary layer where the shear due to the relative motion is concentrated (just as in the case of shell-ocean coupling). Equation (A.9) is valid if a geostrophic balance exists within the boundary layer (cf. Greenspan, 1968). ν , ρ , a , and n are the kinematic viscosity and density of water, the radius of Europa and the mean motion, respectively. A torque equal and opposite to (A.9) is exerted on the core.

If the flow in the ocean due to the relative motion between the core and the shell is turbulent, Equation (A.9) no longer applies. The condition for turbulence is that the Reynolds number

$$\text{Re} = \frac{u\ell}{\nu} \gg 300 \quad , \quad (\text{A.12})$$

where u is the characteristic relative velocity between the core and the shell (i.e. $u \sim a|\vec{\omega}_c - \vec{\omega}_s|$), and ℓ is the characteristic lengthscale of the turbulence (cf. Jeffreys, 1970).

If the motion is turbulent, the coupling torque is

$$\vec{\Gamma}_{\text{turb}} \simeq C_T |\vec{\omega}_c - \vec{\omega}_s| (\vec{\omega}_c - \vec{\omega}_s) \quad , \quad (\text{A.13})$$

where

$$C_T \sim \alpha \rho a^5 \quad (\text{A.14})$$

and $\alpha \sim 0.002$ is the coefficient of skin friction (Jeffreys, 1970).

Taking the ratio of (A.13) to (A.9), it is seen that the turbulent coupling torque is generally much smaller than the viscous torque. For example, even if $|\vec{\omega}_c - \vec{\omega}_s|$ is as large as $\sim 10^{-2} \text{ yr}^{-1}$, (A.13) is smaller than (A.9) by more than a factor of 20. However, we shall see that even the viscous torque is of negligible importance in coupling the motions of the core and the shell.

Because the largest component of $|\vec{\omega}_{\text{core}} - \vec{\omega}_{\text{shell}}|$ is $\sim \dot{\psi} \sim \frac{1}{\tau_{pw}}$, the magnitude of the coupling torque due to viscous shear is $\Gamma_{\text{viscous}} \sim \frac{C_k}{\tau_{pw}}$, and the ratio $\frac{\Gamma_{\text{viscous}}}{\dot{L}_s}$ is of order $\sim \frac{C_k}{\tau_{pw} n^2 I_o \left(\frac{t}{\tau}\right)}$ which may be written

$$\frac{\Gamma_{\text{viscous}}}{\dot{L}_s} \sim 10^{-8} \left(\frac{10^{-6}}{\frac{t}{\tau}} \right) \left(\frac{10^5 \text{ y}}{\tau_{pw}} \right), \quad (\text{A.15})$$

for reasonable values of $\nu \sim 0.01$ Poise, a thickness of shell plus ocean of $b_o \sim 100$ km, and the known value of $n \simeq 2 \times 10^{-5} \text{ s}^{-1}$ for Europa. The viscous and turbulent coupling torques are clearly utterly negligible.

If polar wander of the shell occurs on a time scale of 10^5 – 10^6 years, the Reynolds number in the boundary layer in the ocean between the core and the shell (Equation (A.12)) is

$$\text{Re} = \frac{u\ell}{\nu} \sim \frac{\alpha\dot{\psi}_s \ell}{\nu} \sim 10^5 - 10^6 \quad (\text{A.16})$$

if the length scale of the turbulence, ℓ , is equated with the radius of Europa. Since the critical Reynolds number is ~ 300 , the frictional coupling torque acting between the core and the shell is turbulent in nature, and is even less effective at coupling the motions of the core and shell than viscous coupling. However, if the length scale of the turbulence is caused by irregularities on the core $\lesssim 1$ – 10 km in length, the Reynolds number could be less than critical and the coupling would be laminar. In neither case is the frictional coupling important.

One more point must be mentioned here: Although we have found no torques capable of inducing significant reorientation of the core during polar wander of the shell, a potential inconsistency exists between our results and those of Lamb (1932). Lamb found that the fluid throughout the interior of a rigid ellipsoidal cavity may reorient as a rigid coherent body in response to imposed motions of the cavity. In the limit where the values of the viscosity and density of the silicate core are the

same as those of the liquid layer, no distinction exists between the core and the ocean, and Lamb's result would indicate that the entire fluid, including the core, would follow the motion of the shell. However, if the viscosity of the core is similar to that of the earth's mantle ($\gtrsim 10^{21}$ Poise), a viscosity contrast of $\gtrsim 10^{23}$ orders of magnitude exists between the core and the liquid water layer, since liquid water has a viscosity of $\sim 10^{-2}$ Poise (cf. Turcotte and Schubert, 1982). We believe that this enormous viscosity contrast, as well as a density contrast of a factor of $\gtrsim 3$ serves to create the critical distinction between our results and those of Lamb.

Appendix B: Viscous Relaxation at the Ice–Ocean Interface

Undulations at the ice–ocean interface are subject to viscous relaxation, despite the isostatic conditions. This problem is very analogous to the classic Rayleigh–Taylor instability (e.g., Chandrasekhar, 1961) except that we must allow for the temperature dependence of the viscosity of ice. Although we are concerned with very long wavelength undulations, an adequate approximation can be obtained from analysis of a Cartesian geometry in which $z = 0$ is the undeformed water–ice interface, and horizontal variations and motions are confined to the x direction. (This can be done without loss of generality because of the linearity of the equations and resulting superposability of solutions.) Let u, w be the horizontal and vertical components of flow, respectively. In the high viscosity limit, the corresponding components of the Navier–Stokes equation are

$$0 = -\frac{\partial p}{\partial x} + \eta \nabla^2 u + \frac{\partial \eta}{\partial z} \cdot \left(\frac{\partial u}{\partial z} + \frac{\partial w}{\partial x} \right) \quad (\text{B.1})$$

$$0 = -\frac{\partial p}{\partial z} + \eta \nabla^2 w + \frac{\partial \eta}{\partial z} \cdot \left(2 \frac{\partial w}{\partial z} \right) \quad , \quad (\text{B.2})$$

where p is the nonhydrostatic pressure and $\eta \equiv \eta(z)$ is the viscosity. We also have the continuity condition for incompressible flow

$$\frac{\partial u}{\partial x} + \frac{\partial w}{\partial z} = 0 \quad . \quad (\text{B.3})$$

If we assume $p, w, \sim \cos kx$ and $u \sim \sin kx$ then these three equations can be combined by eliminating u, p :

$$\frac{d^4 \omega}{dz^4} + \frac{2}{\eta} \frac{d\eta}{dz} \frac{d^3 \omega}{dz^3} + \left(\frac{1}{\eta} \frac{d^2 \eta}{dz^2} - 2k^2 \right) \frac{d^2 \omega}{dz^2} \quad (\text{B.4})$$

$$- \frac{2k^2}{\eta} \frac{d\eta}{dz} \frac{d\omega}{dz} + k^2 \left(\frac{1}{\eta} \frac{d^2 \eta}{dz^2} + k^2 \right) \omega = 0 \quad . \quad (\text{B.5})$$

For simplicity, we approximate $\eta = \eta_o \exp\left(\frac{z}{\delta}\right)$, to represent approximately the rapid increase in viscosity as one goes upwards into the ice. It is also appropriate to assume that the interesting wavelengths of ice undulations are much larger than δ (i.e. $k\delta \ll 1$). Accordingly, the solutions to the above equation that decay as $z \rightarrow \infty$ are:

$$w \propto e^{-z/\delta}, \quad ze^{-z/\delta} \quad . \quad (\text{B.6})$$

For the assumption of zero shear $\left(\frac{\partial w}{\partial z} = 0\right)$ at $z = 0$, appropriate because of the low viscosity of the adjoining water, the solutions of interest are

$$\begin{aligned} u &= \left(1 + \frac{z}{\delta}\right) e^{-z/\delta} \sin kx \\ w &= k\delta \left(2 + \frac{z}{\delta}\right) e^{-z/\delta} \cos kx \\ p &\simeq \frac{\eta_o \cos kx}{k\delta^2} \quad , \end{aligned} \quad (\text{B.7})$$

except for an arbitrary multiplicative function of time. We determine the time-dependence by use of the normal stress boundary condition:

$$\left(-p + 2\eta \frac{\partial w}{\partial z}\right) \Big|_{z=0} = \Delta\rho gh \quad , \quad (\text{B.8})$$

where h is the magnitude of the topography and $\Delta\rho$ is the density difference between water and ice. Taking one time derivative and identifying $w(z=0) = \frac{\partial h}{\partial t}$,

$$\frac{\partial}{\partial t} \left(-p + 2\eta \frac{\partial w}{\partial z}\right) \Big|_{z=0} = \Delta\rho g w \quad , \quad (\text{B.9})$$

from which it follows that

$$\frac{1}{h} \frac{\partial h}{\partial t} \equiv \frac{1}{w} \frac{\partial w}{\partial t} \Big|_{z=0} = -\frac{2g\Delta\rho k^2 \delta^3}{\eta_o} \quad . \quad (\text{B.10})$$

The reciprocal of this is a characteristic time scale τ_r for the relaxation of topography. Scaling to numbers appropriate to Europa,

$$\tau_r \simeq (1 \times 10^7 \text{ yr}) \cdot \left(\frac{1 \text{ km}}{\delta}\right)^3 \cdot \left(\frac{\eta_o}{10^{15} \text{ Poise}}\right) \quad , \quad (\text{B.11})$$

for horizontal wavelengths comparable to the equator-to-pole distance. (In fact, the numerical constant becomes 2.5×10^7 years, if $w \propto P_2(\cos \theta)$, $\theta = \text{colatitude}$.)

The appropriate choice of δ can be estimated from

$$\delta \equiv \left(\frac{d \ln \eta}{d \ln z} \right)^{-1} = \left(\frac{d \ln T}{d \ln \eta} \right) \cdot \left(\frac{d \ln z}{d \ln T} \right) \cdot d \quad , \quad (\text{B.12})$$

where T is the temperature and d is the ice crust thickness. Accordingly, $\delta \sim 0.04d \sim 1$ km. The appropriate choice of η_o may be as low as 10^{14} Poise (the commonly quoted value of terrestrial temperate glacier ice) but could be $\sim 10^{15}$ Poise because of the very low stresses associated with this flow.

We conclude that $\tau_r \sim 10^7$ years for Europa. Thus, there is no strong inequality between this process and the estimated time scales of thermal diffusion or putative polar wander. Nevertheless, the time scale is not significantly shorter than other time scales of interest. Accordingly, the assumed variations in ice thickness used in the Europa models may not be in error by a large factor. More importantly, the qualitative behavior of ice thickness variation is correct.

Acknowledgements

This work was supported by NASA Grant NAGW-185 to the California Institute of Technology and in part by NASA Grant NAGW-944 to the Lunar and Planetary Laboratory of the University of Arizona. Both grants are part of the NASA Planetary Geology and Geophysics program. We would like to thank Dr. Peter Goldreich for very helpful conversations.

References

- Chandrasekhar, S. (1961). *Hydrodynamic and Hydromagnetic Stability*. Dover Publications, New York.
- Crawford, G.D. and Stevenson, D.J. (1988). Gas-driven water volcanism and resurfacing of Europa. *Icarus* **73**, 66–79.
- Danby, J.M. (1962). *Fundamentals of Celestial Mechanics*. MacMillan, New York.
- Darwin, G.H. (1877). On the influence of geological changes on the earth's axis of rotation. *Phil. Trans. Roy. Soc. London* **167**, 271–312.
- Eirich, F.R. (1956). *Rheology: Theory and Applications, Vol. 1* Academic Press, New York.
- Garland, G.D. (1979). *Introduction to Geophysics*. W.P. Saunders Co., Philadelphia.
- Gold, T. (1955). Instability of the earth's axis of rotation. *Nature* **175**, 526–529.
- Goldreich, P. and Toomre, A. (1969). Some remarks on polar wandering. *J. Geophys. Res.* **74**, 2555–2567.
- Goldstein, H. (1970). *Classical Mechanics*. Addison Wesley, Reading, Massachusetts.
- Gordon, R.G. (1987). Polar wandering and paleomagnetism. *Ann. Rev. Earth Planet. Sci.* **15**, 567–593.
- Greenberg, R. and Weidenschilling, S.J. (1984). How fast do the Galilean satellites

spin? *Icarus* **58**, 186–196.

Greenspan, H.P. (1968). *The Theory of Rotating Fluids*. Cambridge University Press, New York.

Hobbs, P.V. (1974). *Ice Physics*. Oxford University Press, London.

Jeffreys, H. (1976). *The Earth, 6th ed.* Cambridge University Press, Cambridge.

Lamb, H. (1932). *Hydrodynamics*. Cambridge University Press, London.

Lambeck, K. (1980). *The Earth's Variable Rotation: Geophysical Causes and Consequences* Cambridge University Press, Cambridge.

Mathews, J. and Walker, R.L. (1970). *Mathematical Methods of Physics*. The Benjamin Cummings Publishing Co., Menlo Park, California.

Milankovich (1934). Der mechanismus der polverlagerungen und die daraus sich ergebenden polbahkurven. *Gerlands Beitr. z. Geoph.* **42**, 70.

Munk, W. and McDonald, G.J.F. (1960). *The Rotation of the Earth*. Cambridge University Press, New York.

Ojakangas, G.W. and Stevenson, D.J. (1988). Thermal state of an ice shell on Europa Submitted to *Icarus*.

Rochester, M.G. (1976). The secular decrease of obliquity due to dissipative core-mantle coupling. *Geophys. J. R. astr. Soc.* **46**, 109–126.

Ross, M.N. and Schubert, G. (1987). Tidal heating in an internal ocean model of Europa. *Nature* **325**, 133–134.

- Schubert, G., Cassen, P., and Young, R.E. (1977). Subsolidus convection models of the lunar internal temperature. *Phil. Trans. Roy. Soc. London* **285**, 523–536.
- Turcotte, D.L. and Schubert, G. (1982). *Geodynamics*. John Wiley and Sons, New York.
- Turcotte, D.L. and Willemann, R.J. (1981). Role of membrane stresses in the support of planetary topography. *J. Geophys. Res.* **86**, 3951–3959.
- Vening-Meinesz, F.A. (1947). Shear patterns of the earth's crust. *Trans. Amer. Geophys. Union* **28**, 1–61.
- Willemann, R.J. (1984). Reorientation of planets with elastic lithospheres. *Icarus* **60**, 701–709.
- Willemann, R.J. and Turcotte, D.L. (1981). Support of topographic and other loads on the moon and on the terrestrial planets. *Proc. Lunar Planet. Sci. B* **12**, 837–851.
- Willemann, R.J. and Turcotte, D.L. (1982). The role of lithospheric stress in the support of the Tharsis rise. *J. Geophys. Res.* **87**, 9793–9801.